Dissertation
submitted to the
Combined Faculty of Natural Sciences and Mathematics
of the Ruperto Carola University Heidelberg, Germany
for the degree of
Doctor of Natural Sciences

presented by

M. Sc. Simone Sander

born in Neumünster

Oral examination:

Relevance of ACSL3-mediated ACS activity and ACSL3 localization in anabolic and catabolic lipid droplet metabolism

Referees: Prof. Dr. Britta Brügger

apl. Prof. Dr. Joachim Füllekrug

Table of contents

List of figures and tables

List of abbreviations

A3-RNAi	cells with a knockdown of ACSL3 caused by RNA interference
ACAT	acyl-CoA:cholesterol acyltransferase
ACSL	long chain acyl-CoA synthetases
ACSL3	long chain acyl-CoA synthetase 3
ACSVL	very long chain acyl-CoA synthetases
AGPAT	acylglycerolphosphate acyltransferase
AMP	adenosine monophosphate
APS	ammoniun persulfate
ATGL	adipose triglyceride lipase
ATP	adenosine triphosphate
BCA	bicinchoninic acid
BSA	bovine serum albumine
$CaCl_2$	calcium chloride
CDP	cytidine diphosphate
CCT	CTP:phosphocholine cytidylyltransferase
CGI-58	comparative gene identification-58
CIDEA	cell death activator A
CIDEC	cell death activator C
CMP	cytidine monophosphate
CTP	cytidine triphosphate
CH	cholesterol
DAG	diacylglycerol
DGAT	diglyceride acyltransferase
DNA	deoxyribonucleic acid
ER	endoplasmic reticulum
ERAD	ER-assisted degradation
FA	non-esterified fatty acid
FAS	fatty acid synthase
FATP	fatty acid transport protein
FCS	fetal calf serum
FIT	fat storage-inducing transmembrane protein
FSP27	fat-specific protein 27
G02S	G0/G1 switch gene 2
GFP	green fluorescent protein
GFP_A3ko	ACSL3-knockout cells expressing cytosolic GFP
GPAT	glycerol 3-phosphate acyltransferases
GST-ACSL3	ACSL3 bound to glutathione S-transferase

HA	hemaglutinin
HCl	hydrochloric acid
HCV	hepatitis C virus
HDR	homology-directed repair
HEPES	4-(2-hydroxyethyl)-1-piperazineethanesulfonic acid
HSL	hormone-sensitive lipase
KCl	potassium chloride
LD	lipid droplet
LPCAT	lysophosphatidylcholine acyltransferace
MDH	monodansylpentane
MGL	monoacylglycerol lipase
ms	mouse
MTT	3-(4,5-dimethylthiazol-2-yl)-2,5-diphenyl tetrazolium bromide
Na_2HPO_4	disodium phosphate
NaCl	sodium chloride
NaOH	sodium hydroxide
NHEJ	non-homologous end joining
OA	oleic acid/oleate
PA	phosphatidic acid
PAM	protospacer adjacent motif
PAP	phosphatidic acid phosphatase
PC	phosphatidylcholine
PE	phosphatidylethanolamine
PFA	paraformaldehyde
Phx-gp	Phoenix gag-pol cells
PI	phosphatidylinositol
PS	phosphatidylserine
P/S	penicillin/streptomycin
rb	rabbit
SDS	sodium dodecyl sulfate
SG buffer	saponin-gelatin buffer
SGB buffer	saponin-gelatin-BSA buffer
SM	sphingomyelin
TEMED	tetramethylethylendiamin
TG	triglyceride
TLC	thin layer chromatography
wt	wildtype
wtCOS-7	wildtype COS-7 cells

1. Summary

Lipid droplets (LD) are intracellular storage organelles that are found in most of all cell types and play an important role in the pathology of various human diseases like diabetes type II, cardiomyopathy and atherosclerosis. The core of the LD consists of different neutral lipids, mainly triglycerides and cholesteryl esters. This hydrophobic core is surrounded by a phospholipid monolayer embedding specific proteins and enzymes. One of these enzymes is the long chain acyl-CoA synthetase 3 (ACSL3) that belongs to the family of acyl-CoA synthetases (ACS). Proteins of the ACS family catalyze the esterification of fatty acids with coenzyme A, which is an essential prerequisite for further metabolism. Among all ACS family members, ACSL3 is the only ACS enzyme that is consistently found on LD. ACSL3 is characterized by a dual localization on LD and the endoplasmic reticulum (ER). It translocates from the ER to the LD upon fatty acid supplementation and is already present on nascent LD. Based on the current data, ACSL3 localization on LD and the ACS activity mediated by ACSL3 is presumed to be biologically relevant.

This work investigated the relevance of ACSL3-mediated ACS activity and ACSL3 localization in anabolic and catabolic lipid metabolism. The main approach was based on the depletion of ACSL3 in COS-7 cells by RNA interference or CRISPR/Cas9 knockout. ACSL3-knockout cells were transduced with genetically modified enzyme variants and lipid metabolism was investigated. A mutated ACSL3 variant lacking ACS activity was applied to identify potential ACSL3 functions independent of ACS activity. An ACSL3 variant localized to the ER but excluded from the LD was supposed to elucidate the importance of ACSL3 localization on LD. Experimental approaches included radiolabelling and quantification of intracellular lipid species by ^{14}C-oleic acid and ^{14}C-acetate, quantification of newly synthesized LD in starved cells and intracellular triglyceride measurement during basal lipolysis. Molar quantification of ACSL3 in A431 cells was carried out to calculate the metabolic capacity of LD-associated ACSL3 for triglyceride synthesis.

ACSL3-knockout reduced ACS activity by 93 % indicating that ACSL3 is the dominant ACS family member in COS-7 cells. Incorporation of ^{14}C-oleic acid was significantly decreased by 33 % in the ACSL3-knockout cells compared to wildtype COS-7 cells. Triglyceride synthesis was markedly reduced by approximately 50 % and LD biogenesis was decreased by 65 % in the ACSL3-knockout cells compared to wildtype COS-7 cells. The basal lipolytic rate was increased in the ACSL3-knockout cells resulting in intracellular triglyceride levels that were

46 % lower than the triglyceride levels measured in the control cells after 6 h of starvation. Cells expressing the ACSL3 variant lacking ACS activity were slightly reduced in basal lipolysis and thus exhibited triglyceride levels elevated by 24 % compared to the ACSL3-knockout cells after 6 h of starvation. Cells expressing only ER-localized ACSL3 were increased in triglyceride synthesis, but decreased in LD biogenesis by 54 % compared to cells expressing also LD-associated ACSL3. Model calculations in A431 cells estimated that local triglyceride synthesis on LD accounted to 3.3 % of total cellular triglyceride synthesis.

In conclusion, this study revealed that ACSL3 is essential for triglyceride synthesis and LD biogenesis by activating fatty acids and delivering them to enzymes involved in lipid synthesis. However, the metabolic capacity of LD-associated ACSL3 is too low to significantly contribute to LD growth. Thus, LD expansion is probably dependent on lipid transfer from the ER to the LD. Moreover, ACSL3 decreases lipolysis maybe by re-esterification of fatty acids deliberated during lipolysis but also possibly by recruitment of antilipolytic proteins to the LD. ER-localized ACSL3 is superior in triglyceride synthesis probably due to the proximity of lipogenic enzymes harboured in the ER membrane. Furthermore, ACSL3 localization appears to be important for LD formation.

ACSL3 is an important key player involved in lipid metabolism. Future studies of its underlying functional mechanism are promising to advance the understanding of diseases associated with lipid metabolism and to develop new therapeutic strategies.

1. Zusammenfassung

Lipidtröpfchen sind Speicherorganellen, die in fast allen Zelltypen vorkommen, und spielen vermutlich bei der Pathogenese verschiedener Krankheiten eine wichtige Rolle, z.B. Diabetes Typ II, Kardiomyopathie und Atherosklerose. Der Kern von Lipidtröpfchen enthält verschiedene Neutrallipide, hauptsächlich Triglyceride und Cholesterinester. Dieser hydrophobe Kern ist von einer Monomembran aus Phospholipiden umhüllt, in die verschiedene Proteine und Enzyme eingebettet sind. Darunter ist auch die Acyl-CoA-Synthetase 3 (ACSL3), die zur Familie der Acyl-CoA-Synthetasen (ACS) gehört. Proteine aus der ACS-Familie katalysieren die Veresterung von Fettsäuren mit Coenzym A, welche eine wichtige Voraussetzung für die weitere Verstoffwechselung der Fettsäuren darstellt. Von allen Proteinen aus der ACS-Familie ist ACSL3 das einzige Enzym, das konsistent auf Lipidtröpfchen zu finden ist. ACSL3 ist durch eine duale Lokalisation auf den Lipidtröpfchen und dem endoplasmatischen Retikulum (ER) charakterisiert. ACSL3 transloziert nach Supplementierung von Fettsäuren vom ER zu den Lipidtröpfchen und ist bereits auf entstehenden Lipidtröpfchen detektierbar. Basierend auf den vorliegenden Erkenntnissen wird die durch ACSL3-vermittelte ACS-Aktivität und die ACSL3-Lokalisation auf Lipidtröpfchen als biologisch relevant angesehen.

In dieser Arbeit wurde die Relevanz der ACSL3-vermittelten ACS-Aktivität und der ACSL3-Lokalisation im anabolischen und katabolischen Lipidstoffwechsel untersucht. Die wesentliche Herangehensweise basierte auf der Reduktion der ACSL3-Quantität in COS-7 Zellen durch RNA-Interferenz oder einen CRISPR/Cas9-knockout. ACSL3-knockout-Zellen wurden mit modifizierten ACSL3-Varianten transduziert und der Lipidstoffwechsel untersucht. Eine ACSL3-Variante, die durch eine Mutation ihre ACS-Aktivität verloren hat, diente zur Untersuchung von ACSL3-Funtionen, die unabhängig von der ACS-Aktivität sind. Außerdem sollte durch eine andere ACSL3-Variante, die im ER und nicht auf Lipidtröpfchen lokalisiert ist, die Wichtigkeit der ACSL3-Lokalisation auf Lipidtröpfchen erläutert werden. Das experimentelle Vorgehen umfasste dabei die Markierung und Quantifizierung intrazellulärer Lipidspezies mit ^{14}C-Oleat und ^{14}C-Acetat, die Quantifizierung neu synthetisierter Lipidtröpfchen in gehungerten Zellen und die Bestimmung der Triglyceridsynthese während basaler Lipolyse. Die molare Menge von ACSL3 wurde in A431-Zellen quantifiziert, um die metabolische Kapazität von Lipidtröpfchen-assoziiertem ACSL3 für die zelluläre Triglyceridsynthese zu schätzen.

Der ACSL3-knockout führte zu einer Reduktion der ACS-Aktivität um 93 %, wodurch deutlich wird, dass ACSL3 das dominante ACS-Enzym in COS-7 Zellen ist. Die Inkorporation von ^{14}C-Oleat war in den ACSL3-knockout-Zellen im Vergleich zu den wildtyp COS-7-Zellen um 33 % reduziert. Die ACSL3-knockout-Zellen zeigten eine 50 % niedrigere Triglyceridsynthese und eine 65 % geringere Lipidtröpfchenbiogenese als die wildtyp COS-7-Zellen. Die basale Lipolyserate hingegen war in den ACSL3-knockout-Zellen erhöht, wodurch die intrazelluläre Triglyceridmenge nach einer Hungerperiode von 6 h um 46 % nierdriger war als die in den Kontrollzellen gemessene Triglyceridmenge. Die Zellen mit der ACSL3-Variante ohne ACS-Aktivität waren in der basalen Lipolyse leicht herabgesetzt und wiesen nach einer 6-stündigen Hungerperiode 24 % mehr intrazelluläre Triglyceride auf als die ACSL3-knockout-Zellen. Zellen, die nur ER-lokalisiertes ACSL3 exprimierten, waren in ihrer Triglyceridsynthese erhöht, aber synthetisierten nach einer Hungerperiode 54 % weniger Lipidtröpfchen im Vergleich zu den Zellen, die ACSL3 zusätzlich auf den Lipidtröpfchen exprimierten. Anhand von Modellberechnungen in A431 Zellen wurde geschätzt, dass die lokale Triglyceridsynthese auf den Lipidtröpfchen 3.3 % der gesamten zellulären Triglyceridsynthese ausmacht.

Die Ergebnisse zeigen, dass ACSL3 für die Triglyceridsynthese und Lipidtröpfchenbiogenese unverzichtbar ist, indem es effizient Fettsäuren aktiviert und den Enzymen der Lipidsynthese zur Verfügung stellt. Jedoch ist die metabolische Kapazität von Lipidtröpfchen-assoziiertem ACSL3 zu gering um maßgeblilch zum Lipidtröpfchenwachstum beizutragen. Daher ist das Lipidtröpfchenwachstum wahrscheinlich auf den Lipidtransfer vom ER zu den Lipidtröpfchen angewiesen. Desweiteren reduziert ACSL3 die basale Lipolyse vermutlich durch Re-Esterifizierung von freigesetzten Fettsäuren und möglicherweise durch Rekrutierung antilipolytischer Proteine auf die Lipidtröpfchen. ER-lokalisiertes ACSL3 ist in der Triglyceridsynthese vermutlich effizienter durch die Nähe zu den Enzymen, die an der Lipidsynthese beteiligt und in der ER-Membran zu finden sind. Außerdem ist die Lokalisation von ACSL3 wichtig für die Lipidtröpfchenbiogenese.

ACSL3 ist ein bedeutendes Protein des Lipidstoffwechsels. Zukünftige Untersuchungen der durch ACSL3 vermittelten Wirkungsmechanismen sind vielverprechend, um das Verständnis von Lipidstoffwechsel-assoziierten Krankheiten zu vertiefen und neue Therapieansätze zu entwickeln.

2. Fundamental information

2.1 Lipid droplets in lipid metabolism

General features of lipid droplets

Lipid droplets (LD) are intracellular storage organelles that occur in all eukaryotic cell types and also some actinobacteria and cyanobacteria. LD are composed of a neutral lipid core mainly containing triglycerides (TG) and cholesteryl esters, but also retinyl esters, wax esters and ether lipids can be included. The core is surrounded by a phospholipid monolayer which is made up of mostly phosphatidylcholine (PC) and phosphatidylethanolamine (PE). PC acts as a surfactant impeding merging of LDs and keeps them in a size manageable for the cell. The phospholipid membrane harbours various proteins and enzymes that are involved in lipid metabolism (Wilfling et al., 2014a; Zhang and Liu, 2017). The size depends on the nutritional status, maturity and can also vary among different cell types. The diameter varies from 0.1-0.3 µm in nascent LD up to 1 µm in most cell types. LD in adipose tissue are an exception and can achieve diameters in the 100 µm range (Suzuki et al., 2011; Thiam and Beller, 2017).

Lipid droplet life cycle

LD are presumed to originate from the endoplasmic reticulum (ER). The LD life cycle comprises the stages of lense formation, growth, budding and further growth as depicted in *figure 1*. Upon demand of energy, lipids are mobilized from LD and hydrolyzed in lipolysis. Depending on the stage of LD maturity, different kinds of proteins are involved in the dynamic change of the organelle (Thiam and Beller, 2017).

LD biogenesis occurs at nucleation sites in the ER. TG accumulate and form a lense. Nucleation can take place as spontaneous events, when lense formation is facilitated by membrane curvature, e. g. by certain lipid species or curvature-inducing proteins (McMahon and Boucrot, 2015). Nucleation can also be regulated by a high local concentraction of TG due to lipogenic enzymes, like diglyceride acyltransferase family member 1 (DGAT1) and long chain acyl-CoA synthetase family member 3 (ACSL3). Once the lense has grown bigger and reached the solubility threshold, the nascent LD is released into the cytosol, a process called ‘budding’. LD budding is probably dependent on the fat storage-inducing transmembrane (FIT) proteins, since the depletion of FIT proteins caused the LD to remain at the ER (Choudhary et al., 2015).

Being present in the cytosol, the LD continues to grow by local TG synthesis on LD or lipid transfer from the ER to the LD via LD-ER-membrane bridges. These contact sites are formed

by continuities between the outer leaflet of the ER bilayer and the LD monolayer and are regulated by seipin (Prinz, 2013; Salo et al., 2016; Schuldiner and Bohnert, 2017). The Arf1/COPI machinery has been shown to favour the formation of LD-ER-membrane bridges by removal of phospholipids from the LD membrane, which increases the surface tension and promotes fusion of LD and ER membrane (Wilfling et al., 2014b). In principle, LD can also grow by fusion with existing LD, however, this event is rarely observed (Wilfling et al., 2014a).

TG and cholesterol esters are the constituents required for the growth of the neutral lipid core. TG and cholesterol ester synthesis is mainly localized in the ER and depends on activated fatty acids, fatty acyl-CoA molecules, that are generated by acyl-CoA-synthetases through esterification of fatty acids with Coenzyme A (CoA). Members of the diglyceride acyltransferase family, DGAT1 and DGAT2, use fatty acyl-CoA and diacylglycerol (DAG) for the formation of TG. DAG originates from dephosphorylation of phosphatidic acid (PA), a reaction that is catalyzed by the enzyme phosphatidic acid phosphatase (PAP). The synthesis of cholesterol esters is carried out by members of the ER-localized acyl-CoA:cholesterol acyltransferase (ACAT) family, ACAT1 and ACAT2, that catalyze the formation of cholesterol esters using fatty acyl-CoA and cholesterol (Lagace and Ridgway, 2013; Ruggles et al., 2013; Wilfling et al., 2014a).

As the neutral lipid core grows, also phospholipids are needed to maintain the phospholipid monolayer surrounding the expanding neutral lipid core. Like neutral lipid synthesis, phospholipid synthesis occurs in the ER. An important precursor for phospholipid synthesis is PA. PA can be converted into phosphatidylinositol (PI) and PA can be dephosphorylated to DAG, which is used for the synthesis of PC and PE. The most abundant phospholipid is PC. PC can be also synthesized by the Kennedy pathway and the Land's cycle. The Kennedy pathway describes the de novo synthesis of PC and includes three catalytic reactions. First, choline is phosphorylated to phosphocholine by the choline kinase. The CTP:phosphocholine cytidylyltransferase (CCT) transfers cytidine monophosphate (CMP) from cytidine triphosphate (CTP) to phosphocholine resulting in the formation of CDP-choline. Finally the CDP-cholinephosphotransferase transfers phosphocholine from CDP-choline to diacylglycerol resulting in PC. In the Land's cycle fatty acyl-CoA and lysophosphatidylcholine are converted into PC by the lysophosphatidylcholine acyltransferase (LPCAT) (Lagace and Ridgway, 2013; Pol et al., 2014).

In periods of nutrient deprivation or high energy demand, fatty acids are mobilized from the LD by lipolysis and used for ATP production by β-oxidation. Most work studying regulation of lipolysis focused on white adipose tissue. Still there are remaining questions about underlying mechanisms and tissue-specific features. The most important lipases identified are adipose triglyceride lipase (ATGL), hormone-sensitive lipase (HSL) and monoacylglycerol lipase (MGL). ATGL hydrolyses TG into free fatty acids and DAG and has been shown to be activated by comparative gene identification-58 (CGI-58). CGI-58 in turn is activated by long chain fatty acyl-CoAs (Sanders et al., 2015). Inhibition is achieved through G0/G1 switch gene 2 (G0S2). HSL hydrolyzes DAG into a free fatty acid and monoacylglycerol. MGL completes TG hydrolyzation and converts monoacylglycerol into a free fatty acid and glycerol. Lipolysis can be controlled by many mechanisms, e. g. alteration of lipase expression, regulation of access to TG, up- and downregulation of CGI-58 and G0S2 or posttranslational modifications (Schweiger et al., 2014).

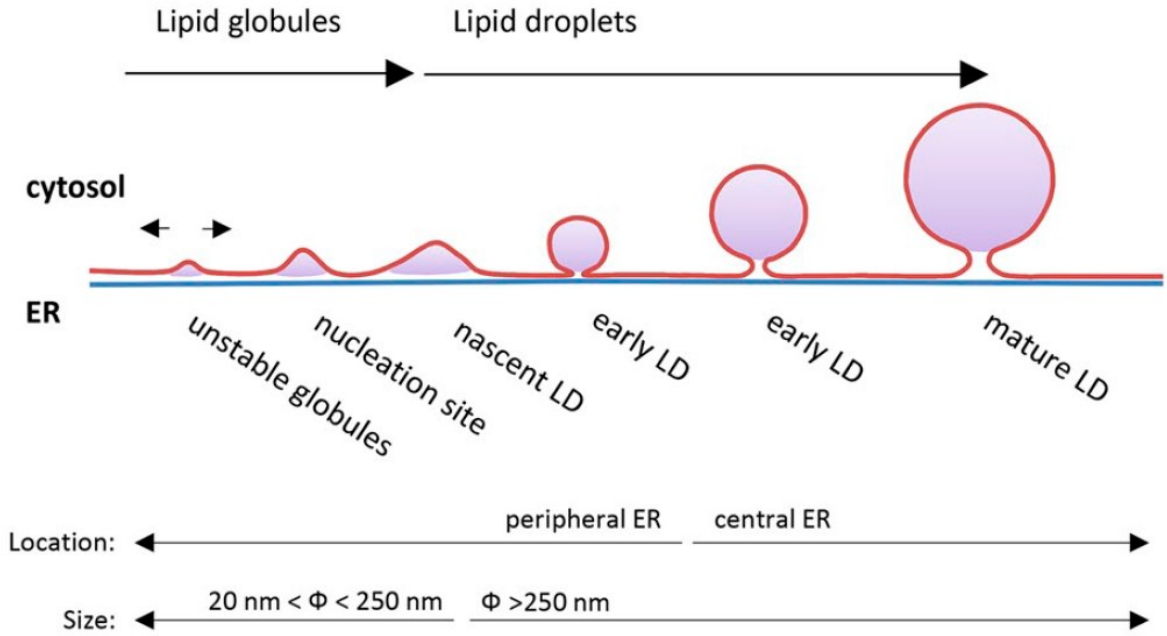

***Fig. 1*: Model of lipid droplet nucleation and growth.** Neutral lipids accumulate between the two ER membrane leaflets at nucleation sites in the ER periphery and form a lense (globule). The lipid globule of 20 nm in diameter expands to a diameter of 250 nm upon lipid synthesis. The growing early lipid droplet migrates to more central regions and eventually buds off as a mature LD (Pol et al., 2014).

Protein targeting to lipid droplets

Many studies investigated the LD proteome in different tissues and cell lines. The general procedure includes the generation of a homogenate, ultracentrifugation and purification of the floating LD followed by identification of the proteins by mass spectrometry. Contaminations

caused by contact sites between LD and other organelles, e. g. mitochondria and ER, can impede the correct assignment of proteins to the LD fraction (Goodman, 2018). Moreover, the unique structure of LD restricts possible protein topologies and makes it difficult to understand backgrounds and explicit mechanisms of protein targeting to LD. Additionally, the phospholipid monolayer has distinct features from lipid bilayers that are more common surroundings of organelles. LD are characterized by a looser packaging of membrane lipids and more packaging defects. Packaging defects are defined regions, where the hydrophobic parts of the phospholipids are not completely shielded from the cytosolic environment. Another challenge for tracking the routes of protein targeting is that LDs are lacking a certain protein import machinery known for other organelles, e. g. the TIM/TOM complex found in the mitochondria (Prevost et al., 2018).

The neutral lipid core is devoid of proteins and membrane proteins are embedded in the phospholipid monolayer by hydrophobic hairpins or amphipathic helices (Bersuker and Olzmann, 2018). The proteins targeting the LD by a hydrophobic hairpin motif are specified as class I proteins and have a dual localization on the ER and the LDs. They approach the LD from the ER via LD-ER-membrane bridges. The hairpin conformation is often due to one or more proline residues in the middle of the hydrophobic sequence leading to a kink of the helical formation and both ends of the protein facing the cytosol. Examples for class I proteins are DGAT2 and GPAT4. Class II proteins access the LD from the cytosol via amphipatic helices. When they are embedded in the LD membrane, their hydrophobic residues are anchored in the acyl-chain of the membrane and the hydrophilic parts are directed to the cytosol or interact with polar headgroups of the phospholipids. An example for a class II protein is CCTα, which is involved in the synthesis of PC. However, there are proteins that can not be assigned to class I or II and might be bound to LDs by interactions with other proteins or by posttranslational modifications, e. g. palmitoylation leading to a formation of a lipid anchor (Bersuker and Olzmann, 2017; Kory et al., 2016; Ohsaki et al., 2014). *Figure 2* illustrates possible targeting mechanisms of proteins on LD. However, the targeting mechanisms of proteins are highly diverse and poorly understood.

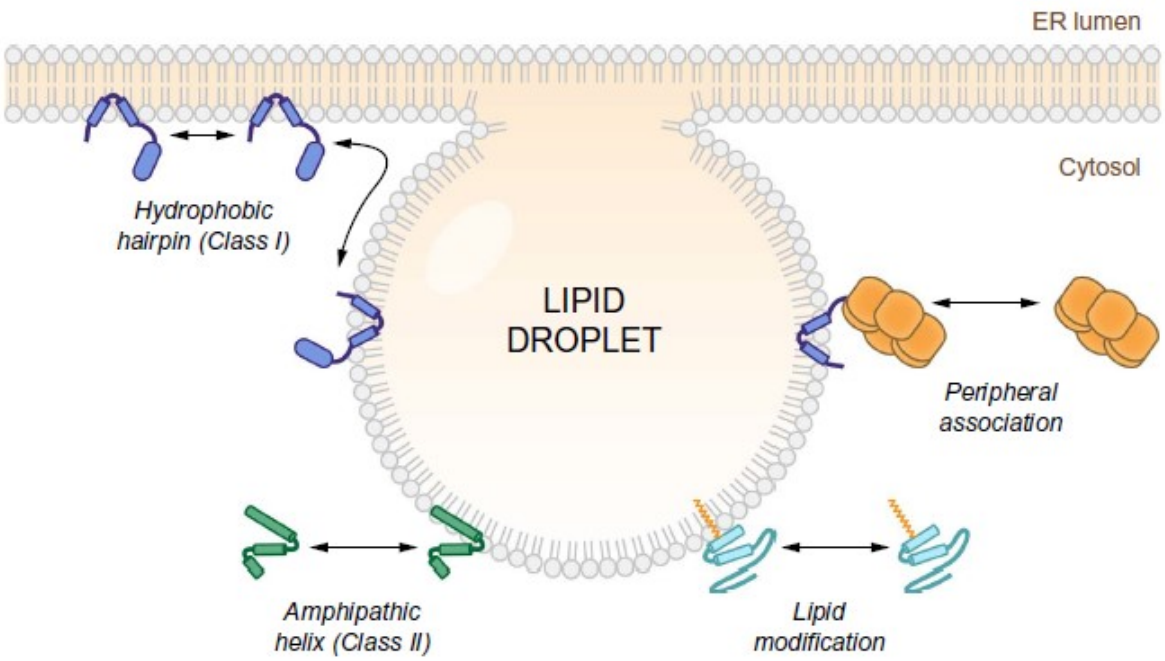

Fig. 2: **Targeting mechanisms of proteins on LD**. Class I proteins are targeted to the LD from the ER by a hydrophobic hairpin. Class II proteins are targeted to the LD from the cytosol by an amphiathic helix. Lipid modification and peripheral association due to protein-protein interaction are also possible targeting mechanisms (Bersuker and Olzmann, 2017).

More than 200 LD-associated proteins have been identified being functional in lipid metabolism and regulation, membrane trafficking, cell signaling or acting as scaffolding proteins (Rosen and Spiegelman, 2014). One important group of LD-associated proteins is the perilipin (PLIN) family which comprises five members, PLIN1-PLIN5. The PLIN proteins are a good example of the dynamic LD proteome that is adjusted to the metabolic situation of the cells. The occurrence of PLIN proteins on LD is linked to a remodeling process during LD maturation. PLIN3 and PLIN4 are predominantly found on small lipid droplets. Upon LD growth these proteins are replaced with PLIN2, which is found on medium-sized lipid droplets, and PLIN1 is the predominant PLIN family member on large LD (Bersuker and Olzmann, 2017; Gemmink et al., 2017; Khor et al., 2013). Other validated proteins are the lipogenic proteins glycerol-3-phosphate acyltransferase 4 (GPAT4), DGAT2 and ACSL3 and the lipolytic proteins ATGL, HSL, G0S2 and CGI-58. Cell death activator A (CIDEA) and cell death activator C (CIDEC), also called fat-specific protein 27 (FSP27), are found on LD and are implicated in LD fusion. Other proteins are involved in protein transport, membrane trafficking or ubiquitination, e. g. caveolins, the Ras-related proteins Rab18 and Rab8a and ancient ubiquitous protein 1 (AUP1) (Bersuker and Olzmann, 2017; Khor et al., 2013; Larsson et al., 2012; Rosen and Spiegelman, 2014).

LD functions and implication in diseases

For decades LD were assumed to be passive organelles serving as energy reservoirs. By now the understanding has changed and it has been shown, that LD play a central role in many fields of cellular biology.

The most obvious function of LD is to store energy and provide substrates for the ATP production during nutrient-deprivation or periods of high energy demand. Excess of non-esterified fatty acids are converted into TG and stored in the form of lipid droplets which protect the cells from lipotoxicity (Barbosa and Siniossoglou, 2017).

As neutral lipid stores, LD provide substrates not only for energy metabolism, but also building blocks for membrane synthesis and they are the source of lipid derived metabolites like bile salts or hormones (Pol et al., 2014). By their chemical properties, LD store lipid-soluble vitamins like vitamin E, vitamin K and vitamin A as well as signaling precursors like eicosanoids and steroids (Bozza et al., 2011; Schreiber et al., 2012; Shen et al., 2016; Spicher and Kessler, 2015). Also a function in chromatin packaging is attributed to embryonic LD, as they are associated to the histone proteins H2A, H2B, H2Av, which are recruited to the LD by the protein Jabba. As embryonic development proceeds, the histones are delivered to the nucleus and used for chromatin assembly (Cermelli et al., 2006; Li et al., 2012).

As LD build contact sites with many organelles, their implication in cellular processes is assumed versatile, although deeper knowledge of detailed mechanisms and the functional relevance of these contact sites for the most part is missing until now.

Membrane bridges between the ER and LD enable the trafficking of proteins and lipids between the two organelles. Moreover, LD act as a temporary intermediate store for misfolded proteins during ER stress until the misfolded proteins are degraded. Proteins involved in ER-assisted degradation (ERAD) are found on LD suggesting a promoting role for LD in protein degradation (Gao and Goodman, 2015; Welte and Gould, 2017). LD are also implicated in viral replication that is elaborately investigated for hepatitis C virus (HCV). After infection, non-structural HCV proteins are transferred from the ER to the LD suggesting a role of LD in virus assembly thus contributing to HCV-induced liver damage (Shyu et al., 2018). Connections between LD and mitochondria are upregulated upon exercise training facilitating rapid oxidation of the substrates mobilized from the LD (Tarnopolsky et al., 2007). In addition, LD connections to lysosomes and peroxisomes have been verified indicating a function of LD in

autophagy and peroxisomal lipid metabolism, but understanding of the exact function is missing (Schrader, 2001; Schuldiner and Bohnert, 2017).

Since LD are the cellular lipid storage sites, they are the hub of diseases related to lipid metabolism. Immoderate accumulation of lipid droplets causes the metabolic syndrome, an umbrella term including obesity, inflammation and insulin resistance leading to the development of diabetes. Excess lipids in hepatocytes damages the liver and can cause fibrosis or hepatocellular cancer. When the arterial walls are effected from augmented cholesterol accumulation, artherosclerosis is the consequence which increases the chance for strokes and heart failure (Gemmink et al., 2017; Mashek et al., 2015; Onal et al., 2017; Shi and Burn, 2004). Not only excess occurrence of LD is problematic, but also the severe diminishment of adipose tissue, called 'lipodystrophy', that is caused by impairment of LD synthesis and regulation (Walther and Farese Jr, 2012). Lipodystrophy leads to metabolic complications as it results in ectopic lipid storage in organs like liver and muscle compromising optimal organ function and leading to insulin resistance and diabetes (Brown et al., 2016). Therapeutic approaches against cancer increasingly focus on LD, because LD number as well as lipogenic enzymes like acetyl-CoA-carboxylase, the fatty acid synthase and acyl-CoA synthetases are upregulated. The increased lipid turnover is assumed to fuel the increased proliferation of cancer cells (Shyu et al., 2018; Tang et al., 2018).

2.2 Acyl-CoA synthetase family

Fatty acids are of great importance for the production of ATP and for the biosynthesis of membrane lipids and lipid-derived signaling molecules. Fatty acids can orginate from de novo synthesis by the fatty acid synthase complex (Chakravarty et al., 2004) or enter the cell from extracellular environment. There are three models about how fatty acids can enter the cell from the outside: 1) diffusion across the lipid bilayer by flip-flop mechanism (Hamilton et al., 2002), 2) facilitated transport by proteins, e. g. CD36 (Su and Abumrad, 2009) and 3) metabolic trapping (Füllekrug et al., 2012). Independent of the origin, all fatty acids have to be activated before they can enter the different pathways of lipid metabolism, because by their biochemical properties as aliphatic hydrocarbon chains they are inert molecules. Activation means esterification with the polar molecule CoA whereby the unpolar fatty acids become amphipathic.

The activation of fatty acids is carried out as an adenosine triphosphate (ATP)-dependent two-step reaction and requires the presence of Mg^{2+}. ATP is converted into pyrophosphate (PPi) and

adenosine monophosphate (AMP), which is used for the formation of acyl adenylate in the first reaction. Then AMP is removed and the fatty acid is bound to CoA by a thioester bond, forming acyl-CoA. (Watkins, 2008; Yan et al., 2015). The reaction is shown below:

Fatty acid + ATP → acyl-AMP + PPi
Acyl-AMP + CoA → acyl-CoA + AMP

Activation of fatty acids in mammalian cells is catalyzed by 26 acyl-CoA synthetases (ACS). Thirteen members of the ACS family activate fatty acids with a chain length of 16-22 carbon atoms and are divided into three subfamilies according to their substrate specificity. The five long chain acyl-CoA synthetases (ACSL) numbered as ACSL1, ACSL3, ACSL4, ACSL5 and ACSL6, activate fatty acids containing 12-20 carbon atoms. The six very long chain acyl-CoA synthetases (ACSVL), also called fatty acid transport proteins (FATP), numbered FATP1-FATP6, esterify long chain fatty acids like the ACSL enzymes but also very long chain fatty acids with more than 22 and more carbon atoms (Ellis et al., 2010; Mashek et al., 2007; Watkins, 2008). The two bubblegum proteins are not investigated in detail (Fraisl et al., 2006; Steinberg et al., 2000).

All ACS enzymes contain two conserved protein domains, the AMP-binding domain (Motif I) and a fatty acid-binding signature (FACS) motif (Motif II), which is involved in fatty acid binding (Black and DiRusso, 2003; Watkins, 2008). ACSL1, ACSL3 and ACSL4 can be inhibited by Triacsin C, which competes for binding with long chain fatty acids (Mashek et al., 2007; Tomoda et al., 1987).

Hypothesis of metabolic channeling

The ACS enzymes are characterized by a tissue-specific expression, but can also be co-expressed in the same cell type. For instance, ACSL1, ACSL4, ACSL5, FATP2, FATP4 and FATP5 are expressed in the liver. ACSL3 and ACSL6 are found in the brain and the gonads (Mashek et al., 2007). ACS enzymes not only vary in tissue distribution, but also subcellular localization, e. g. ACSL1 has been reported to be localized on mitochondria, ACSL4 on peroxisomes, microsomes, plasma membrane and the cytosol, FATP4 in the ER and ACSL3 in the ER and on LD (Küch et al., 2014; Milger et al., 2006; Poppelreuther et al., 2012; Poppelreuther et al., 2018; Smith et al., 2013). The concept of metabolic channeling addresses the high number of ACS enzymes that are co-expressed in the same tissue though they are functionally redundant. The channeling hypothesis is based on the assumption, that the different subcellular localization of ACS enzymes is important to deliver fatty acyl-CoA for specific

pathways. ACS enzymes found in the ER membrane might channel fatty acids into lipid synthesis, whereas mitochondria-associated ACS enzymes could fuel beta-oxidation for ATP production (Digel et al., 2009).

Model of metabolic trapping

ACS enzymes are hypothesized to mediate fatty acid uptake by metabolic trapping. This model suggests, that the fatty acid uptake is dependent on the cellular ACS activity. Fatty acids from the extracellular environment enter the cell, equilibrate in the ER membrane and become activated by esterification with CoA by ACS enzymes in the ER. The fatty acyl-CoA molecules can enter downstream pathways of lipid metabolism. An increase in ACS activity is assumed to deplete fatty acids from the ER membrane. The temporary deficit in fatty acids is replenished from the plasma membrane which in turn drives fatty acid uptake from the extracellular space due to a change in concentration gradient (Füllekrug et al., 2012).

2.3 ACSL3

ACSL family member 3 (ACSL3) activates long chain fatty acids with a preference for unsaturated fatty acids with a chain length of 16-20 carbon atoms (Fujino et al., 1996). Human ACSL3 comprises 720 amino acids, has a molecular weight of 80.3 kDa and is encoded on chromosome 2 (Minekura et al., 1997). There is evidence for ubiquitous ACSL3 expression, but it is predominantly found in the brain and the gonads (Fujino et al., 1996; Mashek et al., 2006). Regulation of ACSL3 expression varies in the tissues and is dependent on the diet. High-fructose diet downregulated hepatic ACSL3 expression probably due to modulating liver X receptor/retinoid X receptor signaling (Dong et al., 2013). High-fat palm oil diet reduced the ACSL3 expression in the small intestine (Beilstein et al., 2016).

ACSL3 is a bona fide LD protein as it is found abundantly on LD and is recruited to LD already in early stages of formation (Fujimoto et al., 2004; Kassan et al., 2013). ACSL3 is the only ACS family member certainly localized to LD. ACSL1 and ACSL4 were also reported as LD-associated proteins (Brasaemle et al., 2004; Hodges and Wu, 2010), however this could not be shown consistently indicating an outstanding role of ACSL3 in lipid metabolism. Only the long isoform of ACSL4 has been shown to be localized on LD, but its expression is restricted to neurons (Küch et al., 2014).

ACSL3 is characterized by a dual localization on the ER and LD, which is dependent on the nutrient supply. Translocation from the ER to the LD takes place upon fatty acid

supplementation, which increases neutral lipid synthesis and LD growth. It has been shown, that the N-terminus of the ACSL3 protein is crucial for LD targeting and for the function as an ACS enzyme (Poppelreuther et al., 2012). Recent studies revealed that ACSL3 translocation from the ER to the LD is facilitated by syntaxin 17, because cells depleted from syntaxin 17 showed a remarkable reduction of ACSL3 recruitment to LD. Redistribution of ACSL3 from the ER to the LD is probably mediated by interaction of ACSL3 with the SNARE domain of syntaxin 17 (Kimura et al., 2018).

ACSL3 was previously assumed to target LD by a hydrophobic hairpin motif as N- and C-terminus have been shown to be oriented towards the cytosol (Poppelreuther et al., 2012). However, recent proteomic analysis suggest targeting via an interfacial amphipathic helix (Pataki et al., 2018).

ACSL3 is a lipogenic enzyme that is involved in LD formation and growth by TG synthesis (Kassan et al., 2013). Moreover, ACSL3 has been reported to play a role in the fatty acid incorporation into PC and the secretion of very low density proteins from hepatocytes (Yao and Ye, 2008). Bu et al. (2009) carried out further investigations about the transcriptional control of hepatic lipogenesis and found out, that ACSL3 acts as a regulator of transcriptional activity for peroxisome proliferator-activated receptor-γ, carbohydrate-responsive element-binding protein, sterol-regulatory element- binding protein and liver X receptor-α. This broadens the presumed scope of action mediated through ACSL3 and emphasizes the great significance of ACSL3 for lipid metabolism.

Hypothesis of local triglyceride synthesis on LD

Based on the experiments implicating an important role of ACSL3 in LD metabolism and the unique localization of ACSL3 on LD, ACSL3 has been hypothesized to drive LD growth by local triglyceride synthesis on LD (Fujimoto et al., 2007; Poppelreuther et al., 2018). The hypothesis is supported by the finding, that at least one member of each protein family involved in TG synthesis is also present on LDs: DGAT2, acylglycerolphosphate acyltransferase family member 3 (AGPAT3), GPAT4 and PAP (Pol et al., 2014). LD-associated ACSL3 activates fatty acids to fatty acyl-CoA. AGPAT3 and GPAT4 are involved in the synthesis of phosphtidic acid (PA), which is utilized by PAP to generate DAG. DGAT2 in turn catalyzes TG synthesis from fatty-acyl CoA and DAG. Thus, by creating a high local concentration of fatty acyl-CoA, LD-associated ACSL3 might be an important driver of TG syntesis on LD. An alternative way for LD growth is the synthesis of TG in the ER involving ER-localized ACS enzymes like ACSL3,

DGAT1, DGAT2, members of the GPAT and AGPAT family and PAP (Lagace and Ridgway, 2013; Ruggles et al., 2013). The TG generated in the ER are transferred to the LD via membrane bridges (Prinz, 2013). A schema summarizing the main aspects of the model are shown in *figure 3*.

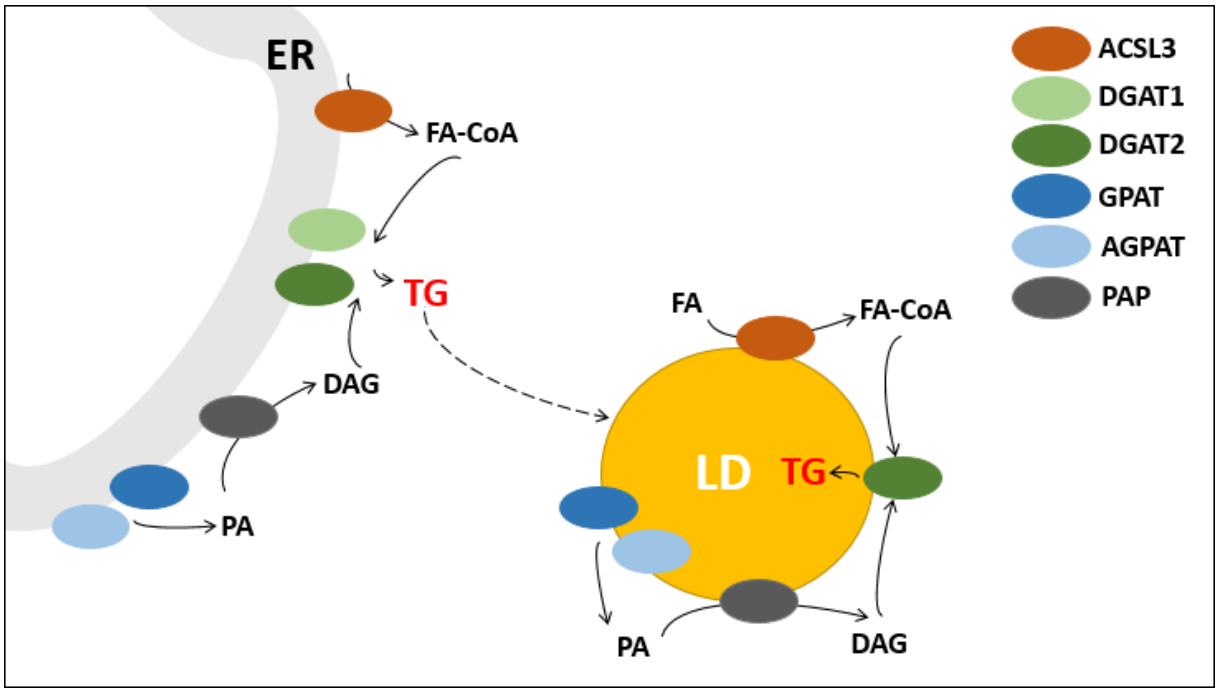

***Fig. 3*: Hypothesis of local of triglyceride synthesis on LD.** LD and ER membrane-associated proteins are shown as coloured oval structures. ACSL3 activates fatty acids to fatty acyl-CoA. LD-associated members of the GPAT and AGPAT family, GPAT4 and AGPAT3, deliver PA which is used for DAG synthesis by PAP. DGAT2 on LD catalyzes the final step of TG synthesis using fatty acyl-CoA and DAG. By creating a high local concentration of fatty acyl-CoA, LD-associated ACSL3 might be an important driver of TG syntesis on LD. Alternatively, TG can also be synthesized at the ER, where the main lipogenic enzyme machinery is harboured, and transferred to the LD, where they are incorporated into the growing neutral lipid core. ACSL3, acyl-CoA synthetase 3; DGAT1, diglyceride acyltransferase 1; DGAT2, diglyceride acyltransferase 2, GPAT, glycerol 3-phosphate acyltransferase; AGPAT, acylglycerolphosphate acyltransferase, PAP, phosphatidic acid phosphatase; FA, fatty acid; FA-CoA, fatty acyl-CoA, DAG, diacylglycerol, PA, phosphatidic acid, TG, triglycerides.

3. Aim of this work

Previous studies showed a key role of ACSL3 in fatty acid activation and lipid droplet biogenesis. ACSL3 is characterized by a dual localization on LD and the ER, which is unique among the ACS protein family and therefore is presumed to be biologically relevant. LD-associated ACSL3 is hypothesized to be crucial for LD growth by local triglyceride synthesis. Moreover, it has been hypothesized, that ACSL3 counteracts lipolysis by re-esterification of liberated fatty acids thus not only modulating anabolic but also catabolic pathways in lipid metabolism.

The aim of this work was to investigate the relevance of ACSL3-mediated ACS activity and ACSL3 localization on lipid species synthesis, LD biogenesis and basal lipolysis. The main approach was the generation of an ACSL3-knockout in COS-7 cells and the complementation of these knockout cells with different modified enzyme variants fused to green fluorescent protein (GFP) to gain deeper insight into ACSL3 function: GFP-ACSL3, GFP-AA-ACSL3 and GFP-ER-ACSL3. Cytosolic GFP only was transduced into the knockout cells as a negative control (GFP_A3ko cells). GFP-ACSL3 was wildtype ACSL3 fused to GFP and transduced as a positive control. The GFP_A3ko cells were studied to assess the general impact of ACSL3-mediated ACS activity on lipid metabolism. GFP-AA-ACSL3 was a mutant variant, where serine at the positions 288 and 290 was replaced with alanine. This functional mutation in the AMP-binding site of the protein diminished ACS activity and allowed to investigate functions of ACSL3 independent of its ACS activity, e. g. function as scaffolding protein. The GFP-ER-ACSL3 variant was excluded from LD by replacement of the N-terminal LD targeting sequence with the transmembrane domain of FATP4, an integral ER membrane protein. In contrast to GFP-ACSL3, GFP-ER-ACSL3 could not translocate to the LD upon fatty acid supplementation and was restricted to the ER. Therefore, comparison of GFP-ER-ACSL3 with GFP-ACSL3 expressing cells revealed the impact of ACSL3 localization on protein function.

Experimental approaches included radiolabelling with acetate and oleic acid (OA) to investigate lipid synthesis from endogenously synthesized and exogenously supplied fatty acids and to assess the hydrolysis of intracellular TG during basal lipolysis. The capacity for LD biogenesis in the cells was examined by determining the number of generated LD after starvation. Moreover, A431 cells were applied for subcellular fractionation, molar quantification of ACSL3 and model calculations to estimate the metabolic capacity of LD-associated ACSL3 in LD growth as assumed by the hypothesis of local triglyceride synthesis.

4. Materials and Methods

4.1 Materials

4.1.1 General equipment, materials and kits

Material	Supplier
Biological safety cabinet ‚Herasafe™‘	Thermofisher Scientific, Waltham (USA)
Centrifuge ‚5415R‘	Eppendorf AG, Hamburg (Germany)
Centrifuge ‚5804R‘	Eppendorf AG, Hamburg (Germany)
Centrifuge ‚C-1200‘	National Labent Co., Edison (USA)
Cryovials ‚Cryo.s™‘	Greiner Bio-One GmbH Kremsmünster (Austria)
Falcon tube 15 mL, 50 mL	Greiner Bio-One GmbH Kremsmünster (Austria)
Filter paper	Ahlstrom Corporation, Helsinki (Finland)
Gel clean up kit ‘Nucleospin® Gel and PCR clean up’	Macherey-Nagel GmbH & Co. KG, Düren (Germany)
Heating block ‚Thermomixer compact‘	Eppendorf AG, Hamburg (Germany)
Inoculation tubes 14 mL	Greiner Bio-One GmbH, Kremsmünster (Austria)
LSC cocktail ‚Ultima Gold‘	Perkin Elmer, Waltham (USA)
Microscope ‘Leica DMIL’	Leica Microsystems GmbH, Wetzlar (Germany)
Miniprep kit ‘Nucleospin® Plasmid’	Macherey-Nagel GmbH & Co. KG, Düren (Germany)
Multichannel pipette	Eppendorf AG, Hamburg (Germany)
Odyssey Classic 900 infrared scanner	LI-COR Inc., Lincoln (USA)
Oven ‘Heraeus function line’	Thermofisher Scientific, Waltham (USA)
Petri dish	Sarstedt AG & Co., Nümbrecht (Germany)
Phosphorimaging reader ‘BAS-1500’	Fujifilm Holdings K.K., Minato (Japan)
Phosphorimaging cassette ‘BAS cassette 2040’	Fujifilm Holdings K.K., Minato (Japan)
Photometer ‘PHOmo’	Anthos Mikrosysteme GmbH, Krefeld (Germany)
Pipettes (P2, P10, P20, P200, P1000)	Gilson Incorporation, Middleton (USA)
Pipette tips 10µL	Kisker Biotech GmbH & Co. KG, Steinfurt (Germany)
Pipette tips 200 µL, 1000 µL	Greiner Bio-One GmbH, Kremsmünster (Austria)
Pipetus ‚Integra Pipetboy 2‘	Integra Biosciences Corporation, Hudson (USA)
Reaction tubes 1.5 mL, 2 mL (safe-seal)	Sarstedt AG & Co., Nümbrecht (Germany)
Reaction tubes 2 mL (chloroform-resistant)	Eppendorf AG, Hamburg
Scintillation vials	Zinsser Analytic GmbH, Frankfurt am Main (USA)
Scintillation counter ‘Wallac 1414’	Perkin Elmer, Waltham (USA)

Serological pipettes (5 mL, 10 mL, 25 mL)	Corning Incorporation, Corning (USA)
Shaker ‘SM-30 control/TH30’	Edmund Bühler GmbH, Tübingen (Germany)
Thin layer chromatography chamber	Desaga GmbH, Wiesloch (Germany)
Thin layer chromatograpy plates ,TLC silica gel 60 with concentrating zone 20x2.5 cm	Merck KgaA, Darmstadt
Ultracentrifuge (SW41 Ti rotor)	Beckman Coulter Inc., Indianapolis (USA)
Vortexer ‚Reax top‘	Heidolph Instruments GmbH & Co KG, Schwabach (Germany)

4.1.2 Cell biological methods

Material	Supplier
Oleic acid, #O1383	Sigma-Aldrich Chemie GmbH, Steinheim (Germany)
1-^{14}C-oleic acid (51.3 mCi/mmol; 0.1 mCi/mL; 1.96 mM in ethanol), #MC-406	Moravek Inc., Brea (USA)
1-^{14}C-sodium acetate (50.5 mCi/mmol, 1.0 mCi/mL, 20 mM in ethanol), #NEC084HSB	Perkin Elmer, Waltham (USA)
Cell culture dishes (100 mm, 145 mm)	neoLab Migge GmbH, Heidelberg (Germany)
Cell culture plates (6-well, 12-wel, 24-well, 48-well, 96-well)	Thermofisher Scientific, Waltham (USA)
Cerulenin, #C2389	Sigma-Aldrich Chemie GmbH, Steinheim (Germany)
Coenzyme A sodium salt hydrate, #C4780	Sigma-Aldrich Chemie GmbH, Steinheim (Germany)
Dimethyl sulfoxide Hybri Max®	Sigma-Aldrich Chemie GmbH, Steinheim (Germany)
Dulbecco’s modified Eagle medium 1x (+GlutaMAX™, 4.5 g/L glucose, without pyruvate), #61965026	Thermofisher Scientific, Waltham (USA)
Dulbecco’s modified Eagle medium 1x (+GlutaMAX™, 1 g/L glucose, with pyruvate #21885025	Thermofisher Scientific, Waltham (USA)
Fetal calf serum, #10270106	Thermofisher Scientific, Waltham (USA)
Fugene HD transfection reagent, #E2311	Promega Corporation, Madison (USA)
Gelatine (from teleostan)	Sigma-Aldrich Chemie GmbH, Steinheim (Germany)
Glass plates (Ø 10 mm)	Paul Marienfeld GmbH & Co. KG, Lauda-Königshofen (Germany)
Hoechst 33342	Invitrogen, Carlsbad (USA)
Monodansylpentane (MDH) (named AUTOdot autophagy visualization dye)	Abgent, San Diego (USA)
MTT	Sigma-Aldrich Chemie GmbH, Steinheim (Germany)
mowiol	Merck KGaA, Darmstadt (Germany)

Opti-MEM	Thermofisher Scientific, Waltham (USA)
Non-essential amino acid solution (100x)	Sigma-Aldrich Chemie GmbH, Steinheim (Germany)
Orange G	Sigma-Aldrich Chemie GmbH, Steinheim (Germany)
Paraformaldehyde	Riedel-de Haen, Seelze (Germany)
Penicillin (10,000 U/mL)/streptomycin (10,000 µg/mL)	Thermofisher Scientific, Waltham (USA)
Polybrene (Hexadimethrin bromide)	Sigma-Aldrich Chemie GmbH, Steinheim (Germany)
Puromycin	Thermofisher Scientific, Waltham (USA)
Saponin, #S7900	Sigma-Aldrich Chemie GmbH, Steinheim (Germany)
Sodium azide	Sigma-Aldrich Chemie GmbH, Steinheim (Germany)
Sodium pyruvate 100 mM	Sigma-Aldrich Chemie GmbH, Steinheim (Germany)
Trypsin/EDTA solution 1x (0.05%)	Thermofisher Scientific, Waltham (USA)

4.1.3 Biomolecular and biochemical methods

Material	**Supplier**
Acetic acid	Carl Roth GmbH & Co. KG, Karlsruhe (Germany)
30 % acrylamide/bis solution 29:1	Bio-Rad Laboratories Inc., Hercules (USA)
Agarose ultrapure, #15510-027	Invitrogen, Carlsbad (USA)
Ammonium persulfate	Sigma-Aldrich Chemie GmbH, Steinheim (Germany)
Bacto tryptone	Becton Dickinson, Erembodegem (Belgium)
Bacto yeast extract	Becton Dickinson, Erembodegem (Belgium)
Bicinchoninic acid, #B9643	Sigma-Aldrich Chemie GmbH, Steinheim (Germany)
Bio-Rad protein assay dye reagent concentrate	Bio-Rad Laboratories Inc., Hercules (USA)
Bovine serum albumine, fatty-acid free, #P06-139450	Pan-Biotech GmbH, Aidenbach (Germany)
Bromophenol blue	Sigma-Aldrich Chemie GmbH, Steinheim (Germany)
Calcium chloride (dihydrate)	Merck KGaA, Darmstadt (Germany)
Chloroform Rotipuran ≥99% p.a., #3313.2	Carl Roth GmbH & Co. KG, Karlsruhe (Germany)
Disodium phosphate	Applichem GmbH, Darmstadt (Germany)
DNA ladder Gene Ruler™ 1 kb	Thermofisher Scientific, Waltham (USA)
E. coli DH5α	Invitrogen AG, Frankfurt am Main (Germany)

Ethanol Rotipuran® >99.8 % p.a.	Carl Roth GmbH & Co. KG, Karlsruhe (Germany)
Glycerol	Invitrogen, Carlsbad (USA)
Glycine	Thermofisher Scientific, Waltham (USA)
Glucose	Merck KGaA, Darmstadt (Germany)
Glutathione sepharose 4B beads	Sigma-Aldrich Chemie GmbH, Steinheim (Germany)
N-heptane	Merck KGaA, Darmstadt (Germany)
4-(2-hydroxyethyl)-1-piperazineethanesulfonic acid	Carl Roth GmbH & Co. KG, Karlsruhe (Germany)
Hydrochloric acid	Carl Roth GmbH & Co. KG, Karlsruhe (Germany)
Isopropanol	Sigma-Aldrich Chemie GmbH, Steinheim (Germany)
Methanol	Honeywell Specialty Chemicals Seelze GmbH, Seelze (Germany)
Milk protein	Carl Roth GmbH & Co. KG, Karlsruhe (Germany)
Nitrocellulose membrane 0.45 µm, #88018	Thermofisher Scientific, Waltham (USA)
Page Ruler prestained protein ladder	Sigma-Aldrich Chemie GmbH, Steinheim (Germany)
Peqgreen DNA staining reagent, #37-5000	Peqlab Biotechnologie GmbH, Erlangen (Germany)
Ponceau S solution	Sigma-Aldrich Chemie GmbH, Steinheim (Germany)
Potassium dihydrogenphosphate	Gerbu Biotechnik GmbH, Gaiberg (Germany)
Potassium chloride	Thermofisher Scientific, Waltham (USA)
Select agar	Invitrogen, Carlsbad (USA)
Sodium dodecyl sulfate	Merck KGaA, Darmstadt (Germany)
Sodium hydroxide 1M	Honeywell Specialty Chemicals Seelze GmbH, Seelze (Germany)
Sodium chloride	Sigma-Aldrich Chemie GmbH, Steinheim (Germany)
Sucrose	Riedel-de Haen, Seelze (Germany)
Sulphuric acid	Merck KGaA, Darmstadt (Germany)
T4 DNA ligase	Promega Corporation, Madison (USA)
T4 DNA ligase buffer 10x	Promega Corporation, Madison (USA)
Taq DNA polymerase	Qiagen N.V., Venlo (Netherlands)
Tetramethylethylendiamin	Sigma-Aldrich Chemie GmbH, Steinheim (Germany)
Triethylamine <99.5 %	Carl Roth GmbH & Co. KG, Karlsruhe (Germany)
Tris base	Carl Roth GmbH & Co. KG, Karlsruhe (Germany)
Tris HCl	Applichem GmbH, Darmstadt (Germany)

Triton X-100	Sigma-Aldrich Chemie GmbH, Steinheim (Germany)
Tween®-20	Carl Roth GmbH & Co. KG, Karlsruhe (Germany)
Water (aqua ad iniectibilia)	B. Braun Melsungen AG, Melsungen (Germany)
Xylene cyanol	Sigma-Aldrich Chemie GmbH, Steinheim (Germany)

4.1.4 Self-manufactured buffers and solutions

Experiment	Buffer	Composition
Agarose gel electrophoresis	6x DNA loading dye	38 % (w/v) glycerol, 0.08 % w/v bromophenol blue, 0.08 % w/v xylene cyanol
	TAE buffer	40 mM Tris/Acetat pH 8.0, 10 mM EDTA/NaOH pH 8.0
ACS assay	KTx-lysis buffer	130 mM KCl, 25 mM Tris-HCl, pH 7.4, 1 % (w/v) Triton X-100
	Dole's solution	Isopropanol:Heptane:H_2SO_4(conc.) 40:10:1
	TBS	20 mM Tris/HCl pH 7.4, 130 mM NaCl
Cell culture	PBS	0.2 g/L KCl, 0.2 g/L KH_2PO_4, 8 g/L NaCl, 1.15 g/L Na_2HPO_4
Cloning	LB medium pH 7.0	10 g/L bacto tryptone, 5 g/L bacto yeast extract, 1 g/L NaCl
	LB agar	10 g/L bacto tryptone, 5 g/L bacto yeast extract, 1 g/L NaCl, 15 g/L select agar
Immunofluorescence/ dSTORM microscopy	SG buffer	0.01 % w/v saponin, 0.2 % w/v gelatine, 0.02 % v/v azide, in PBS
	SGB buffer	0.1 % w/v saponin, 0.5 % (w/v) gelatine, 5mg/mL BSA, 0.02 % v/v azide, filter sterilized (0.45 µm), in PBS
	4% PFA	4 % PFA in PBS, pH 7.4
	Mowiol	10 g mowiol dissolved in 40 mL PBS, stirred for 24 h, 20 mL glycerol added, stirred for 24 h, centrifuged at 4,000 rpm for 15 min, use supernatant
	Triton X-100 permeabilization buffer	0.5 % v/v Triton X-100 in PBS
	Washing buffer	0.05 % v/v Triton X-100, 1 % BSA in PBS
	Imaging buffer	100 mM β-mercaptoethylamine, 10 % w/v glucose, 50 U/mL glucose oxidase, 5000 U/mL catalase, 2.5 mM KCl, 1.1 mM Tris-HCl pH 7.5, 2.5 % glycerol, 0.2 mM Tris(2-carboxylethyl)phosphine hydrochloride; in PBS; pH adjusted to 8 with 1 M NaOH
Molar quantification of ACSL3	TNEX buffer	150 mM NaCl, 20 mM Tris/HCl pH 7.4, 1 mM EDTA, 0.2% w/v Triton X-100, 1 mM DTT
	TNE buffer	150 mM NaCl, 20 mM Tris/HCl pH 7.4, 1 mM EDTA, 1 mM DTT

	Coomassie brilliant blue R250 staining solution	0.1 % w/v Coomassie brilliant blue R250 mixed in 300 mL methanol, 100 mL acetic acid and 600 mL water
	Destaining solution	30 % v/v methanol, 10 % v/v acetic acid in water
Subcellular fractionation	Non reducing lysis buffer	62 mM Tris-HCl pH 6.8, 2 % SDS, 10 % w/v glycerol
	Sucrose buffer B	50mM Tris/HCl pH 7.4, 2 M sucrose
Western Blot	4x-O buffer	8 % w/v SDS, 250 mM Tris/HCl pH 6.8, 40 % v/v glycerol, 400 mM β-mercaptoethanol, 0.2 % w/v Orange G
	Running buffer	25 mM Tris, 190 mM glycine, 0.1% w/v SDS
	Transfer buffer	25 mM Tris, 190 mM glycine, 20 % v/v methanol
	TBS-T	10 mM Tris/HCl pH 7.4, 150 mM NaCl, 0.1 % Tween
	Blocking solution	2 % w/v milk protein in TBS-T
	4x separating buffer	1.5 M Tris/HCl pH 8.8, 0.4 % w/v SDS
	Stacking gel buffer	150 mM Tris/HCl (pH 6.8); 0.12% (w/v) SDS
Virus production	2x HBS	280 mM NaCl, 50 mM HEPES, 12 mM glucose, 10 mM KCl, 1.5 mM Na_2HPO_4; pH 6.95

4.1.5 Cell lines

Internal number	Description	Short name
	COS-7 cells	
C001a	Wildtype COS-7 (DSMZ, #ACC 60)	wtCOS-7
C208	Wildtype COS-7 transduced with pRVH1 plasmid lacking sequence for RNA interference	control cells
C211a	COS-7 cells with ACSL3-knockdown by RNA interference	A3-RNAi
C232	Pool of six ACSL3-knockout clones	A3ko-pool
C233	GFP-expressing A3ko-pool	GFP_A3ko
C234d	GFP-ACSL3 expressing A3ko-pool	GFP-ACSL3
C235	GFP-ER-ACSL3 expressing A3ko-pool (low expressing variant)	GFP-ER-ACSL3(L)
C235d	GFP-ER-ACSL3 expressing A3ko-pool (high expressing variant)	GFP-ER-ACSL3(H)
C236	GFP-AA-ACSL3 expressing A3ko-pool	GFP-AA-ACSL3
C239	A3Nt-mcherry expressing wildtype COS-7	-
C240	A3Nt-mcherry expressing C233	-
C241	A3Nt-mcherry expressing C234d	-

C243	A3Nt-mcherry expressing C235	-
C244	A3Nt-mcherry expressing C235d	-
C245	A3Nt-mcherry expressing C236	-
A431 cells		
C320b	Wt A431 (ATCC, #CRL-1555™) transduced with pRVH1 plasmid	A431 pRVH1
C341	A431 ACSL3-knockout cell line	A431 A3KO
Other cell lines		
C010	Phoenix gp (ATCC, #SD-3514)	Phx-gp

4.1.6 Growth media

Name	Composition	Application
Standard growth medium	DMEM GlutaMAX 4.5 g/L glucose (Thermofisher Scientific #61965026), 10 % FCS, 1 % P/S	Routine cell cultivation of wtCOS-7 cells and Phx-gp cells
Cryomedium	10 % v/v DMSO in standard growth medium	Cryoconservation of cells
Low glucose growth medium	DMEM 1 g/L glucose (Thermofisher Scientific #31885023), 10 % FCS, 1 % P/S	Production of retroviral particles
Starvation medium	DMEM 4.5 g/L glucose (Thermofisher Scientific #61965026), 1 % P/S, 1 mM sodium pyruvate, 1x non-essential amino acids, without FCS	Starving for LD biogenesis assay
LD induction medium	DMEM 4.5 g/L glucose (Thermofosher Scientific #61965026), 1 % P/S, 600 µM OA:BSA 6:1, without FCS	LD induction for LD biogenesis assay
Lipolysis medium	4.5 g/L glucose (Thermofisher Scientific #61965026), 1 % P/S, without FCS, 100 µM fatty acid free BSA, 1 mM sodium pyruvate, 1x non-essential amino acids, 4.5 g/L glucose	Induce lipolysis in lipolysis assay

4.1.7 Plasmids

Internal number	Name	Application
JF007	pBS SK(-)	Evaluation of competence of *E. coli*
JF067	pEGFP-N1	Transfection control

JF380	pVSV-G	Production of retroviral particles
JF424	pRVH1-hygro	Competitive retroviral plasmid to generate cell lines with different expression levels of GFP-ACSL3 and GFP-ER-ACSL3
JF623	GFP.pRJ	Generation of cell line C233
JF825	GFP-ACSL3.pRIJ	Generation of cell line C234d
JF827	GFP-ER-ACSL3.pRIJ	Generation of cell lines C235 and C235d
JF844	GFP-ACSL3_AA.pRIJ	Generation of cell line C236
JF1045	eCas9-puro	Basal CRISPR plasmid encoding enhanced Cas9 machinery and puromycin resistance
JF1052	gRNA(1)-ACSL3-Chl.eCas9	CRISPR plasmid containing guide RNA 1 for ACSL3-knockout
JF1053	gRNA(2)-ACSL3-Chl.eCas9	CRISPR plasmid containing guide RNA 2 for ACSL3-knockout
JF1262	A3Nt-mCherry.pRHYGRO	Generation of A3Nt-mcherry expressing cell lines C239-C245

4.1.8 Oligonucleotides

Internal primer number and name	Sequence (5'→3')	application
#592 seq_hU6fwd	GAGGGCCTATTTCCCATGATTCC	Sequencing of JF1052 and JF1053
#675 seq_BGHrev	TAGAAGGCACAGTCGAGG	Sequencing of JF1045
#597 s-gACSL3-E5 (5'→3'; sense)	CACCGCGAGTGGATGATAGCTGCAC	CRISPR/Cas9 guide RNA for JF1052
#598 a-gACSL3-E5 (5'→3'; antisense)	AAACGTGCAGCTATCATCCACTCGC	CRISPR/Cas9 guide RNA for JF1052
#691 s-gACSL3-Chl (5'→3'; sense)	CACCGGGGGTCATCGTGCATACCA	CRISPR/Cas9 guide RNA for JF1053
#692 a-gACSL3-Chl (5'→3'; antisense)	AAACTGGTATGCACGATGACCCCC	CRISPR/Cas9 guide RNA for JF1053

4.1.9 Restriction enzymes and buffers

Enzyme	Buffer	application
BbsI	NEB2.1	Cloning and screening digest of JF 1052 and JF1053
FseI	CutSmart buffer	Cloning of JF1045
NotI-HF	CutSmart buffer	Cloning of JF1045; screening digest of JF1052 and JF1053

All enzymes and buffers were purchased from New England Biolabs GmbH (Frankfurt am Main, Germany).

4.1.10 Antibodies

Antibody (internal number)	Description	Manufacturer	Applied dilution
αms 680RD (J092)	Fluorescing secondary antibody, raised in goat	LI-COR Inc., Lincoln (USA); #926-68070	1:5,000-1:10,000
αms 800CW (J093)	Fluorescing secondary antibody, raised in goat	LI-COR Inc., Lincoln (USA); #926-32210	1:5,000-1:10,000
αrb 800CW (J091)	Fluorescing secondary antibody, raised in goat	LI-COR Inc., Lincoln (USA); #926-32211	1:5000-1:10,000
αms Alexa Fluor 647	Fluorescing secondary antibody, raised in donkey	Thermofisher Scientific, Waltham (USA); # A-31571	1:1000
αms Cy3 (J101)	Cy3-konjugated anti mouse antibody, raised in donkey	Dianova GmbH, Hamburg (Germany); #715-165-151	1:1000
msαACSL3 (J059d)	Mouse, polyclonal	Abnova, Taipeh (Taiwan); #H00002181-B01P	1:2,2000-1:3,000 (Western Blot) 1:600 (immunofluorescence) 1:1000 (subcellular fractionation)
msαβ-actin (J061)	Mouse, monoclonal	Sigma-Aldrich Inc., St. Louis (USA); #A5441	1:30,000-1:40,000
rbαcalnexin (J065c)	Rabbit, polyclonal	Thermofisher Scientific, Waltham (USA); #PA1-30197	1:444
msαTip47/perilipin3 (J078b)	Mouse, monoclonal	R&D Sytems Inc., Minneapolis (USA) #MAB76641	1:888

4.1.11 Software

Software/tool	Company	Application
Adobe Photoshop version 6.0.1	Adobe Systems Incorporated, 1989-2001	Illustration of microscopic pictures
AIDA (Advanced Image Data Analyzer) version 4.27.039	raytest Isotopenmeßgeräte GmbH, 1996-2010	Analysis of Scan of phosphorimaging plate
BASReader version 3.14	raytest Isotopenmeßgeräte GmbH, 2000-2002	Scanning of phosphorimaging plate (TLC)
CRISPRdirect (https://crispr.dbcls.jp/)	Database Center for Life Science, 2015 Naito Y, Hino K, Bono H, Ui-Tei K. (2015) CRISPRdirect: software for designing CRISPR/Cas guide RNA with reduced off-target sites. *Bioinformatics*, 31, 1120-1123.	Design of guide RNAs for ACSL3-knockout
ExPASy ProtParam tool	SIB Swiss Institute of Bioinformatics (https://web.expasy.org/protparam/)	Calculation of molecular weight of amino acid sequences
ImageJ version 2.0.0	National Institutes of Health, 2004	Analysis of microscopic pictures (Lipid droplet biogenesis assay)
Image Studio Lite version 4.0.21	LI-COR Inc., 2014	Analysis of Western Blot membrane scans
NCBI	National Center for Biotechnology Information (https://www.ncbi.nlm.nih.gov/)	Genomic sequences analysis
PhosphoSitePlus®	Cell Signaling Technology Inc., 2003-2018 (Hornbeck et al., 2015) (https://www.phosphosite.org/homeAction.action)	Inquiry for phosphorylation sites in human ACSL3
SnapGene Viewer version 4.0.6.	GSL Biotech LLC, 2017	Creation of plasmid maps

4.2. Methods

4.2.1 Biomolecular methods

4.2.1.1 Restriction digest of DNA

Restriction enzymes were used for subcloning of plasmids. Restriction enzymes derive from bacteria and cut deoxyribonucleic acid (DNA) at specific recognition sites (Mühlhardt, 2009).

The amount of enzyme applied in the preparation was calculated based on 1 U enzyme cutting 1 µg DNA in 1 h in a volume of 50 µL. For the generation of a new plasmid, the vector was digested in a 10x overdigest, i.e. 2 µg vector DNA was mixed with 20 U enzyme and the enzyme-specific buffers (according to manufacturer) in a total volume of 50 µL. The preparation was incubated at 37 °C for 1 h. As a vector control, one preparation contained water instead of restriction enzymes in order to distinguish cut and uncut vector DNA. Subsequently, the DNA fragments were separated by gel electrophoresis.

If the DNA fragments were directly used for subcloning without prior gel electrophoresis, the digested DNA was purified with the Nucleospin® Gel and PCR clean up kit from Macherey-Nagel.

For a digestive screening to verify a newly cloned plasmid, 0.5 µg plasmid DNA was cut in a 5x overdigest and the fragments were analyzed by gel electrophoresis (see section 4.2.1.2).

4.2.1.2 Gel electrophoresis

The DNA fragments were separated by their size by gel electrophoresis. A 0.8 % agarose gel was prepared by dissolving 0.4 g agarose in 50 mL TAE buffer (40 mM Tris/Acetat pH 8.0, 10 mM EDTA/NaOH pH 8.0). The solution was heated up, cooled down and 2.5 µL 20,000x concentrated peqgreen was added as DNA staining reagent before the solution was poured into the gel preparation device containing a comb to form the slots for the samples. When the gel was polymerized, the samples were diluted in a 6x loading dye and loaded on the gel. A 1 kbp ladder indicated the length of the contained fragments.

For subsequent cloning of the DNA fragments, the respective band was cut and purified with the Nucleospin® Gel and PCR clean up kit from Macherey-Nagel.

4.2.1.3 Ligation

For the ligation of the vector and the insert, 0.5 µL vector DNA was mixed with 1.5 µL insert DNA, 0.5 µL T4-ligase (400 U/µL), 0.5 µL 10x ligation buffer and 2.0 µL water and the

preparation was incubated at room temperature for 10 min. In order to evaluate the probability for unsuccessful ligation, a vector control containing water instead of insert DNA was prepared and treated like the samples.

4.2.1.4 Production of LB medium and agar plates

For the production of agar plates, 5 g Bacto tryptone, 2.5 g Bacto yeast extract and 5 g sodium chloride (NaCl) were dissolved in water by stirring and the pH was checked with a pH paper. If necessary, the pH was adjusted to 7.0 with 1 M sodium hydroxide (NaOH), otherwise an amount of 7.5 g select agar was added. The solution was autoclaved and cooled down to 50-60 °C before ampicillin was added to a final concentration of 50 µg/mL. A volume of 20-25 mL of the solution was poured in every petri dish and cooled down until polymerization.

For the production of LB medium 10 g bacto tryptone, 5 g bacto yeast extract and 10 g NaCl were dissolved in water by stirring and the pH was checked with a pH paper. If necessary, the pH was adjusted to 7.0 with 1 M NaOH. The solution was autoclaved and stored at room temperature.

4.2.1.5 Preparation of competent *E. coli*

LB agar plates and LB medium without antibiotics were prepared according to section 4.2.1.4. *E. coli* from a DH5α glycerol stock were plated on an antibiotic-free agar plate and incubated overnight at 37 °C. Then one colony was inoculated and pre-cultured at 37 °C in LB medium without antibiotics for 8 h. The preculture was diluted in LB medium without antibiotics and incubated at room temperature and 230 rpm in a shaker. When the bacteria reached an OD_{600} between 0.55 and 0.6, they were made chemically competent using calcium chloride following the instructions of the standard protocol described in Inoue et al. (1990).

The competence of the *E. coli* was tested by transformation with 50 pg and 5 pg of the plasmid containing an ampicillin resistance (JF007) (see section 4.2.1.6). The grown colonies were counted and the number of colonies per µg DNA was calculated. The competence of the *E. coli* was approved as sufficient, if the number of colonies was at least 1 x 10^7 colonies/µg DNA.

4.2.1.6 Transformation of plasmid DNA in *E. coli*

The ligation product was gently mixed with 50 µL *E. coli*. Subsequently, the preparation was incubated on ice for 15 min and a heat shock was performed at 42 °C for 1 min. Then the

bacteria were plated on a pre-warmed agar plate containing 50 µg/ mL ampicillin for selection of the transformed *E. coli*. The plates were incubated at 37 °C overnight.

4.2.1.7 Inoculation and minipreparation of plasmids

A number of 1-5 colonies of each plasmid was picked and incubated in inoculation tubes containing 2 mL LB-medium with 100 µg/mL ampicillin at 37 °C and 230 rpm for 16 h.

The minipreparation was performed using the "Nucleospin®Plasmid" kit from Macherey-Nagel (Ref.: 740588.250) according to the manual.

4.2.1.8 CRISPR/Cas9

The ACSL3-knockout was performed in wildtype (wt) COS-7 cells by applying the CRISPR/Cas9 method. CRISPR/Cas9 describes a tool for genome editing gaining increasing popularity in the field of life science. The technique is based on the Cas9 protein, which is an RNA guided endonuclease, that is directed to a target in the genome of an organism or cell and generates a gene knockout by inducing a double strand break (Komor et al., 2017). The system originates from bacteria which express Cas9 endonucleases for protection against external nucleic acids, e.g. from viruses. The most frequently applied Cas9 endonuclease derives from *Streptococcus pyogenes* (Sander and Joung, 2014).

In order to perform a CRISPR/Cas9 knockout, the gene locus to be cut has to be identified and the CRISPR plasmid coding for the Cas9 protein and the guiding RNA needs to be cloned. The guide RNA usually includes 20 nucleotides that are complementary to the gene locus to be modified. When the CRISPR plasmid is brought into the target cells, the Cas9 endonuclease is expressed, the guide RNA is transcribed and both form a complex. By following the rules of Watson-Crick base pairing, the guide RNA directs Cas9 to the target sequence in the gene locus and a double strand break is induced. Each variant of Cas9 endonucleases requires the presence of a different Protospacer Adjacent Motif (PAM) sequence occurring immediately downstream (3') of the target sequence (Addgene, 2016). Once a double strand break has been induced, the cellular repair mechanisms non-homologous end joining (NHEJ) or homology-directed repair (HDR) are implemented. While by HDR it is possible to insert specific DNA sequences for a knock-in or modification, NHEJ produces indel mutations often causing a frameshift in the coding sequence resulting in a knockout (Ran et al., 2013).

Search for target sequence and design of guide sequence

The target sequence was identified using the CRISPRdirect tool (https://crispr.dbcls.jp/) which scans the delivered input sequence of the investigated species for suitable target sequences including the required 5'NGG PAM sequence. Moreover, it indicates the number of potential off-target sites of each guide RNA sequence in the whole genome. In addition, the tool also gives information about the genomic sites, that are not complementary to the entire target sequence, but to only eight and twelve nucleotides (called 'seed sequences'), which extends the information about the specificity (Naito et al., 2015).

Since the COS-7 cell line originating from the African green monkey (*Chlorocebus sabaeus*) was the biological system meant to be investigated, the genomic data of *Chlorocebus sabaeus* were applied for designing the CRISPR plasmid. Thus, the ACSL3 mRNA (NCBI Reference Sequence: XM_007966443.1) of *Chlorocebus sabaeus* (taxid: 60711) was delivered as input sequence to the CRISPR direct tool to screen the sequence for a target locus including the PAM sequence requirement 'NGG'. 'Green monkey (*Chlorocebus sabaeus*) genome, ChlSab1.1 (Mar, 2014)' was selected for the specificity check.

As output, CRISPRdirect delivered three highly specific target sequences without any off-target sites, thereof the target sequence 3'- GGGGGTCATCGTGCATACCATGG -5' (corresponding to amino acids K249-A257) located in the fourth exon of ACSL3 was selected for the knockout. The other sequences were located in exon 9 and 14 and were therefore excluded from utilization, because they would cause an abruption at the end of the protein which might leave a residual functionality of the enzyme.

In order to increase the probability of an ACSL3-knockout, a second target sequence 3'-CGAGTGGATGATAGCTGCACAGG-5' (corresponding to amino acids A170-A178), which was located in the second exon of ACSL3, was selected, because a double strand break at the beginning of a gene is more likely to produce a non-functional protein. However, this target sequence was not highly specific and exhibited ten potential off-target sites for the seed sequence of 12 nucleotides. See section 10.1.1 for a screenshot of the CRISPR direct tool output and more detailed information about the target sites.

After selecting the target sequences, the sense and the anti-sense oligos were designed to generate the double stranded DNA coding for the guide RNA for each of the two CRISPR plasmids JF1052 and JF1053. Since the vector was digested with BbsI, an overhang had to be added to the oligos to enable later ligation of the digested vector and the annealed oligos. For

the guide RNA in JF1052 a guanine had to be added in sense-direction and a cytosine in anti-sense for efficient transcription by RNA polymerase (*table 1*). The oligos were ordered from Sigma-Aldrich (Sigma-Aldrich Chemie GmbH, Steinheim).

Table 1: **The oligo sequences for the design of the guide RNAs.**

Plasmid name and internal number	Oligo name and number	Oligo sequence	Annealed oligos
A3-ex2 (JF1052)	#597 s-gACSL3-E5 (5'→3'; sense)	CACCGCGAGTGGATGATAGCTGCAC	CACCGCGAGTGGATGATAGCTGCAC CGCTCACCTACTATCGACGTGCAAA
	#598 a-gACSL3-E5 (5'→3'; antisense)	AAACGTGCAGCTATCATCCACTCGC	
A3-ex4 (JF1053)	#691 s-gACSL3-Chl (5'→3'; sense)	CACCGGGGGTCATCGTGCATACCA	CACCGGGGGTCATCGTGCATACCA CCCCCAGTAGCACGTATGGTCAAA
	#692 a-gACSL3-Chl (5'→3'; antisense)	AAACTGGTATGCACGATGACCCCC	

The 20 nucleotides of the target sequences are not highlighted. The BbsI overhang (highlighted in green) was added to the 20 nucleotides of the target sequence to enable subcloning into the CRISPR plasmid. The nucleotide guanine and cytosine (highlighted in grey) were added in JF1052 to increase efficiency of cutting. The guide RNA for the plasmid JF1053 was designed by Susanne Domschke (medical doctoral candidate).

Cloning of puromycin resistance into the CRISPR plasmid

The basis for the CRISPR plasmids was the eSpCas9(v1.1)-plasmid (Addgene, internal number JF1039), which codes for the improved Cas9 enzyme holding less off-target activity than wt Cas9 (Slaymaker et al., 2016). This plasmid did not contain an antibiotic resistance for mammalian cells. Therefore a puromycin resistance gene, deriving from the plasmid with the internal number JF988 (Addgene, #62988), was subcloned into the eSpCas9(v1.1)-plasmid. For this purpose, JF988 and JF1039 were cut with the restriction enzymes NotI-HF and FseI (see section 4.2.1.1) and the fragments were separated by gel electrophoresis (see section 4.2.1.2). The insert and the vector were ligated (see section 4.2.1.3) resulting in the new CRISPR plasmid eCas9-puro (internal number JF1045) coding for the enhanced CRISPR/Cas9 machinery, the puromycin resistance and an ampicillin resistance (see plasmid map in *figure 4*). Amplification of the plasmid by inoculation and minipreparation was done according to section 4.2.1.7.

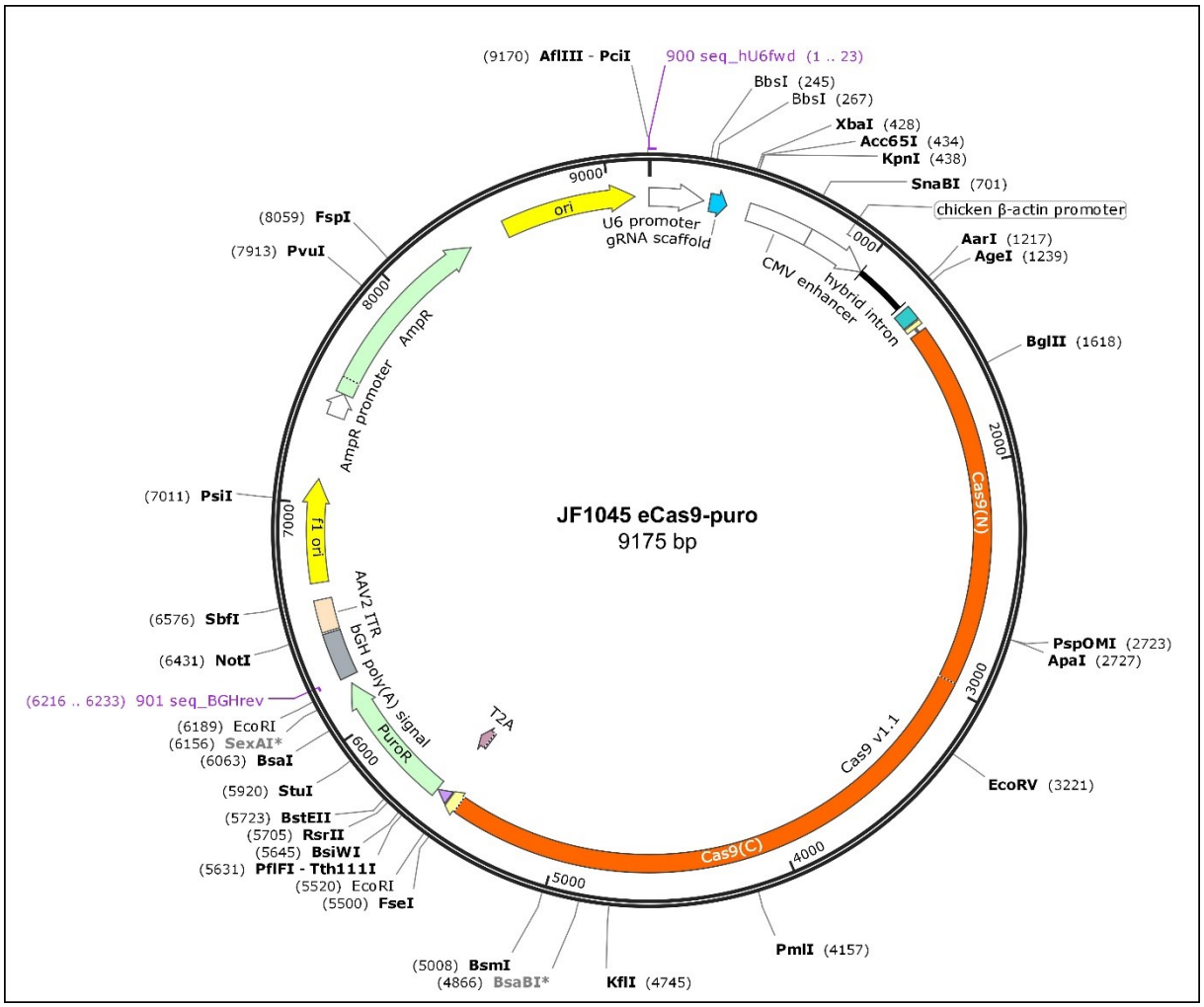

***Fig. 4*: Plasmid map of the CRISPR plasmid eCas9-puro.** The plasmids encodes the Cas9 endonuclease (shown in orange) and the antibiotic resistance genes for puromycin and ampicillin (shown in green). The guide sequences are cloned into the plasmid before gRNA scaffold (shown as blue arrow) by cutting the plasmid with the restriction enzyme BbsI. The primer binding sites for seq_BGHrev and seq_hU6fwd (highlighted in purple letters) were used for verification of correct insertion of the puromycin resistance gene and the guide sequences (see section 4.2.1.9). This map was created with SnapGene Viewer version 4.0.6.

Cloning of guide sequences into CRISPR plasmid eCas9-puro

Two final CRISPR plasmids containing a different guiding sequence for ACSL3 were prepared. The guiding sequences were cloned into the CRISPR plasmid JF1045, containing the sequence for the enhanced CRISPR/Cas9 machinery, an ampicillin resistance for transformed *E. coli* selection and a puromycin resistance, which allows the selection of transfected cells.

The oligos were annealed by mixing each 20 µL 100 µM #597 and #598 or 100µM #691 and #692 respectively, and heating at 95 °C for 10 min in a heating block. Subsequent cooling to room temperature resulted in 50 µM annealed oligos forming the insert guide sequence for A3-ex2 (JF1052) or A3-ex4 (JF1053) respectively.

The target vector JF1045 was digested with BbsI in a 10x overdigest (see section 4.2.1.1). The annealed oligos were diluted to 0.1 µM and 1.5 µL was mixed with 0.5 µL of the digested vector JF1045. Ligation was performed according to section 4.2.1.3 and the plasmid was amplified in *E. coli* and isolated (see section 4.2.1.7).

4.2.1.9 Verification of newly cloned plasmids

In principle, there are different ways to verify the correct cloning of a generated plasmid.

In a digestive screening (see section 4.2.1.1), the generated plasmids were cut with restriction enzymes in order to check the length of generated fragments or restriction sites, which might be added or disappeared during correct cloning. A digestive screening was performed for the ACSL3-knockout CRISPR plasmids JF1052 and JF1053.

In addition, the sequence of plasmids was verified by Sanger sequencing performed by GATC Biotech AG (Konstanz, Germany). For this purpose, 0.5 µg plasmid DNA was mixed with 5 µL of the 5 µM sequencing primer. For verification of JF1052 and JF1053 the sequencing primer #592 seq_hU6fwd (5'-GAGGGCCTATTTCCCATGATTCC-3') and for verification of JF1045 the sequencing primer #675 seq_BGHrev (5'- TAGAAGGCACAGTCGAGG-3') was applied. The preparation was sent to GATC and the chromatogram was analyzed to confirm the correct ligation of vector and insert.

4.2.1.10 Characteristics of applied retroviral plasmids

The applied retroviral plasmids were based on the retroviral expression vector pQCXIP (Becton Dickinson, Erembodegem, Belgium). The vector pQCXIP contains a multiple cloning site for simple insertion of the target genes and encodes a puromycin resistance gene that is co-transcribed with the inserted gene of interest. The 5' and 3' long terminal repeats (LTRs) flanking the target gene and the extended packaging signal psi^+ (Ψ^+) are also included.

The retroviral plasmids JF623, JF825, JF827, JF844 and JF1262 had already been subcloned and were kindly provided by Margarete Poppelreuther, Kathrin Seeburger and Tarik Exner. See section 10.2 for the DNA and amino acid sequence of the transduced proteins GFP, GFP-ACSL3, GFP-ER-ACSL3 and GFP-AA-ACSL3. The enzyme variants GFP-ACSL3, GFP-ER-ACSL3 and GFP-AA-ACSL3 were additionally tagged with a hemaglutinin (HA) epitope.

4.2.2 Cell biological methods

All cells were grown at 37 °C with 5 % CO_2 supply and 95 % relative humidity except as noted otherwise.

4.2.2.1 Cultivation of COS-7 cells

The COS-7 cell line (DSMZ, #ACC 60) is a kidney fibroblast-like cell lines originating from the African Green Monkey (*Chlorocebus aethiops,* synonym *Chlorocebus sabaeus*). It was immortalized by transfection with simian virus 40 which is incapable of replication due to a mutation in the replication origin. The cells are standard cultivated at 5 % CO_2 and 37 °C and exhibit a doubling time of approximately 35-48 hours (DSMZ).

COS-7 cells were cultured in standard growth medium (DMEM GlutaMAX 4.5 g/L glucose, 10% FCS, 1 % P/S) except as noted otherwise. The cells were passaged every 2-3 days in a ratio of 1:3-1:5. For passaging, the medium was removed, the cells were washed with PBS and trysinized to become dissociated from the dish surface. The impact of trypsin on the cells was inhibited by resuspending the cells with standard growth medium and then the cells were seeded in a fresh dish.

4.2.2.2 Cultivation of A431 cells

The A431 cell line (ATCC, #CRL-1555™) is a human cancer cell line originating from an epidermoid carcinoma. A431 cells were cultured in standard growth medium (DMEM GlutaMAX 4.5 g/L glucose, 10% FCS, 1 % P/S) except as noted otherwise. Cells were grown at a temperature of 37 °C with 5 % CO2 supply and a relative humidity of 95 %. The cells were passaged every 2-3 days in a ratio of 1:5-1:10. For passaging, the medium was removed, the cells were washed with PBS and trysinized to become dissociated from the dish surface. The impact of trypsin on the cells was inhibited by resuspending the cells with standard growth medium and then the cells were seeded in a fresh dish.

4.2.2.3 Cultivation of Phoenix gag-pol cells

Phoenix gag-pol (Phx-gp) (ATCC, # SD-3514) were generated from 293T cells by stable transfection with a Moloney GagPol-IResLyt2 construct (Nolan, 2018).

Phx-gp cells were were cultured in standard growth medium (DMEM GlutaMAX 4.5 g/L glucose, 10% FCS, 1 % P/S) except as noted otherwise. The cells were passaged every second

day in a ratio of 1:6. For passaging, the cells were detached from the dish surface by gentle mechanical force achieved by pipetting up and down carefully.

4.2.2.4 Cryoconservation and thawing of the cells

In order to ensure a high viability of the cells throughout the freezing process, the cryo-stocks were produced from cells with approximately 80 % confluence. The cells were washed and trypsinized and resuspended in cold standard growth medium. The cell number was determined by applying a hemacytometer. After centrifugation at 150 x g for 5 min, the supernatant was removed and the cell pellet was resuspended in cold cryo-medium containing dimethyl sulfoxide (DMSO) (10 % v/v DMSO in standard growth medium) and the cells were distributed to cryotubes as 1 mL aliquots comprising approximately 2 x 10^6 cells. The tubes were placed in an isopropanol tank at 80 °C and transferred to liquid nitrogen after some days.

For thawing, the cells were warmed-up at 37 °C and transferred in a fresh cell culture dish with standard growth medium. The growth medium was replaced 1 d after thawing to get rid of residual cytotoxic DMSO.

4.2.2.5 Generation of standard cell pellets

Cells were grown under standard growth condition until harvesting. The cells were washed, trypsinized and resuspended in cold standard growth medium. The number of cells was determined by counting with a hemacytometer and an amount of 6 x 10^6 cells was transferred into a 50 mL falcon tube. The cells were centrifuged at 500 x g and 4 °C for 10 min and resuspended in 6 mL PBS. Then 1 ml of the suspension corresponding to 1 x 10^6 cells were transferred to a 1.5 mL tube and centrifuged at 500 x g and 4 °C for 5 min. The supernatant was removed and the cell pellets were stored at -80 °C.

4.2.2.6 Transient transfection of CRISPR plasmids

Wildtype COS-7 cells (wtCOS-7) were seeded in a 6-well plate and incubated for 1 d. The next day, when the cells reached 80 % confluence, the cells were transfected applying Fugene. One hundred µL Opti-MEM were provided in a 1.5 mL tube. Two µg of the CRISPR plasmids JF1052 or JF1053 was added, mixed and incubated for 5 min at room temperature. Then, 10 µL of Fugene Transfection reagent was added, mixed and incubated at room temperature for 20 min. In the meanwhile, the growth medium of the cells was replaced with medium without antibiotics. The transfection reagent was added to the cells under swirling and the cells were incubated under standard conditions for 1 d. Three controls were run during the whole

procedure. The transfection control was transfected with the cloning vector pEGFP-N1 (NCBI Genbank accession: U55762; internal plasmid number JF067) coding for eGFP but devoid of a puromycin resistance gene. A selection control was seeded, but not transfected to monitor how untransfected wt cells react to the subsequent antibiotic selection. A viability control was cultivated under standard growth conditions to make sure that the selected cells in the other wells only die due to the antibiotic. Puromycin selection was performed in order to kill the untransfected cells lacking incorporation of the CRISPR plasmids. For this purpose, the medium was removed and replaced with fresh standard growth medium containing 6 µg/ µL puromycin. The viability control was incubated in puromycin-free medium. Fourty-eight hours after starting the puromycin selection, the cells were detached from the flask surface by trypsinization and resuspended in standard growth medium. The cells were counted and a dilution series was generated (3.5 cells/well; 35 cells/well). The cells were seeded on 96-well plates in a fashion, that statistically 0.7 or 7 cells were contained in one well with a working volume of 200 µL. The aim was to obtain single cells in each well which produce colonies of the same genotype. The cells were incubated at standard growth conditions for five weeks before cryostocks were generated (see section 4.2.2.4). Meanwhile, the wells were monitored for single cells, the arising clonal colonies were grown and the growth medium was replaced with fresh medium every 3-6 days or when the cells were passaged. Four clones were obtained from the CRISPR plasmid A3-ex2 (JF1052) and 8 clones from A3-ex4 (JF1053).

4.2.2.7 Verification of the ACSL3-knockout in clones

The ACSL3-knockout was confirmed in all clones by Western Blot analysis (see section 4.2.3.1). After pooling of six cell clones (see section 4.2.2.8) the ACSL3-knockout was additionally confirmed by indirect immunofluorescence (see section 4.2.2.11).

4.2.2.8 Pooling of ACSL3-knockout clones

The confirmed ACSL3-knockout clones were examined regarding morphology and cellular behavior in cell culture routine in order to find clones that were maybe damaged during the CRISPR procedure. Each three inconspicuous cell clones transduced with the CRISPR plasmid A3-ex2 (JF1052) or A3-ex4 (JF1053) were selected and pooled in order to level out potential off-target effects between the cell clones. For this purpose, clone 2, 5 and 7 transduced with JF1052 and clone 1, 4 and 8 transduced with JF1053 were pooled by combining a number of 0.2×10^6 cells of each cell clone.

4.2.2.9 Production of retroviral particles

The production of the retrovirus for the proteins GFP, GFP-ACSL3, GFP-ER-ACSL3, GFP-AA-ACSL3 and A3Nt-mcherry encoded on the retroviral plasmids JF623, JF825, JF827, JF844 and JF1262 was performed with the packaging cell line Phx-gp. The vectors produced by Phx-gp cells are based on the Moloney Murine Leukemia Virus (MMULV) infecting murine cells (Nolan, 2018). The retroviral plasmids were taken up into the Phx-gp cells by calcium-phosphate precipitation, which is a method developed by F. L. Graham and A. J. van der Eb. Using this technique, a buffer containing phosphate ions is mixed with calcium chloride and the retroviral plasmids meant to be transfected. The calcium and phosphate ions form a precipitate while the DNA co-precipitates. The preciptate together with the DNA is taken up into the cells (Graham and van der Eb, 1973). Efficient generation of the retroviral particles is achieved by the proviral genes *gag* and *pol* expressed in the Phx-gp cells. *Gag* is a polyprotein forming the core structure of the retrovirus. *Pol* encodes for the integrase and reverse transcriptase required for transcription of the viral genes. Together with the proviral genes, the transgenes are packaged into retroviral particles and released into the medium. Phx-gp cells do not express an envelope protein by themselves. Pseudotyping was done with the glycoprotein of the vesicular stomatitis virus (VSV-G) that is frequently used to change the tropism of viral vectors (Cronin et al., 2005; Nolan, 2018).

The protocol was based on the procedure described in Schuck et al. (2004). Phx-pg cells were seeded in an amount of 1.2 x 10^6 cells in a 100 mm cell culture dish and incubated at 37 °C and 5 % CO_2. After 2 d of incubation, the transfection reagent was prepared in a 50 mL falcon tube. Water was provided first to a final volume of 540 µL. A quantity of 4.5 µg VSV-G plasmid DNA (JF380), 13.5 µg retroviral plasmid DNA, 132 µL 1 M $CaCl_2$ were added and mixed thoroughly. While vortexing the DNA/$CaCl_2$ mix, 540 µL 2x HBS buffer (280 mM NaCl, 50 mM HEPES, 12 mM glucose, 10 mM KCl, 1.5 mM Na2HPO4; pH 6.95) was added dropwise. The whole preparation was incubated at room temperature for 5 min. The growth medium of the Phx-gp cells was replaced with fresh one and the transfection mix was added dropwise to the cells. After swirling gently, the cells were incubated at 37 °C and 5 % CO_2 for 16 h. Then the transfection mix was removed and replaced with 5 mL low glucose growth medium (DMEM, 1 g/L glucose, 10 % FCS, 1 % P/S). The cells were grown at 32 °C to increase the stability of the retroviral particles. After 24 h of incubation at 32 °C, the virus was harvested. For this purpose, 4.5 mL supernatant was collected and filtered through a 0.45 µm filter. The filtered retroviral supernatant was distributed to four aliquots à 1 mL, flash freezed in liquid

nitrogen and stored at -80 °C until utilization. The Phx-gp cells were provided with fresh low glucose growth medium and the harvesting was repeated every 24 h for 5 d post transfection.

The retroviral particles for the plasmids encoding GFP, GFP-ACSL3, GFP-ER-ACSL3 and GFP-AA-ACSL3 had already been generated according to the protocol and were kindly provided by Marga Poppelreuther and Katrin Seeburger.

4.2.2.10 Retroviral transduction

COS-7 derived cell lines were seeded from a confluent 100 mm cell culture flask into 6-well plates in a number of 50,000 cells/well. One well was seeded for each plasmid to be transduced. One selection control was seeded additionally. The cells were incubated for 1 d to 50-60 % confluency. Since the retroviral particles only infect dividing cells, this density gives an efficient transduction rate. The supernatant was removed and the cells were incubated with 1 mL retroviral supernatant for 24 at 32 °C, because at this temperature, the viral particles are more stable. In order to increase the transduction efficiency, polybrene was added in each 6-well in a final concentration of 4 µg/mL. The selection control was treated with polybrene in normal growth medium only. Twenty-four hours after the infection, the medium was replaced with fresh standard growth medium and the cells were placed to 37 °C for another 24 h. Untransduced cells were killed by antibiotic selection either with puromycin or hygromycin, depending on the resistance gene encoded by the transduced retrovirus. For puromycin selection, the cells were incubated in standard growth medium containing 6 µg/mL puromycin for 48 h. After 1 day the selection medium was replaced with fresh one. Hygromycin selection was carried out at a concentration of 500 µg/mL for six days including the exchange to fresh selection medium after 3 days. The selection control was also treated with the respective antibiotic to ensure that the period of time was enough to kill all untransduced cells. After completion of selection, the medium was changed to normal growth medium and the cells were subcultivated until a sufficient amount of cells was obtained for further experiments.

In order to obtain cell lines with different expression levels of GFP-ACSL3 or GFP-ER-ACSL3, the pooled ACSL3-knockout cells (C232) were co-infected with varying amounts of retrovirus encoding the respective transgene and retrovirus encoding only a hygromycin resistance gene (JF424) (table 2). Assuming that the cells would incorporate different amounts of the retroviral particles encoding the transgene and the competing plasmid, the expression of GFP-ACSL3 and GFP-ER-ACSL3 in the cells would be altered accordingly. Cells only transduced with

JF424 did not survive the puromycin selection, since JF424 did not contain a puromycin resistance gene.

Table 2: **Amounts of retrovirus used for co-transduction of the retroviral transgene and a competing hygromycin resistance gene.**

Internal cell line number	JF825 (mL)	JF827 (mL)	JF424 (mL)
C234d	0.25 mL		0.75 mL
C235		1.00 mL	0.00 mL
C235d		0.50 mL	0.50 mL

4.2.2.11 Indirect immunofluorescence

Standard immunofluorescence

COS-7 or A431 cells were grown on a glass plate (Ø10 mm) in a 24-well plate in a number of 20,000 cells/well and incubated for 4-5 h until the cells were attached. The cells were washed 3x in PBS and fixed in 4 % PFA for 20 min. The PFA was removed and after three subsequent washing steps in PBS the cells were permeabilized with SGB buffer (saponing-gelatin-BSA buffer) for 10 min. The supernatant was removed and the primary antibody diluted in SGB buffer was added for 1 h. Then, the cells were washed 3x in SG buffer (saponin-gelatin buffer) and the solution containing the secondary antibody diluted 1:1000 in SG buffer was added for 1 h. Following each two washing steps in SG buffer and PBS, the cells were mounted in mowiol containing 1 µg/mL Hoechst for staining of the nuclei. Microscopy was performed using an Olympus Bx41 microscope (see section 4.2.2.14 for details).

Immunofluorescence for dSTORM microscopy

A431 pRVH1 (control cells) and A431 ACSL3-knockout cells (A431 A3KO) were seeded in 8-well chambers in a number of 20,000 cells/well. The cells were grown for 24 h either in standard growth medium or standard growth medium supplemented with 600 µM OA for 24 h. Then the cells were washed in PBS, fixed in 4 % PFA for 10 min and washed three times in PBS for each 3 min. Permeabilization was done in Triton X-100 permeabilization buffer (0.5 % v/v Triton X-100 in PBS) for 10 min and the cells were blocked with SGB buffer for 60 min at gentle shaking. The primary antibody was diluted in SGB buffer and incubated for 90 min at gentle shaking. The solution was removed and the cells were washed three times in washing buffer (0.05 % v/v Triton X-100, 1 % BSA in PBS) each for 3 min. The secondary antibody Alexa Fluor 647 was diluted 1:1000 in SGB buffer and added to the cells for 60 min. The plate was covered with aluminium foil to prevent photobleaching. After incubation at gentle shaking, the cells were washed in washing buffer three times for each 3 min. Fixation was repeated in

4 % PFA for 10 min followed by three washing steps in PBS for each 3 min. The cells were stored in PBS containing 0.01 % w/v sodium azide at 4 °C until dSTORM microscopy was performed (see section 4.2.2.14).

4.2.2.12 Cell proliferation assay

MTT [3-(4,5-dimethylthiazol-2-yl)-2,5-diphenyl tetrazolium bromide] assay was first described by Mosmann in the year 1983 and is a widely used colorimetric method to determine mammalian cell viability and activity. It is based on the principle, that the tetrazolium ring of MTT is cleaved by mitochondrial dehydrogenases in living cells resulting in the purple colored product formazan (Mosmann, 1983).

MTT assay was performed in order to investigate the growth of COS-7 cells in the presence of cerulenin, which acts as an inhibitor of the fatty acid synthase (Omura, 1976). The experiments were performed with COS-7 cells exhibiting an ACSL3 knockdown induced by RNA interference (A3-RNAi cells) and wtCOS-7 cells transfected with a pRVH1 plasmid without small hairpin RNA sequence as control cells.

The cells were seeded in a 96-well plate in a number of 6,000 cells/well and incubated under standard growth conditions. Cerulenin stock solution (5 mg/mL in DMSO) was diluted in standard growth medium to the final concentrations 2 µg/mL, 4 µg/mL or 6 µg/mL. The supernatant was removed from the cells and the medium containing cerulenin was added. Each concentration was tested in sixfold determination. Six wells served as control and were cultured in standard growth medium only. Cell viability was determined by MTT-assay 4 h, 24 h and 48 h after seeding. For the MTT assay, the growth medium was removed and replaced with 120µL standard growth medium containing 0.83 mg/mL MTT. After 3 h of incubation, the supernatant was gently removed and the formazan crystals were dissolved in 200 µL/well DMSO. To ensure that no formazan clumps remained, the cells were incubated at room temperature for 5 min and the plate was shaken on a thermomixer at 300 rpm for 5 min. The absorbance of each well was measured in a photometer at a wavelength of 595 nm.

4.2.2.13 Lipid droplet biogenesis assay

For the lipid droplet biogenesis assay, wtCOS-7 cells and the cell lines GFP_A3ko (C233), GFP-ACSL3 (C234d), GFP-ER-ACSL3(H) (C235d) and GFP-AA-ACSL3 (C236) were stably transduced with A3Nt-mcherry resulting in new cell lines with the internal numbers C239, C240, C241, C244 and C245. The lipid droplet biogenesis assays required the insertion of

A3Nt-mcherry as a lipid droplet marker into the rescue cell lines. The reason was that early lipid droplets were not sufficiently stained by monodansylpentane (MDH) to make them detectable in the microscope. Other more sensitive neutral lipid dyes, e.g. Bodipy 493/503, were not appropriate, since the channel for green fluoresence was already occupied by the GFP transduced into the cells. A3Nt is a protein comprising the N-terminus, amino acid 1-135, of the human ACSL3 and was first designed as a GFP fusion protein by Poppelreuther et al., who report that the N-terminal region of ACSL3 is essential for targeting the protein to the lipid droplets and the endoplasmic reticulum. A3Nt translocated to the lipid droplets upon fatty acid supplementation like endogenous ACSL3 and epitope-tagged full length ACSL3 (Poppelreuther et al., 2012). Therefore, A3Nt is an adequate lipid droplet marker. For this work, A3Nt was fused to mcherry, a red fluorescent protein, to enable microscopic analysis of two color images in the biogenesis assay. See section 10.2 for the DNA and amino acid sequence of A3Nt-mcherry.

The cells were seeded in a 24-well plate on a cover slip (Ø10 mm) in a number of 40,000 cells/well. For each cell line two wells were required: one well as a starving control and one well for lipid droplet induction. After seeding the cells were incubated for 20-24 h under standard growth conditions. The supernatant was removed, the cells were washed twice with PBS and starvation medium (DMEM 4.5 g/L glucose [Thermofisher Scientific #61965026], 1 % P/S, 1 mM sodium pyruvate, 1x non-essential amino acids, without FCS) was added. After 24 h of starvation, the starving controls were washed 3x with PBS and fixed in 4 % paraformaldehyde for 20 min at room temperature. Following three washing steps in PBS the cells were mounted in mowiol containing 1 µg/mL Hoechst for staining of the nuclei. The cells destined for lipid droplet biogenesis were washed 2x in PBS and incubated in lipid droplet induction medium (DMEM 4.5 g/L glucose [Thermofisher Scientific #61965026], 1 % P/S, 600 µM OA bound to 100 µM BSA, without FCS) for exactly 20 min. The lipid droplet induction medium was removed, the cells were washed 4x with PBS and fixed and mounted like the starving control. For a control experiment, starved cells were incubated in lipid droplet induction medium for 60 min instead of 20 min in order to investigate, if the differences observed between the GFP-ACSL3 and GFP-ER-ACSL3 cells are valid for early stages of LD biogenesis or sustained throughout a longer period of time.

The detection of the early lipid droplets, labelled by A3Nt-mcherry, was carried out in the red channel (filter: U-MNG2). The pictures were taken in the high sensitivity mode 8, with a gamma of 1.4 and with the 60x objective. A cell was imaged with the exposition time suggested

by the auto-mode of the software. Cells were excluded from microscopic analysis, if the suggested exposition time failed to be in the range of 100 ms to 700 ms in order to select for cells with a moderate expression of the lipid droplet marker. Furthermore, cells were excluded from microscopy if they had more than one nucleus, exhibited an irregular spindular shape or if they were not efficiently starved and possessed big lipid droplets with the surrounding monolayer clearly distinguishable from the neutral lipid core.

For the cell lines expressing GFP-ACSL3 and GFP-ER-ACSL3 the cells were also imaged in the green channel to quantify the GFP expression and relate the number of generated lipid droplets to the expression of GFP. For this purpose, the GFP in the GFP-ACSL3 and GFP-ER-ACSL3 cells was imaged with an exposition time of 500 ms. In order to ensure proper quantification of the GFP fluorescence, cells with a really low or high GFP protein expression (more than 20 % overexposed pixels) were excluded. The GFP fluorescence was quantified by ImageJ by calculating the integrated density of fluorescence.

The number of lipid droplets was quantified by ImageJ using a novel automated method developed and validated by Tarik Exner (medical doctoral candidate; manuscript submitted for publication). The automated quantification of lipid droplets was based on the analysis of fluorescence intensity reflected by the tonal distribution of the grey values in the image. Lipid droplets were identified according to their characteristical fluorescence intensity maximum in the center and a circular shape. The plugin ‘find maxima’ was used to identify pixels higher in brightness, compared to their neighbouring pixels. With the settings for size and circularity of the particles the properties of structures counted as lipid droplets was defined. Before the algorithms for lipid droplet quantification was applied, the original images were modified by ImageJ to optimize the analytical conditions. One amplification cycle was performed to increase the signal-to-noise ratio. The image was convoluted using Gaussian blurring to diminish unspecific fluorescence maxima and reduce false-positive counts.

Validation of this method was done by comparison of the algorithm’s output with numbers obtained from manual counting in 3750 images. The results derived from automated and manual analysis were highly similar independent from the lipid droplet staining technique, metabolic state or cell line. To compare the results from manual and automated counting, linear regression analysis was performed by plotting numbers of the manual counts against the numbers of the algorithm. The Pearson correlation coefficient (R^2) for the quantification in COS-7 cells

transduced with A3Nt as lipid droplet marker was 0.7843 indicating that the algorithm delivers reliable output (performed by Tarik Exner, manuscript submitted for publication).

4.2.2.14 Microscopy

Wide-field microscopy

Microscopy was performed using an Olympus Bx41 microscope. Green fluorescing GFP was detected with the filter block *U-M41028*. The filter block *U-MNG2* was applied to detect red fluorescence by Cy3 and mcherry and the filter *U-MF2 with F36-500 HC-Set DAPI* was used to detect blue fluorescent Hoechst and MDH. Gamma was 1 if not stated otherwise and when necessary, high sensitivity mode 8 was applied in order to reduce bleeching caused by high exposition times. The merged pictures and panels were generated using Adobe Photoshop version 6.0.1.

dSTORM microscopy

dSTORM (direct stochastic optical reconstruction microscopy) is a novel method for super-resolution fluorescence imaging and allows the localization of single molecules in cellular structures. The spatial resolution in conventional microscopy is limited leading to optical blurring of light spots positioned too close together as they could be displayed as separate objects. This often restricts clear imaging of fluorescent molecules in the subcellular compartments. dSTORM allows imaging of fluorophores at a resolution of approximately 20 nm by a selective reversible switching of fluorophores into an active or passive state. Organic fluorophores, like Alexa Fluor, can be switched of using reducing thiol compounds like mercaptoethylamine. The deactivated state is quite stable. This is why only the minority of fluorescing molecules randomly return back to ‚on state' at the same time. The fluorescence can be also switched on by applying UV-light. Consecutive imaging of the cell during repeating cycles of deactivation and activation and subsequent reconstruction of single molecule localization give a super resolved fluorescence image (Borlinghaus et al., 2015; van de Linde et al., 2010).

dSTORM microscopy was performed using a N-STORM microscope (Nikon) with a 100x oil immersion objective (NA 1.49). Irradiation of the ACSL3-bound Alexa Fluor 647 was carried out with a 647 nm laser with an intensity of approximately 0.5 kW/cm^2. A 405 nm laser was applied to recover the fluorescence. Fluorescence emission and excitation light were separated with a dichroic mirror transmitting light above 660 nm and a bandpass filter (705/72 nm). Fluorescence emission was detected with an EMCCD camera (iXon Ultra 897, Andor).

Imaging buffer (100 mM β-mercaptoethylamine, 10 % w/v glucose, 50 U/mL glucose oxidase, 5000 U/mL catalase, 2.5 mM KCl, 1.1 mM Tris-HCl pH 7.5, 2.5 % glycerol, 0.2 mM Tris(2-carboxylethyl)phosphine hydrochloride; in PBS; pH adjusted to 8 with 1 M NaOH) was added to the samples to switch off Alexa Fluor 647 fluorescence. The oxygen scavenger system containing catalase and oxidase and the β-mercaptoethylamine provoked a stable 'off-state' of the molecules. By a stochastic process, the Alexa Fluor 647 reverted back to fluorescing state which could be detected as flashing regions in the samples. When necessary, fluorescence was additionally induced by UV-light.

4.2.3 Biochemical methods

4.2.3.1 Western Blot

Western Blotting allows to detect a specific protein in a complex mixture of proteins. First, the proteins are separated according to their molecular weight by electrophoresis in an SDS-polyacrylamide gel. Then, the proteins are transferred to a membrane by applying an electric field to enable easy access of the antibodies during immunostaining. A primary antibody binding to the destined protein is added. The protein-antibody complex can be made visible by addition of a secondary antibody that is fluorescently labelled (Berg et al., 2013).

SDS-polyacrylamide gel electrophoresis

The raw material for Western Blot analysis was a standard cell pellet (see section 4.2.2.5) or the subfractions obtained from subcellular fractionation (see section 4.2.3.7). For sample preparation, the cell pellets were resuspended in 200 µL 4x SDS-PAGE sample buffer, called 'O buffer' (4x: 8 % w/v SDS, 250 mM Tris/HCl pH 6.8, 40 % v/v glycerol, 400 mM β-mercaptoethanol, 0.2 % w/v Orange G). For the subcellular fractions, 150 µL of each fraction was diluted in 50 µL 4x O-buffer. The samples were shaken in a heatable shaker at 1000 rpm and 95 °C for 5 min to ensure complete denaturation of the proteins and binding to SDS, which makes the proteins move from the cathode to the anode in an electric field. The running gel and the stacking gel were prepared by mixing the following components and volumes shown in *table 3* (for 2 gels).

Table 3: **The components of a running and stacking gel.**

	running gel (8 %)	**stacking gel (4 %)**
Water	5.7 mL	
4 x Separating buffer (1.5 M Tris/HCl pH 8.8, 0.4 % w/v SDS)	3.0 mL	
30 % Acrylamide solution	3.18 mL	0.96 mL
Stacking gel buffer (150 mM Tris/HCl pH 6.8, 0.12 % w/v SDS)		5.98 mL
TEMED	20 µL	10 µL
10 % APS	200 µL	100 µL

First, the solution for the running gel was prepared, filled between two glass plates, fixed in a device and the running gel was overlaid with isopropanol to straighten the gel front. After polymerization, the isopropanol was removed and the stacking gel solution was poured onto the running gel. A comb was utilized to build the wells for the samples. After polymerization, the protein samples were loaded on the gel, which was placed in a gel electrophoresis chamber containing running buffer (25 mM Tris, 190 mM glycine, 0.1% w/v SDS). Gel electrophoresis was performed at 160-180 V for approximately 1 h.

Semi-dry Western Blot

After gel electrophoresis the proteins were transferred onto a nitrocellulose membrane by applying a semi-dry Western Blot system. Filter paper and the nitrocellulose membrane were soaked with transfer buffer (25 mM Tris, 190 mM glycine, 20 % v/v methanol) and a stack was built containing two layers of filter paper on the upper site, the gel, the membrane and two filter papers on the bottom site. The stack was placed in the Western Blot chamber and the air bubbles were eliminated. The proteins were blotted at a current of 100 mA per gel for 1 h. Reversible Ponceau protein staining was performed to survey an efficient transfer of the proteins from the gel onto the membrane. For this purpose, the membrane was incubated with ponceau red for 30-60 s, the excess staining was removed with water and the membrane was scanned.

Indirect Immunostaining

The membrane was blocked by incubation on the shaker for 1 h in blocking solution (2 % milk protein in TBS-T). The primary antibody was diluted in blocking solution and the membrane was incubated in the primary antibody solution at 4 °C overnight. The primary antibody solution was removed by washing the membrane for three times in TBS-T for 5 min each. The secondary antibody was diluted in blocking solution and the membrane was incubated in that solution for 1 h at room temperature. The secondary antibody solution was removed by washing

the membrane for three times in TBS-T for 5 min each. The fluorescence signal was detected by scanning the membrane with an Odyssey infrared scanner (LI-COR, Lincoln, USA). The fluorescence signal was analyzed using the software Image Studio Lite version 4.0.21 (LI-COR Inc., 2014).

4.2.3.2 ACS assay

The ACS assay is a radiometric assay applied to determine the ACS activity in cell lysates or the subfractions obtained from subcellular fractionation (see section 4.2.3.7). In principle, the samples are incubated with radiolabelled OA and the components required for the enzymatic reaction: ATP, Mg^{2+}, CoA. The acyl-CoA-synthetases catalyze the esterification of CoA with oleic acid. Phase partitioning of oleic acid and the amphipathic oleoyl-CoA is achieved by heptane extraction and the produced oleoyl-CoA is quantified by liquid scintillation counting. The ACS assay was performed according to the protocol in the method article 'Measurement of Long-Chain Fatty Acyl-CoA Synthetase Activity' (Fullekrug and Poppelreuther, 2016).

Usually, the basic material was a standard cell pellet à 1 x 10^6 cells (see section 4.2.2.5). The cell pellet was lysed in KTx buffer (130mM KCl, 25mM Tris-HCl, pH 7.4, 1% Tx-100) for 30 min and incubated on ice. For complete solubilization of ACSL enzymes, the lysate was gently mixed by pipetting up and down after 10 and 20 min during this incubation time. A solubilization efficiency of > 90 % was verified for wt ACSL3, GFP-ACSL3 and GFP-ER-ACSL3 by Western Blot analysis. The lysate was centrifuged at 10,000 g and 4 °C for 5 min before 180 µL of the supernatant was transferred to a fresh tube. During the whole preparation the lysates were handled on ice to prevent proteolysis. The ACS activity was determined in triplicates for each sample. Ten microliter of lysate were transferred to a 1.5 mL tube and incubated in a heatable shaker with 90 µL labelling mix (100 mM Tris pH 7.4, 5 mM $MgCl_2$, 200 µM DTT, 10 mM ATP, 0.1 % Triton X-100, 20 µM ^{14}C-OA, 200 µM CoA) at 30 °C and 300 rpm for exactly 10 min. As a negative control, 10 µL lysate were incubated in labelling mix lacking CoA in order to calculate the background esterification of OA (minus CoA control). The reaction was stopped with 0.6 mL Dole's solution (400 mL isopropanol, 100 mL heptane, 10 mL concentrated sulphuric acid). The polar oleoyl-CoA molecules were separated from the unpolar unreacted molecules by heptane extraction. For this purpose, 250 µL water and 400 µL heptane was added. The tubes were vortexed and centrifuged at 16,000 x g for 1 min to achieve phase separation. The upper phase was removed and 600 µL heptane was added and the

extraction steps were repeated for 4 times resulting in the polar bottom phase (in total 600 µL) containing the converted labelled product.

For scintillation counting, 20 µL labelling mix was measured as triplicate in each 4 mL LSC cocktail. For the samples, 200 µL of the polar phase, corresponding to fatty acyl-CoA, was mixed in 4 mL LSC cocktail. The vials were vortexed thoroughly and measured with a Wallac Scintillation counter. The protein content in the cell lysates was quantified by a BCA assay in order to normalize the ACS activity to the protein content (see section 4.2.3.6).

The cpm measured in the labelling mix were taken into account to calculate the total radioactivity for each incubation. Considering that 1800 pmol OA were contained in each incubation, the amount of OA in the labelling mix corresponding to one cpm was calculated as nmol/cpm. The average of the background value (minus CoA control) was subtracted from the cpm numbers of the samples and these values were multiplied with the factor 3 to obtain the total cpm in the whole extract. The amount of oleoyl-CoA in the samples was calculated by multiplying the total cpm of the samples with the value for pmol/cpm in the labelling mix. Considering the total protein content in each incubation and the incubation time in the assay, the specific fatty acyl-CoA synthetase activity was calculated as pmol oleoyl-CoA/µg protein/min.

For the determination of the ACS activity in the subcellular fractions, the amount of samples had to be increased from 10 µL to 50 µL for fraction 1 and 2. For the protein-rich fractions 3 and 4, 20 µL of each fraction was diluted with 30 µL sucrose buffer A. In order to keep a total volume of 100 µL in the assay, the concentrations of the components in the labelling mix were adjusted by decreasing the amount of water and 50 µL labelling mix instead of 90 µL was added to each sample. For the negative control, 20 µL of subcellular fraction was diluted in 30 µL sucrose buffer A and incubated with 1 µL water and 49 µL labelling mix without CoA. The ACSL3 content in the fractions was quantified by Western Blot analysis (see section 4.2.3.1) to relate the ACS activity to the ACSL3 amount.

4.2.3.3 Radiolabelling of lipid species by ^{14}C-acetate and ^{14}C-OA incorporation

The lipid species in the cells were radiolabelled by incubation with a radiolabelled substrate in order to investigate the lipid synthesis. Endogenous lipid synthesis was investigated using ^{14}C-acetate as radiolabelled substrate. Acetate is taken up into the cells, where it is activated to acetyl-CoA and carboxylated to malonyl-CoA by the acetyl-CoA carboxylase. Malonyl-CoA is the substrate required for fatty acid synthesis that is catalyzed by the fatty acid synthase

(FAS). The FAS is a multienzyme complex carrying out all reactions that are necessary for the generation of saturated even-numbered fatty acids. In principle, the fatty acids are synthesized by elongation of malonyl-CoA by two carbon atoms originating from acetyl-CoA (Rehner and Daniel, 2010). The lipid synthesis under conditions of exogenous fatty acid supply was analyzed using ^{14}C-OA as radiolabelled substrate. The ^{14}C-OA is taken up into the cells and incorporated as building blocks into various lipid species. Following the radiolabelling, the cellular lipid species were extracted by Folch lipid extraction (see section 4.2.3.4) and the lipid species were analyzed by thin layer chromatography (see section 4.2.3.5). If OA supplementation in the provided growth medium influences the lipid metabolism was analyzed by a double approach in the ^{14}C-acetate and ^{14}C-OA labelling assays. Cells were either pre-incubated in standard growth medium or in standard growth medium supplemented with 600 µM OA bound to 100 µM bovine serum albumin (BSA) for 16 h before the labelling was conducted. This approach was of great importance comparing the GFP-ACSL3 and the GFP-ER-ACSL3 expressing cells, because under OA supplementation, wt ACSL3 and GFP-ACSL3 translocate to the lipid droplets. In the GFP-ER-ACSL3 expressing cells this translocation is not possible, because the ER-ACSL3 is trapped in the ER due to its transmembrane domain. Therefore, an OA pre-incubation was hypothesized to increase potential differences between the GFP-ACSL3 and GFP-ER-ACSL3 expressing cells and allow to draw futher conclusions about the importance of ACSL3 localization.

The cells were seeded in 12-well plates in a number of 80,000 cells/well. The labelling mixes were prepared and added to the cells. Tables 4-7 specifies the composition of the applied ^{14}C-OA mixes containing different OA concentrations depending on the experimental conditions. The ^{14}C-acetate labelling was carried out at a final concentration of 5 µM.

As a biochemical correlate of the lipid droplet biogenesis assay, the lipid species in starved cells were radiolabelled with ^{14}C-OA for 20 min or 3 h.

The lipolysis assay aimed to investigate the degradation of lipids under conditions of nutrient depletion. Therefore, the cells were labelled in ^{14}C-OA following a period of incubation in lipolysis medium (100 µM fatty acid free BSA, 1 mM sodium pyruvate, 1x non-essential amino acids, 4.5 g/L glucose, without FCS). The lipid species were analyzed in the same manner like after the ^{14}C-acetate and ^{14}C-OA incorporation assay.

***Table 4*: ^{14}C-OA labelling mix (3h labelling).**

180 µM ^{14}C-OA labelling mix (10 mL)		
Specific activity: 0.3 Ci/mol		Final concentration
25.3 µL	Cold oleic acid stock solution [71 mM in chloroform]	180 µM
5.4 µL	^{14}C-oleic acid	
86.4 µL	NaOH [25 mM]	216 µM
188 µL	Fatty acid free BSA [1600 mM]	30 µM
9726 µL	FCS-free standard growth medium	

***Table 5*: ^{14}C-OA labelling mix (20 min labelling after starvation).**

600 µM ^{14}C-OA labelling mix (10 mL)		
Specific activity: 0.45 Ci/mol		Final concentration
84.0 µL	Cold oleic acid stock solution [71 mM in chloroform]	600 µM
27.0 µL	^{14}C-oleic acid	
288.0 µL	NaOH [25 mM]	720 µM
625.0 µL	Fatty acid free BSA [1600 mM]	100 µM
9087 µL	FCS-free standard growth medium	

Table 6: **^{14}C-OA labelling mixes used in lipolysis assay for wtCOS-7, GFP_A3ko and GFP-AA-ACSL3 cells.**

600 µM ^{14}C-OA labelling mix (10 mL)		
Specific activity: 0.6 Ci/mol		Final concentration
83.7 µL	Cold oleic acid stock solution [71 mM in chloroform]	600 µM
36 µL	^{14}C-oleic acid	
288 µL	NaOH [25 mM]	720 µM
625 µL	Fatty acid free BSA [1600 mM]	100 µM
9078 µL	FCS-free standard growth medium	
120 µM ^{14}C-OA labelling mix (10 mL)		
Specific activity: 0.6 Ci/mol		Final concentration
17.7 µL	Cold oleic acid stock solution [71 mM in chloroform]	120 µM
7.2 µL	^{14}C-oleic acid	
57.6 µL	NaOH [25 mM]	144 µM
125 µL	Fatty acid free BSA [1600 mM]	20 µM
9817 µL	FCS-free standard growth medium	
60 µM ^{14}C-OA labelling mix (10 mL)		
Specific activity: 0.6 Ci/mol		Final concentration
8.4 µL	Cold oleic acid stock solution [71 mM in chloroform]	60 µM
3.6 µL	^{14}C-oleic acid	
28.8 µL	NaOH [25 mM]	72 µM
63 µL	Fatty acid free BSA [1600 mM]	10 µM
9909 µL	FCS-free standard growth medium	
20 µM ^{14}C-OA labelling mix (10 mL)		
Specific activity: 0.6 Ci/mol		Final concentration
2.8 µL	Cold oleic acid stock solution [71 mM in chloroform]	20 µM
1.2 µL	^{14}C-oleic acid	
9.6 µL	NaOH [25 mM]	24 µM
21 µL	Fatty acid free BSA [1600 mM]	3.33 µM
9970 µL	FCS-free standard growth medium	

Table 7: **^{14}C-OA labelling mixes used in lipolysis assay for wtCOS-7, GFP-ACSL3, GFP-ER-ACSL3(L) and GFP-ER-ACSL3(H) cells.**

120 µM ^{14}C-OA labelling mix (10 mL)		
Specific activity: 0.3 Ci/mol		Final concentration
17.7 µL	Cold oleic acid stock solution [71 mM in chloroform]	120 µM
7.2 µL	^{14}C-oleic acid	
57.6 µL	NaOH [25 mM]	144 µM
125 µL	Fatty acid free BSA [1600 mM]	20 µM
9817 µL	Standard growth medium	
300 µM ^{14}C-OA labelling mix (10 mL)		
Specific activity: 0.3 Ci/mol		Final concentration
17.7 µL	Cold oleic acid stock solution [71 mM in chloroform]	300 µM
7.2 µL	^{14}C-oleic acid	
57.6 µL	NaOH [25 mM]	360 µM
125 µL	Fatty acid free BSA [1600 mM]	50 µM
9817 µL	Standard growth medium	
450 µM ^{14}C-OA labelling mix (10 mL)		
Specific activity: 0.3 Ci/mol		Final concentration
63.2 µL	Cold oleic acid stock solution [71 mM in chloroform]	450 µM
13.5 µL	^{14}C-oleic acid	
216.0 µL	NaOH [25 mM]	540 µM
469.0 µL	Fatty acid free BSA [1600 mM]	75 µM
9315 µL	Standard growth medium	

4.2.3.4 Folch extraction of lipids

The lipids of the cells used in the ^{14}C-OA incorporation assay, ^{14}C-acetate incorporation assay and lipolysis assay were extracted by Folch lipid extraction.

The cells in the 12-well plates were washed twice with 0.9 mL PBS and then lysed in 600 µL methanol:chloroform 2:1 for 5 min. Then the lipids were transferred into 2 mL reaction tubes (chloroform-resistant) containing 600 µL chloroform. The tubes were vortexed thoroughly and centrifuged at 16,000 x g for 5 min. The supernatant was transferred into a fresh 2 mL tube containing 300 µL water. The tubes were vortexed thoroughly and centrifuged at 16,000 x g for 5 min to obtain a clear phase separation. Then the bottom hydrophobic phase (about 800 µL) was transferred into a fresh 2 mL tube and an aliquot of 50 µL was mixed with 4 mL LSC cocktail for liquid scintillation counting.

4.2.3.5 Thin layer chromatography

The lipid extract obtained from Folch lipid extraction (see section 4.2.3.4) was used for thin layer chromatography (TLC) to get insight into the proportion of the intracellular lipid species.

TLC is a widely used method to separate components of a sample according to their subdivision between two phases. The mixture of lipids is spotted on a plate covered with a sorbent material, in this case an aluminium plate covered with a layer of silica gel, which is called the stationary phase. The plate is put in a chamber filled with a running solvent mix, the mobile phase. The running solvent mix is soaked upwards the plate. Depending on their chemical properties, the lipid species are strongly adhered to the stationary phase or associate to the mobile phase and move along the plate resulting in a separation of the different lipid species (Hegyi et al., 2013; Kremer and Bannwarth, 2014).

The TLC plates were labelled and put in a TLC chamber filled with 100 mL methanol for a cleaning pre-run. When the methanol clearly passed a distance of 10 cm, the plates were air-dried for 3 min and then dried in the oven at 105 °C for 1 h to get rid of residual humidity.

The chloroform of the Folch lipid extracts was evaporated and the lipid were sedimented in a speed vacuum centrifuge for 1 h. The lipid pellet was resuspended in 10 µL methanol:chloroform 2:1 and spotted as 0.5 µL aliquots on the TLC plate. The TLC chamber was pre-equilibrated for 1.5-4 h by pouring the running solvent mix (35 mL chloroform, 40 mL ethanol, 9 mL water, 35 mL trimethylamine) into the chamber and depositing one filter paper at the front and the back side of the chamber to allow complete saturation of the air with the evaporating solvent mix. The running mix is called ‘O-mix’, because it clearly separates the non-esterified fatty acids from the polar phospholipids and the unpolar neutral lipids. After pre-equilibration of the chamber, the TLC plate was placed in the chamber for approximately 40 min, until the running front reached a distance of 10 cm. Then the plate was air-dried for 1 h under the extractor hood and placed in a phosphorimaging cassette. The exposition time in the phosphorimaging cassette ranged from 16-136 h depending on the incorporated cpm (counts per minute) in the samples.

The phosphorimaging plate was scanned in the phosphorimaging reader *BAS-1500* and the signal was evaluated with the software AIDA (Advanced Image Data Analyzer) version 4.27.039. The lipid species were identified according to retention factors calculated in previous work. For details see Milger et al. (2006) or the PhD thesis from Eva-Maria Küch (Küch, 2012). The lipid species identified were TG, cholesterol (CH), non-esterified fatty acids (FA), PE,

phosphatidylinositol (PI), phosphatidylserine (PS), PC and sphingomyelin (SM). By densitometry, the AIDA software determined the area under the curve (AUC) of each lipid species and calculated the percentage of total lipids. The absolute amounts of each lipid species were calculated as pmol/µg protein using the percentage given by the software, the substrate incorporation values obtained from liquid scintillation counting and the protein content determined in the Bradford assay. From the total OA contained in the labelling mix, only a small percentage was radiolabelled. The experiment was based on the assumption, that the cells did not distinguish between conventional and radiolabelled OA and metabolize both types equally. However, in the analysis only the radiolabelled OA is included. Therefore, the calculated numbers only represent the amounts of newly synthesized lipids, but do not indicate the amounts of lipids already present in the cells before the labelling.

4.2.3.6 Protein quantification by photometric assays

Bradford assay

The protein content of mock-treated cells was determined by Bradford protein assay for the ^{14}C acetate incorporation assay, ^{14}C-OA incorporation assay and the lipolysis assay.

The Bradford protein assay is a photometric technique to measure the protein content in a sample. It was developed by Marion M. Bradford and applies the dye Coomassie Brilliant Blue G250. Coomassie Brilliant Blue G250 binds to proteins forming a blue colored complex that can be measured at a wavelength of 595 nm (Bradford, 1976).

The cells seeded in 12-well plates (see section 4.2.3.3) were washed with 1 mL PBS. The cells were lysed in 250 µL 1 M NaOH and incubated at room temperature for 1 h. Subsequently, the lysates were transferred to a 1.5 mL tube and vortexed. A protein standard curve was generated by diluting BSA in NaOH in the concentrations of 0-0.5 µg/µL.

A volume of 10 µL lysate or standard solution was pipetted in a 96-well plate. BioRad Bradford reagent containing Coomassie Brilliant Blue G250 was diluted 1:5 in water and 200 µL was added to each well with a multichannel pipette. After 5-10 min of incubation at room temperature the absorbance was measured at a wavelength of 595 nm with a photometer. For calculation of the protein concentrations in the lysates, the absorbance of the blank value was subtracted from the other values and a linear regression curve was generated from the data of the BSA standard to calculate the protein content in the samples.

BCA assay

The total protein was quantified in the samples used in the ACS assay (section 4.2.3.2) by a bicinchoninic acid (BCA) assay in order to normalize the ACS activity to the protein content.

The BCA assay is a photometric method to quantify protein content in a sample. The functional principle of the BCA assay is based on the biuret reaction of proteins with bivalent copper ions in an alkaline environment. The peptide bonds of the proteins bind the bivalent copper ions resulting in monovalent copper ions. BCA forms a blue-purple colored complex with the monovalent copper ions, which can be measured at a wavelength of 562 nm (Smith et al., 1985).

A BSA standard curve including the concentrations 0-10 µg/25 µL was prepared. For the samples, the KTx lysates were diluted 1:5 in order to hit the linear range of the standard curve. A volume of 25 µL standard solution or diluted sample was pipetted into a 96-well plate and 200 µL of 4 % $CuSO_4$ diluted in BCA in a ratio of 1:40 was added with a multichannel pipette. The air bubbles were gently removed with a hairdryer and the plate was incubated at 37 °C for 30 min. The absorption was measured in a photometer at a wavelength of 562 nm. For calculation of the protein concentration, the absorption of the blank was subtracted from the other values and a linear regression curve was generated from the data of the BSA standards to calculate the protein content in the samples.

4.2.3.7 Subcellular fractionation

Subcellular fractionation was performed using a sucrose gradient to collect the proteins of different subcellular compartments in different fractions. The aim of the subcellular fractionation was to investigate ACSL3 amount and ACS activity in the obtained fractions in order to reveal if the ACS activity of lipid droplet-associated and ER-associated ACSL3 is different. See Poppelreuther et al. (2018) for further details about the technical approach.

A431 cells were grown in six 145 mm cell culture dishes. When they reached almost complete confluency, three dishes were treated with standard growth medium and the other three dishes with standard growth medium supplemented with 600 µM OA bound to 100 µM BSA for 24 h. In order to prevent proteolysis, all further steps were performed on ice or at 4 °C. The supernatant was removed and 3 mL ice-cold PBS was added into each dish. The cells of all three equally treated dishes were collected in a 50 mL falcon tube using a rubber policeman. Each dish was flushed two times with 6 mL ice-cold-PBS to prevent loss of material. The cells were centrifuged at 800 x g for 5 min and the supernatant was discarded. Then the cells were resuspended in 1 mL ice-cold sucrose buffer A (50mM Tris/HCl pH 7.4, 20 mM sucrose) and

transferred in a 2 mL reaction tube. A homogenate was prepared passing the cells through a G22 needle for 35 times and a tight dounce homogenizer for 25 times. The lysate was sedimented at 1000 x g for 10 min. A volume of 1 mL of the postnuclear supernatant was mixed with 1 mL sucrose buffer B (50mM Tris/HCl pH 7.4, 2 M sucrose) and transferred in a 4 mL ultracentrifuge tube. The suspension was gently overlayed with 2 mL sucrose buffer A and ultracentrifugation was carried out in a SW41 Ti rotor at 100,000 x g for 3 h. Four fractions of each 1 mL were collected from the top to the bottom with a G22 needle. The two upper fractions contained the lipid droplet fraction. The two bottom fractions contained the cytosolic and membrane components.

The obtained fractions were further analyzed by Western Blot (see section 4.2.3.1) and ACS assay (see section 4.2.3.2).

4.2.3.8 Lipid droplet staining with monodansylpentane (MDH)

MDH is a lipid droplet marker emitting blue-fluorescence, which makes it a good alternative in experimental setups simultaneously applying green or red fluorescing reporter molecules, like LD540, GFP or mcherry (Yang et al., 2012).

Staining of lipid droplets was done in cells seeded on cover slips and fixated in 4 % PFA for 20 min. MDH (purchased from Abgent, named as AUTOdot autophagy visualization dye) was diluted 1:1000 in PBS to a final concentration to 100 µM and a droplet 20 µL was put on a piece of parafilm attached to the work bench. The cover slips with the fixated cells were put onto the droplet with the cells facing the MDH solution. Drying due to evaporation was prevented by covering the cells with a lid from a cell culture dish. Aluminium foil was put on top to prevent bleaching. The cells were incubated in MDH for 30 min at room temperature before they were washed 3-4 times in PBS and mounted in mowiol. The MDH dilution was stored at 4 °C and was used up within 4 weeks after preparation.

4.2.3.9 Molar quantification of ACSL3

Recombinant ACSL3 bound to glutathione S-transferase (GST-ACSL3) was isolated from a bacterial supernantant, which had already been produced by a former lab member. The bacterial supernatant was generated from *E. coli BL21*, which had been transformed with a GST-ACSL3.pGEX-2T vector containing the human ACSL3 complementary DNA fused to GST. Isolation was done with glutathione sepharose 4B beads, which bind to the GST-ACSL3 in the bacterial supernatant. See Poppelreuther et al. (2018) for a detailed description of the procedure.

For pre-equilibration, 50 µL glutathione sepharose 4B beads were washed in TNEX buffer (150 mM NaCl, 20 mM Tris/HCl pH 7.4, 1 mM EDTA, 0.2 % w/v Triton X-100, 1 mM DTT) and sedimented at 1,500 x g for 2 min at 4°C. The supernatant was removed and 1.5 mL bacterial supernatant was added to the beads. The preparation was incubated at 4 °C for 3 h and centrifuged at 1,500 x g for 2 min. The supernatant was removed and the beads were washed twice in TNEX buffer and twice in TNE buffer (150 mM NaCl, 20 mM Tris/HCl pH 7.4, 1 mM EDTA, 1 mM DTT) to get rid of the residual Triton X-100. The preparation was again centrifuged at 1,500 x g for 2 min and the supernatant was removed. The remaining beads were resuspended in 2x SDS-PAGE sample buffer, boiled at 95 °C for 5 min. Following a sedimentation step, the supernatant was collected and flash frozen in liquid nitrogen.

The amount of GST-ACSL3 contained in the preparation was quantified by Western Blot analysis. For this purpose, an aliquot of the GST-ACSL3 preparation and different amounts of BSA were loaded on an 8 % SDS-polyacrylamide gel. The gel preparation and electrophoresis was performed according to the procedure described in section 4.2.3.1. The proteins were stained with Coomassie brilliant blue R250 staining solution (0.1 % w/v Coomassie brilliant blue R250 mixed in 300 mL methanol, 100 mL acetic acid and 600 mL water). After washing in destaining solution (30 % v/v methanol, 10 % v/v acetic acid in water), the gel was scanned. The concentration of GST-ACSL3 in the quantification was determined by densitometric analysis using ImageJ version 2.0.0.

ACSL3 in A431 cells was quantified by Western Blot analysis. Standard cell pellets were generated (see section 4.2.2.5) and boiled in 4x O-buffer for 5 min. Aliquots of the total cell lysate were loaded on an 8 % SDS-polyacrylamide gel as triplicate. GST-ACSL3 was diluted to appropriate concentrations to generate a standard row, which was likewise loaded on the gel. Gel preparation, electrophoresis, semi-dry Western Blot and immunostaining were performed like described in section 4.2.3.1. The membranes were scanned usind an Odyssey Classic 900 infrared scanner. The fluorescence in the lanes was quantified by the LI-COR software Image Studio 4.0.21. The amount of endogenous ACSL3 in the A431 cells was calculated considering the molecular weight difference between endogenous ACSL3 and GST-ACSL3 as 1 ng GST-ACSL3 (M=106.9 kg/mol) corresponds to 0.752 ng of endogenous ACSL3 (M=80.42 kg/mol).

In order to calculate the metabolic capacity of LD-associated ACSL3 the average protein concent in A431 cells was calculated by dissolving standard cell pellets (see section 4.2.2.5) in non reducing lysis buffer (62 mM Tris-HCl pH 6.8, 2 % SDS, 10 % w/v glycerol) and

performing a BCA assay (see section 4.2.3.6). Please note, that the protein quantification in A431 cells was done by a former lab member.

5. Results

Context of applied cell lines as biological system

Most experiments described in this work were done with COS-7 cells. This cell line was advantageous for the current experiments, because their flat morphology enables to investigate subcellular structures in microscopy. COS-7 cells have a high endogenous ACSL3 expression, which makes them a suitable biological system for manipulation of ACSL3 levels to study the metabolic function. Moreover, COS-7 cells can be easily modified, because they efficiently express exogenous DNA.

COS-7 cells which had been depleted of ACSL3 by RNA interference (A3-RNAi cells) were used to get deeper knowledge of the relevance of ACS activity for lipid synthesis. Since the knockdown of ACSL3 still held a remaining ACSL3 quantity of 15 %, residual enzyme activity might mask effects that might be observed in a system devoid of ACSL3. Therefore, a knockout of ACSL3 was produced using the CRISPR/Cas9 method to completely diminish the cells of ACSL3. Via retroviral transduction new cell lines were generated which were rescued with differently modified enzyme variants: GFP-ACSL3, GFP-ER-ACSL3 and GFP-AA-ACSL3. All enzyme variants were fused to GFP in order to monitor the expression and the localization of the proteins. The AMP-binding domain of GFP-AA-ACSL3 was mutated and therefore this protein lacked any ACS activity. The GFP-AA-ACSL3 expressing cells were compared to the ACSL3-knockout cells (GFP_A3ko) to obtain information about ACSL3 functions unrelated to ACS activity. The GFP-ER-ACSL3 contained the transmembrane domain of the ER-localized protein FATP4, an ER localized protein (Milger et al., 2006), and thus was excluded from the LD. The lipid metabolism of the GFP-ER-ACSL3 expressing cells was compared to the GFP-ACSL3 expressing cells to investigate the physiologic role of ACSL3 localization. The approach included investigations about lipid synthesis under normal growth conditions as well as fatty acid supplementation, lipolysis and LD biogenesis. For the experiments investigating LD biogenesis an additional marker for LD, A3Nt-mcherry, was inserted in the cells to look at the newly formed LD after starvation. *Figure 5* gives an overview of the generated cell lines exhibiting an endogenous ACSL3-knockout. In addition, A431 cells were applied as an example for a human cell line to analyze ACSL3 in subcellular fractions and by dSTORM microscopy.

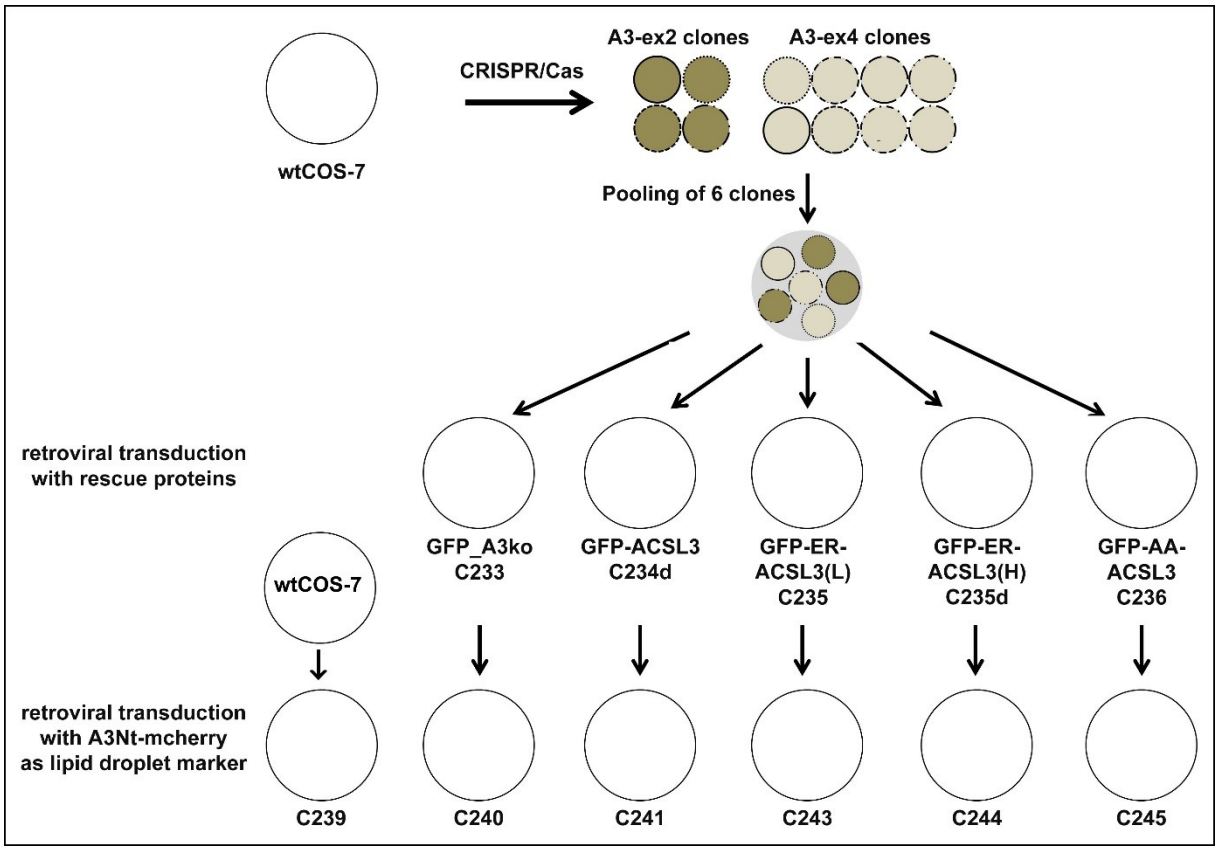

Fig. 5: **Overview of the generated cell lines exhibiting an endogenous ACSL3-knockout.** Using the CRISPR/Cas9 technique an ACSL3-knockout was generated in wtCOS-7 cells. The cells were transfected with two CRISPR plasmids (A3-ex2 and A3-ex4) and single cell clones were grown (shown in green and grey). After confirmation of the ACSL3-knockout, three clones generated from each CRISPR plasmid were pooled. Retroviral particles were applied to stably transduce the pooled ACSL3-knockout cells with modified ACSL3 enzyme variants: GFP-ACSL3, GFP-ER-ACSL3 and GFP-AA-ACSL3. In order to obtain cell lines with a low and high expression level of GFP-ER-ACSL3, the cells were transduced with different amounts of retroviral particles (GFP-ER-ACSL3(L), C235; GFP-ER-ACSL3(H), C235d). As a knockout control, cells were transfected with GFP only. The modified cell lines were transduced a second time with A3Nt-mcherry which was required as a LD marker in the lipid droplet biogenesis assay. The term CXXX designates the internal number of the generated cell lines.

5.1 Cell proliferation and lipid synthesis in ACSL3 knockdown cells

5.1.1 ACSL3 knockdown cells were increased in growth rate and less sensitive to cerulenin

Previous experiments in our research group revealed that ACSL3 depletion causes a significant decrease in fatty acid uptake in COS-7 cells (manuscript submitted, shared first authorship). It has been hypothesized, that this decrease in fatty acid uptake might lead to a decreased membrane phospholipid synthesis and thus decreased cell growth. The aim of the cell proliferation assay was to compare the cell growth of control cells and ACSL3 knockdown cells under standard culture conditions. Cell proliferation was investigated using MTT. MTT is metabolized by mitochondrial dehydrogenases in living cells resulting in the purple colored

product formazan, which can be measured in a photometer. Furthermore, fatty acid synthesis inhibition using cerulenin, a fatty acid synthase inhibitor, was applied in order to analyze how the cells depleted from ACSL3 handle a repression of endogenous fatty acid synthesis compared to control cells and how this impacts cell growth.

Four hours after seeding the absorption measured at 595 nm was not significantly different between the control cells and the ACSL3 knockdown cells (A3-RNAi cells) (*figure 6*). This confirmed, that the same number of cells was initially seeded, which was fundamental for the subsequent analysis of cell proliferation. Unexpectedly, after 24 of seeding, the A3-RNAi cells were significantly increased in cell number by 13 %. It was hypothesized, that the fatty acid synthase might be upregulated in the A3-RNAi cells leading to increased proliferation. Therefore, the cell proliferation was measured after treatment with different concentrations of cerulenin, a fatty acid synthase inhibitor. The dose of 2 µg/mL led to a small, insignificant reduction of cell number compared to standard growth medium lacking cerulenin. The dose of 4 µg/mL led to significant reduction in cell growth in the control cells, but not in the A3-RNAi cells. The dose of 6 µg/mL caused significant cell death in control and A3-RNAi cells with the A3-RNAi cells still having a higher cell number than the control cells (*figure 6*).

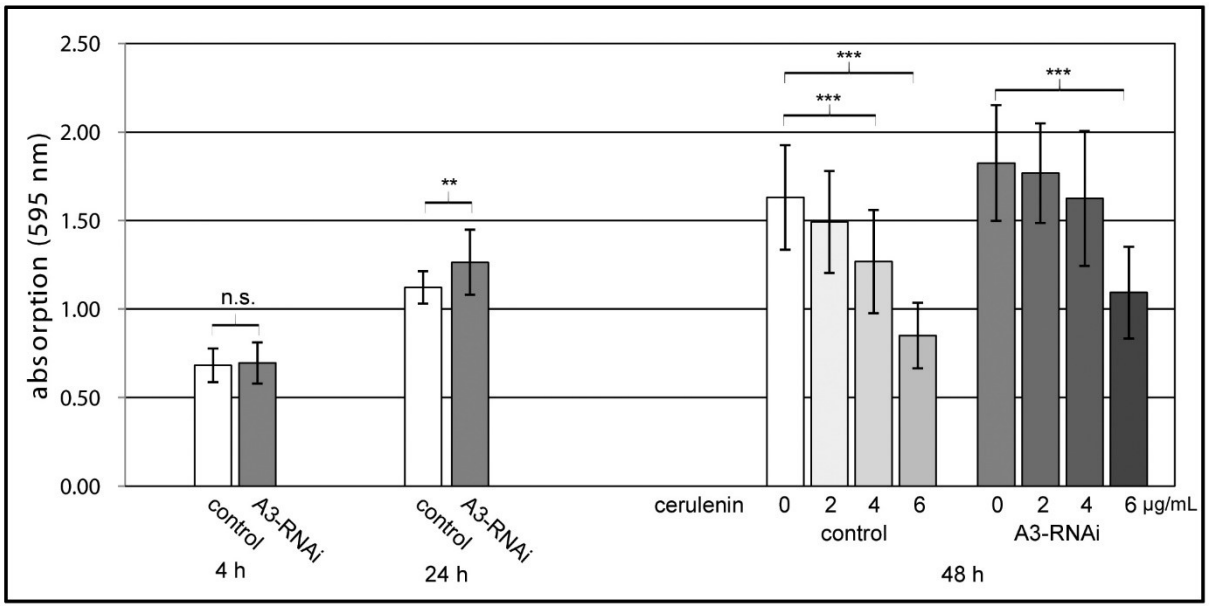

***Fig. 6*: Cell proliferation assay of A3-RNAi and control cells based on formazan formation (MTT cell viability assay).** Same amounts of cells were seeded. Cell proliferation and viability was assessed 4 h, 24 h and 48 h after seeding. Cerulenin was added after 24 h in the concentration 2 µg/mL, 4 µg/mL and 6 µg/mL to investigate, if the fatty acid synthase was upregulated in the A3-RNAi cell leading to higher cell proliferation. Statistical analysis was performed using the Student's T-Test for unequal variances. The level of significance is indicated as follows: $p < 0.01$ (**), $p < 0.001$ (***), not significant (n.s.). n = 3 independent experiments; error bars are SD. (Manuscript submitted for publication, shared first authorship).

5.1.2 ACSL3 knockdown cells showed decreased triglyceride synthesis favouring phospholipid synthesis

Based on the results of the cell proliferation assays the A3-RNAi cells were hypothesized to have a higher phospholipid synthesis to provide membrane lipids for increased cell growth. This was investigated by incubating the cells in radiolabelled acetate, to obtain information about the lipid species synthesized from endogenously synthesized fatty acids.

The TG synthesis in the A3-RNAi cells was significantly reduced by 49 % and phospholipid synthesis was strongly increased, especially for PC (+69 %) and SM (+68 %) (*figure 7*).

The observed differences in lipid synthesis between the A3-RNAi cells and the control cells could be caused by a specific lack of ACS activity on lipid droplets or by a general lack of cellular ACS actvivity. Therefore, A3-RNAi cells rescued with FATP4 were applied to examine, if ACSL3 has a unique function concerning lipid synthesis or if another ACS enzyme can compensate for the ACSL3 knockdown. The ACSL3-RNAi.FATP4 cell line had already been generated in the lab and was suitable, because, FATP4 is an ACS family member localized on the ER but not on LDs and efficiently activates OA (Milger et al., 2006; Watkins, 2008). Analysis of lipid synthesis in these cell lines showed, that FATP4 was not able to compensate for the strong decrease in TG synthesis, whereas phospholipid synthesis was partially decreased to the level of the control cells.

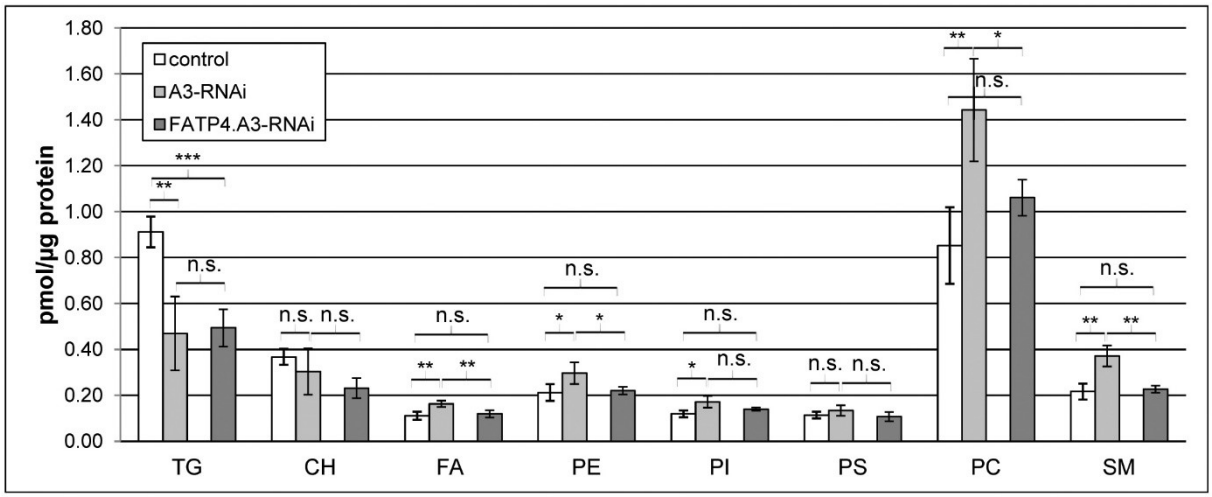

***Fig. 7*: Metabolism of endogenously synthesized fatty acids in A3-RNAi and FATP4 rescue cells.** Synthesized lipids were labelled with ^{14}C-acetate used as substrate for fatty acid synthesis. The lipids were extracted by Folch extraction and quantified by TLC. TG, triglycerides; CH, cholesterol; FA, non-esterified fatty acids; PE, phosphatidylethanolamine; PI, phosphatidylinositol; PS, phosphatidylserine; PC, phosphatidylcholine; SM, sphingomyelin. Statistical analysis was performed using the Student's T-Test for unequal variances. The level of significance is indicated as follows: $p < 0.05$ (*), $p < 0.01$ (**), $p < 0.001$ (***), not significant (n.s.). n = 4 independent experiments; error bars are SD. (Manuscript submitted for publication, shared first authorship).

5.2 Establishment of endogenous ACSL3-knockout in COS-7 cells and rescue with modified ACSL3 variants

5.2.1 Western Blot and immunofluorescence confirmed ACSL3-knockout

Prior to experiments investigating the metabolism of the ACSL3-knockout cells, the ACSL3-knockout in the clones was confirmed by Western Blot analysis (*figure 8*) and indirect immunofluorescence (*figure 9*). Total lysates of all raised clones obtained after transfection with the CRISPR plasmids A3-ex2 (JF1052) and A3-ex4 (JF1053) were screened by Western Blot analysis. WtCOS-7 cells and cells transfected with a CRISPR plasmid leading to a knockout of the FAS enzyme complex but not ACSL3 (CRISPR/Cas controls) were analyzed as positive controls. The wtCOS-7 cells and the CRISPR/Cas controls clearly showed a band between the 95 kDa and 55 kDa ladder representing endogenous ACSL3 (82 kDa), whereas the ACSL3-knockout clones were lacking this band. The CRISPR/Cas9 method was 100 % successfull, since all grown clones featured an ACSL3-knockout. Based on these results, six clones were selected (see section 4.2.2.8) for pooling in order to level out potential off-target effects. The pooled ACSL3-knockout cells were later transduced with GFP (GFP_A3ko cells) and checked for ACSL3-knockout by immunofluorescence (*figure 9*). The wtCOS-7 cells exhibited marked staining of ACSL3 surrounding the lipid droplets, whereas in the GFP_A3ko cells ACSL3 was not detected.

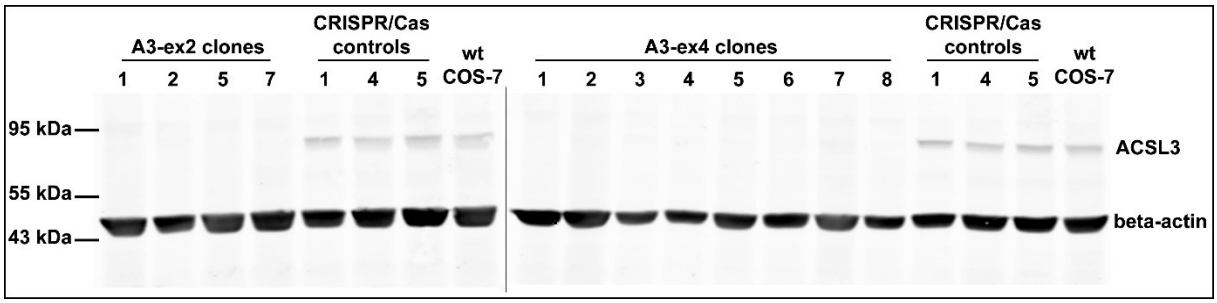

Fig. 8: **Western Blot analysis confirms knockout of ACSL3 in cloned cell lines.** ACSL3 was detected in total lysates with a polyclonal mouse αACSL3 antibody (J059d). Beta-actin (β-actin) was detected as a reference protein for loading control using a monoclonal mouse αβ-actin antibody (J061). The CRISPR/Cas controls were clones transfected with a CRISPR plasmid with a guide RNA targeting FAS (internal plasmid number JF1054). The wtCOS-7 served as second control cell line to confirm the ACSL3-knockout. Please note, that the A3-ex4 clones were blotted on a second membrane (designated by the vertical line).

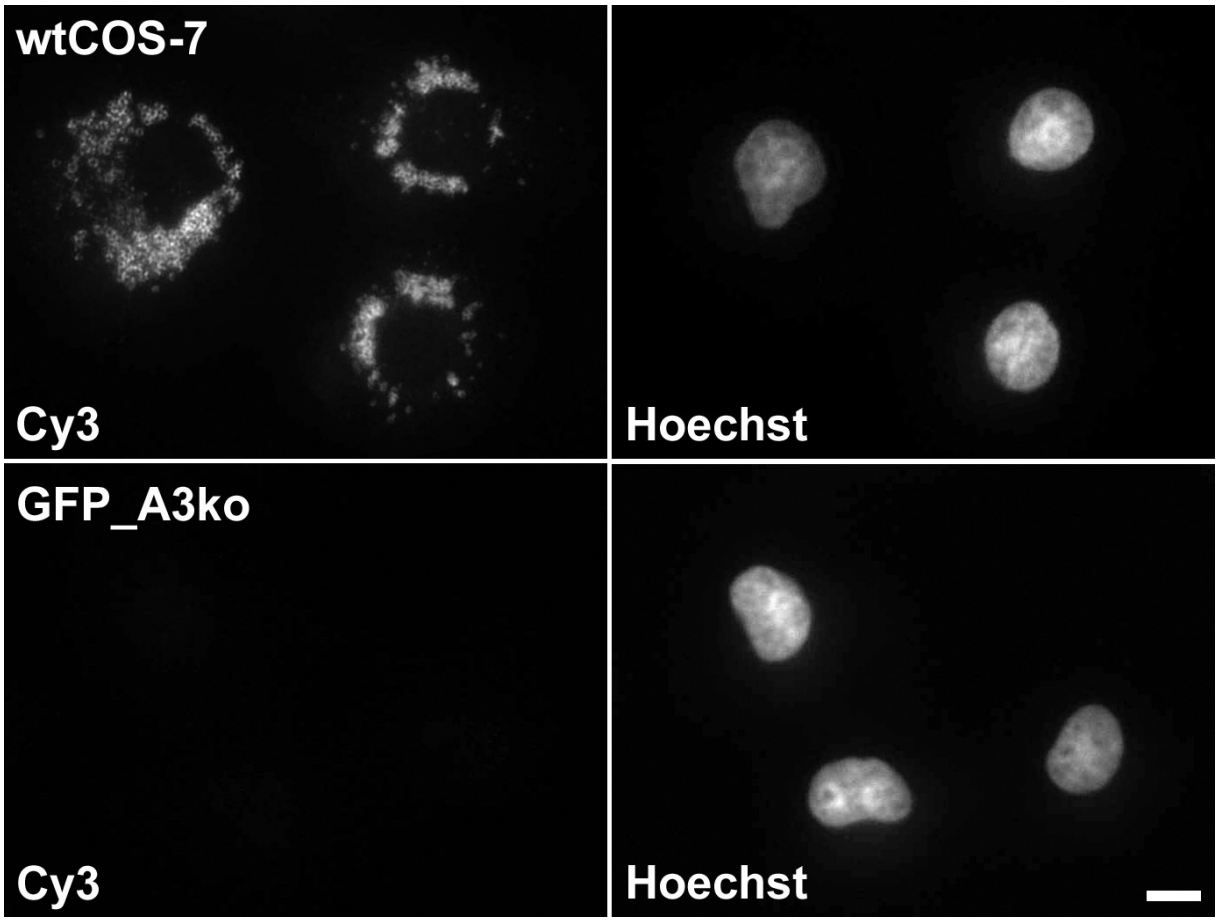

***Fig. 9*: Indirect immunofluorescence confirms knockout of ACSL3 in wtCOS-7 and GFP_A3ko cells.** The GFP_A3ko cells represent the pool of six ACSL3-knockout clones stably transduced with GFP. WtCOS-7 cells clearly showed lipid droplets stained by ACSL3 antibody, while the GFP_A3ko cells lacked ACSL3 protein surrounding lipid droplets. The cells were incubated in 600 µM OA o/n for 16 h. Endogenous ACSL3 was stained using polyclonal mouse αACSL3 antibody (J059d) and Cy3-conjugated αmouse antibody (J101). The nuclei were stained with Hoechst dye. The pictures were taken with an exposition time of 200 ms for Cy3 and 50 ms for Hoechst with 40x objective. Scale bar 10 µm.

5.2.2 Characterization of the ACSL3-knockout cells and rescue cell lines

5.2.2.1 Investigation of ACSL3 variant expression by Western Blot analysis

Total lysates from standard cell pellets (see section 4.2.2.5) were used for Western Blot analysis in order to determine the expression level of the ACSL3 enzyme variants in the transduced ACSL3-knockout cell lines (*figure 10A)*. The wtCOS-7 cells expressed endogenous ACSL3 (82 kDa) and the transduced cell lines expressed the ACSL3 enzyme variants, which had a higher molecular weight because they were fused to GFP and therefore moved slowlier in SDS-polyacrylamide gelelectrophoresis (GFP-ACSL3, 110 kDa; GFP-ER-ACSL3, 109 kDa; GFP-AA-ACSL3, 110 kDa). For the GFP_A3ko cells no ACSL3 band was detectable, because these cells held an endogenous knockout of the protein. The ACSL3 and β-actin signal was quantified using Image Studio Lite version 4.0.21 (LI-COR Inc., 2014) (*figure 10B*). The signal located on 82 kDa level of the GFP_A3ko cells was considered as measure for the background signal

and was subtracted from the ACSL3 signal of the other cell lines, before the ACSL3/β-actin ratio was calculated and normalized to the wtCOS-7 cells. GFP-ACSL3 was overexpressed by the factor 10.2. This value was flanked by the low and the high-expressing GFP-ER-ACSL3 cell lines with the factors 7.8 and 13.9. GFP-AA-ACSL3 was overexpressed by the factor 18.9.

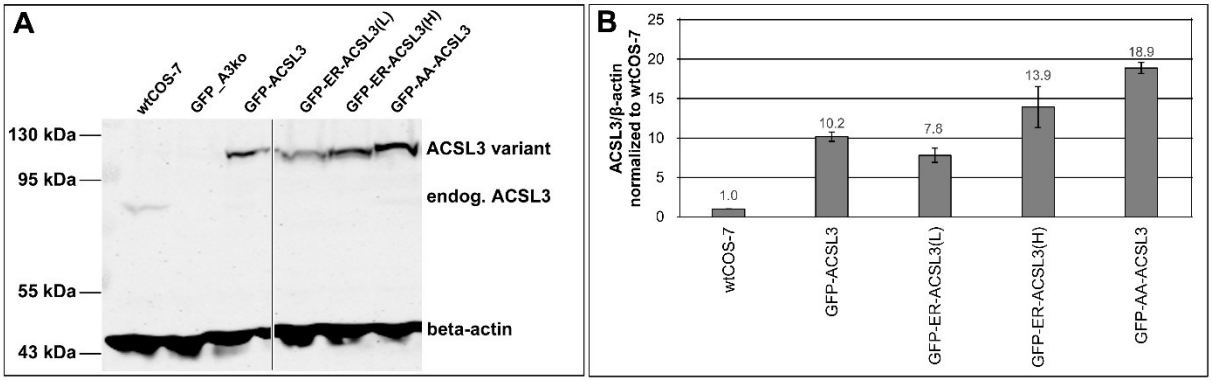

***Fig. 10*: Western Blot analysis showing the ACSL3 expression of the GFP_A3ko cells and the rescue cell lines. (A)** Endogenous ACSL3 (82 kDa) and the ACSL3 variants (GFP-ACSL3, 110 kDa; GFP-ER-ACSL3, 109 kDa; GFP-AA-ACSL3, 110 kDa) were detected in total lysates with a polyclonal mouse αACSL3 antibody (J059d). Beta-actin (β-actin) was detected as a reference protein for loading control using a monoclonal mouse αβ-actin antibody (J061). **(B)** The Western Blot signal was quantified using Image Studio Lite version 4.0.21 (LI-COR Inc., 2014). The signal at 82 kDa of the GFP_A3ko cells was considered as measure for the background signal and was subtracted from the ACSL3 signal values of the other cell lines. The ACSL3/β-actin ratio was calculated and normalized to the wtCOS-7 cells. n = 2 independent experiments including duplicates for each sample; error bars are SD.

5.2.2.2 Determination of ACS activity

The ACS activity in the cell lines was determined by an ACS assay (see *section 4.2.3.2*) and is shown in *figure 11*. The average ACS activity of the wtCOS-7 cells was 2.00 pmol oleoyl-CoA/min/µg protein. The ACSL3-knockout in the GFP_A3ko and GFP-AA-ACSL3 cells led to a significant decrease in ACS activity of 93 % and 96 %. There was no significant difference between the GFP_A3ko and the GFP-AA-ACSL3 cells. The GFP-ACSL3 expressing cells exhibited an ACS activity approximately 2.7-fold and the high GFP-ER-ACSL3 expressing cell line approximately 1.8-fold compared to wtCOS-7. The ACS activity in the low expressing GFP-ER-ACSL3 cell line was comparable to wtCOS-7.

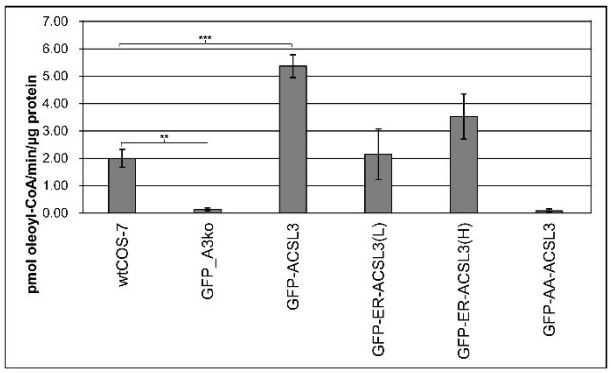

***Fig. 11*: Determination of the ACS activity in the GFP_A3ko cells and the rescue cell lines.** Detergent lysates generated from standard cell pellets were incubated with radiolabelled OA, ATP, Mg^{2+} and CoA. The unreacted OA was separated from the activated oleoyl-CoA by heptane extraction and the produced amount of oeloyl-CoA was measured in a liquid scintillation counter. Protein quantification in the KTx-lysate by BCA assay allowed calculation of the ACS activity as pmol oleoyl-CoA/min/µg protein. The ACS activity of the mutant variant GFP-AA-ACSL3 expressing cells was not significantly different from the ACS activity in the GFP_A3ko cells. The level of significance is indicated as follows: $p < 0.01$ (**), $p < 0.001$ (***). n = 3 independent experiments; error bars are SD.

5.2.2.3 Microscopy of subcellular localization of ACSL3 variants and lipid droplet morpohology

Microscopy was performed using an Olympus Bx41 microscope (see section 4.2.2.14 for details). Since the enzyme variants were fused to GFP, the expression level and the subcellular localization of the proteins could be monitored. Also GFP, expressed in the cytosol of the GFP_A3ko cells, was detected. The size and shape of intracellular lipid droplets was revealed by staining with MDH as a blue fluorescing lipid droplet marker (Yang et al., 2012).

The cells were examined under standard growth conditions (*figure 12*) and after 600 µM OA supplementation (*figure 13*). GFP-ACSL3 and GFP-AA-ACSL3 were localized on the LD and the ER, whereas the GFP-ER-ACSL3 in the low and high-expressing cell lines was only present on the ER. Under standard growth conditions, the wtCOS-7 cells had numerous LD distributed in the ER network but with a higher density in the area near the nucleus. The GFP-ACSL3 and GFP-ER-ACSL3 cell lines were comparable in size, number and distribution of LD. The GFP_A3ko and GFP-AA-ACSL3 cells were markedly reduced in LD size and number. After OA supplementation, the size and number of LD was increased in all cell lines, but most prominently in the wtCOS-7, GFP-ACSL3, low and high GFP-ER-ACSL3 expressing cell lines. The LD tended to form clusters around the nucleus. The LD in the GFP_A3ko and the GFP-AA-ACSL3 cells were smaller and less in number than the other cell lines and sparsely built clusters.

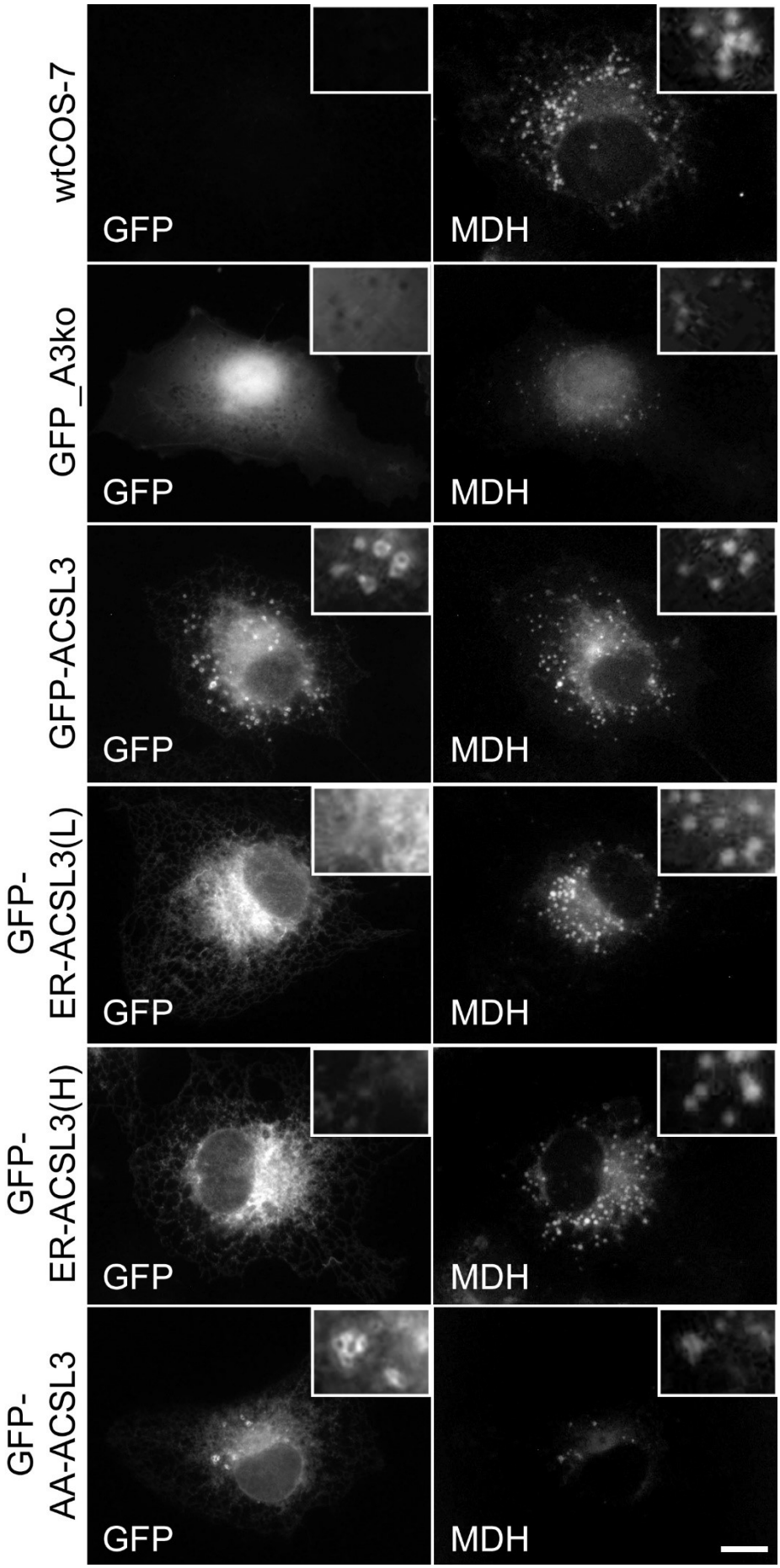

***Fig. 12*: Microscopy of the GFP_A3ko cells and rescue cell lines under standard growth conditions.** The cells were cultivated under standard growth conditions. Lipid droplet staining was performed with 100 µM MDH for 30 min. The pictures were taken with 60x objective. The gamma value was set to 1.4 for the GFP protein to increase the contrast of the ER network. The section in the insets approximates to a 16x magnification. Scale bar 10 µm.

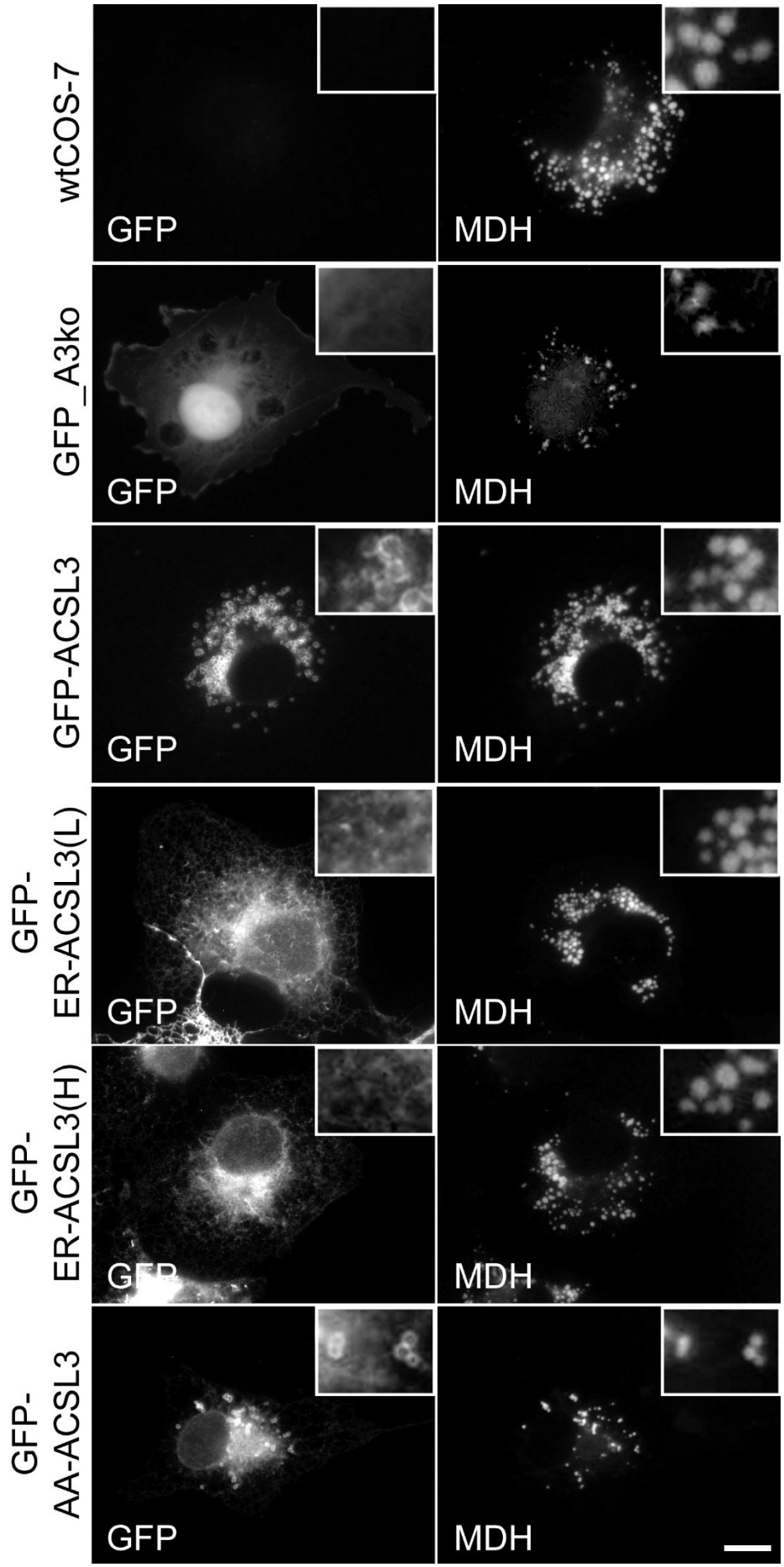

Fig. 13: **Microscopy of the GFP_A3ko cells and rescue cell lines after OA supplementation.** The cells were incubated in standard growth medium supplemented with 600 µM OA for 16 h. Lipid droplet staining was performed with 100 µM MDH for 30 min. The pictures were taken with gamma 1.4 for the GFP protein to increase the contrast of the ER network. The pictures were taken with 60x objective. The section in the insets approximates to a 16x magnification. Scale bar 10 µm.

5.2.2.4 Lipid droplet biogenesis

In order to investigate differences in LD biogenesis between the cell lines, the cells were starved for 24 h following 20 min incubation in 600 µM OA. The cells were fixated, mounted in mowiol and microscopy was performed using specified conditions (see section 4.2.2.13). To keep the size of the experiment manageable, the LD biogenesis assay was only performed with the high expressing GFP-ER-ACSL3 cell line (GFP-ER-ACSL3(H)) instead of the low-expressing cell line. Representative images of 4 independent experiments are given in *figure 14*. The lipid droplets remained in the starved cells and generated during the short OA pulse were quantified using ImageJ version 2.0.0 (*figure 15A*).

The LD number in starved cells ranged between 14 to 28 lipid droplets/cell and was not significantly different between wtCOS-7 and GFP_A3ko cells, GFP_A3ko and GFP-AA-ACSL3 cells, GFP-ACSL3 and GFP-ER-ACSL3(H) cells. Short-term OA incubation increased the average LD number by approximately 5-fold from 19 LD/cell under starved condition to 91 LD/cell in wtCOS-7. A comparable increase was observed in the GFP-ACSL3 cells that exhibited in average 18 LD in starved state and 98 LD after OA supplementation. The LD number in starved GFP-ER-ACSL3 cells was highest with 28 LD/cell and the capacity for LD biogenesis was significantly decreased in the GFP-ER-ACSL3(H) cells by 54 % compared to GFP-ACSL3, since the average LD number in OA treated GFP-ER-ACSL3 expressing cells was 46. The LD biogenesis was limited most heavily in the GFP_A3ko and the GFP-AA-ACSL3 cells that doubled their average LD number from 14 in starved cells to 32 and 34 in OA-treated cells. The capacity for LD biogenesis in the GFP_A3ko was significantly reduced by 65 % compared to wtCOS-7. There was no significant difference in LD biogenesis between the GFP_A3ko and the GFP-AA-ACSL3 cells.

In order to exclude differences in the expression level of GFP-ACSL3 and GFP-ER-ACSL3 as potential reason for differences in LD biogenesis, the GFP-fluorescence intensity in the same cells was quantified by ImageJ version 2.0.0. The GFP-fluorescence intensity was significantly increased in the GFP-ER-ACSL3(H) cells (*figure 15B*) and linear regression analysis did not show any correlation between GFP fluorescence intensity and LD number within the defined range of exposition time (*figure 15C*).

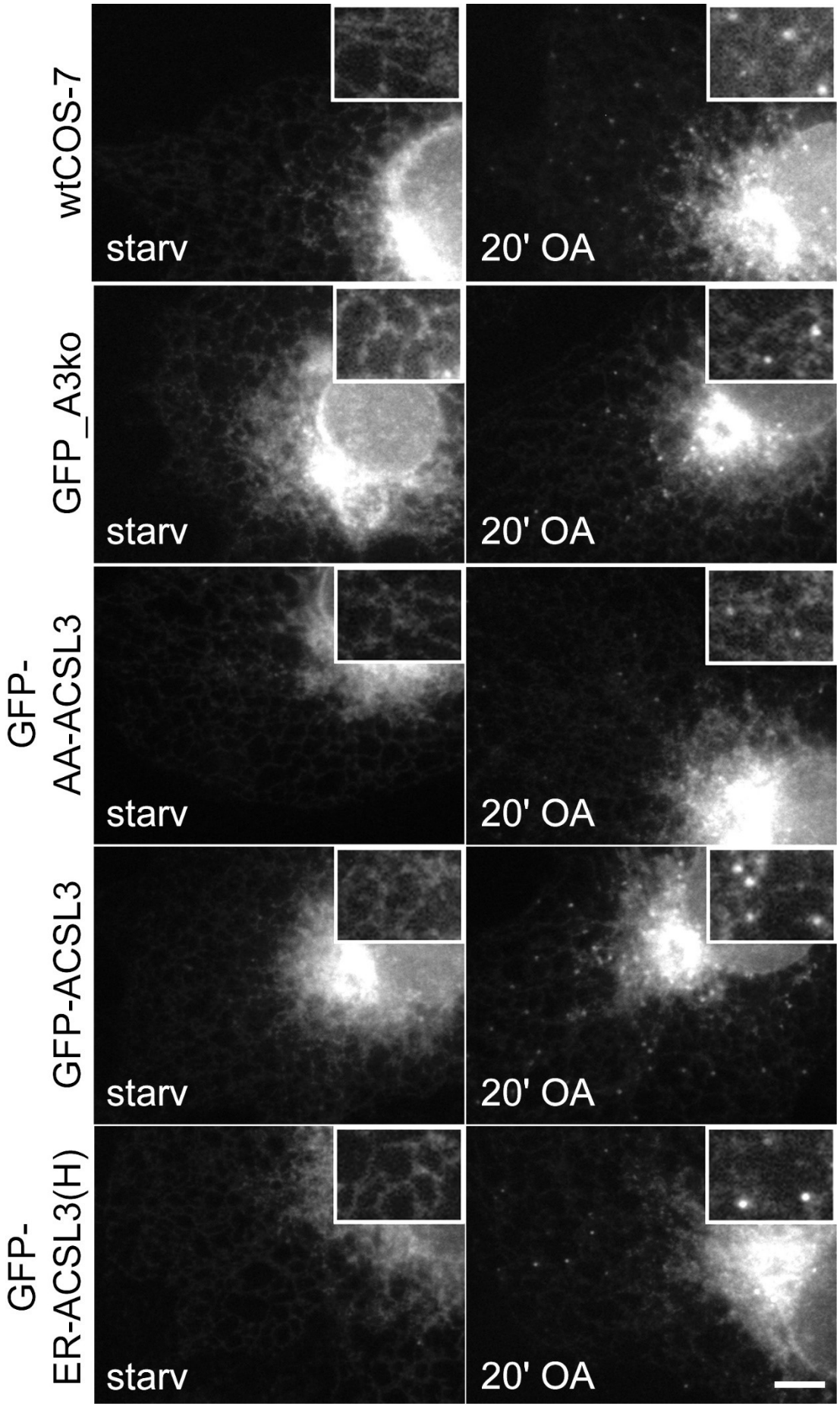
wtCOS-7
GFP_A3ko
GFP-AA-ACSL3
GFP-ACSL3
GFP-ER-ACSL3(H)
starv
20' OA

Fig. 14: **Representative images of LD biogenesis in GFP_A3ko cells and rescue cell lines.** The cells were starved for 24 h and incubated with 600 µM OA for 20 min. Nascent LD labelled by A3Nt-mcherry were detected. Gamma value of 1.4 had been used to detect also small lipid droplets in the periphery, which might be missed with standard microscopy settings. The brightness was elevated equally for all images with Adobe Photoshop version 6.0.21. The brightness in the insets was elevated independent from the image equally for all cell lines. The section in the insets approximates to a 4x magnification. 60x objective. Scale bar 5 µm. The panel shows representative images of n = 4 independent experiments, each included 20 cells for each condition. Please note, that the cell lines were stably transduced with the lipid droplet marker A3Nt-mcherry for this experiment and have the corresponding cell line numbers C239 (wtCOS-7), C240 (GFP_A3ko), C245 (GFP-AA-ACSL3), C241 (GFP-ACSL3) and C244 (GFP-ER-ACSL3(H)).

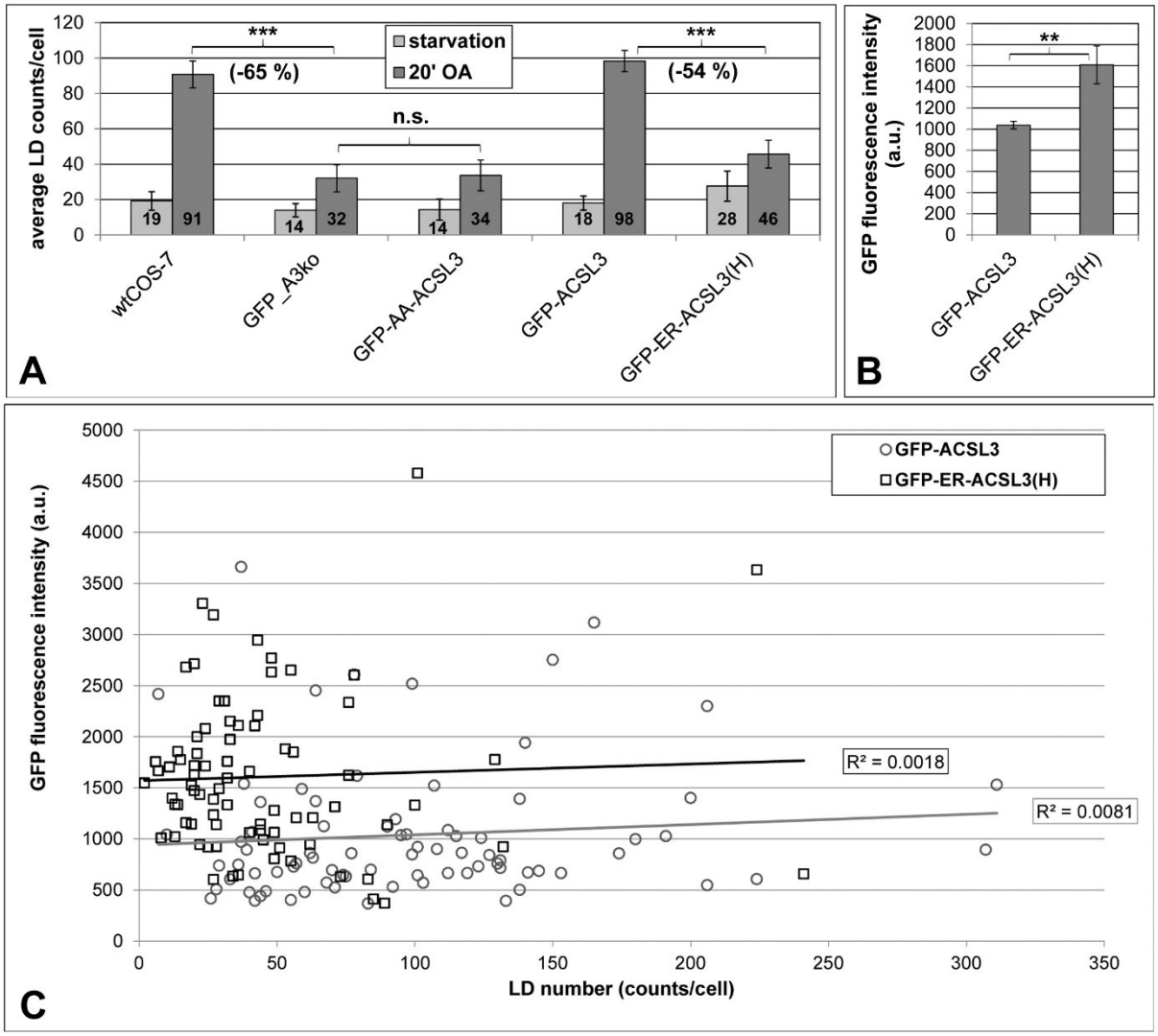

***Fig. 15*: Quantification of LD biogenesis in the GFP_A3ko cells and rescue cell lines. (A)** The lipid droplet number in starved cells and after 20 min OA incubation. **(B)** The GFP expression in the cells was quantified by ImageJ as a measure for expression of GFP-ACSL3 and GFP-ER-ACSL3. **(C)** Linear regression analysis did not show any correlation between GFP expression and LD number. Statistical analysis was performed using the Student's T-Test for unequal variances. The level of significance is indicated as follows: $p < 0.01$ (**), $p < 0.001$ (***) not significant (n.s.). n = 4 independent experiments including 20 images/cell line for each condition; error bars are SD. Please note, that the cell lines were stably transduced with the lipid droplet marker A3Nt-mcherry for this experiment and have the corresponding cell line numbers C239 (wtCOS-7), C240 (GFP_A3ko), C245 (GFP-AA-ACSL3), C241 (GFP-ACSL3) and C244 (GFP-ER-ACSL3(H)).

Starved cells were labelled with ^{14}C-OA for 20 min and the produced lipids were quantified to get deeper insight in the biochemical processes during the lipid droplet biogenesis assay (*figure 16*). The OA incorporation was not significantly different between wtCOS-7, GFP-ACSL3 and GFP-ER-ACSL3(H) cells. Thin layer chromatography did not reveal significant differences in the synthesis of TG or phospholipids and also the non-esterified fatty acids were comparable between the GFP-ACSL3 and the GFP-ER-ACSL3(H) cells. TG synthesis in the GFP-ER-ACSL3(H) was rather higher than in the GFP-ACSL3 cells. TG synthesis was significantly decreased in the GFP-ACSL3 cells compared to the wtCOS-7 cells. In view of the lipid species distribution in the cell lines, the TG level in the wtCOS-7 might appear too large. It arised from the difference in total cellular OA incorporation, which was increased for the wtCOS-7 cells, and slight differences in the other lipid species including three unspecified lipid species, which are not shown.

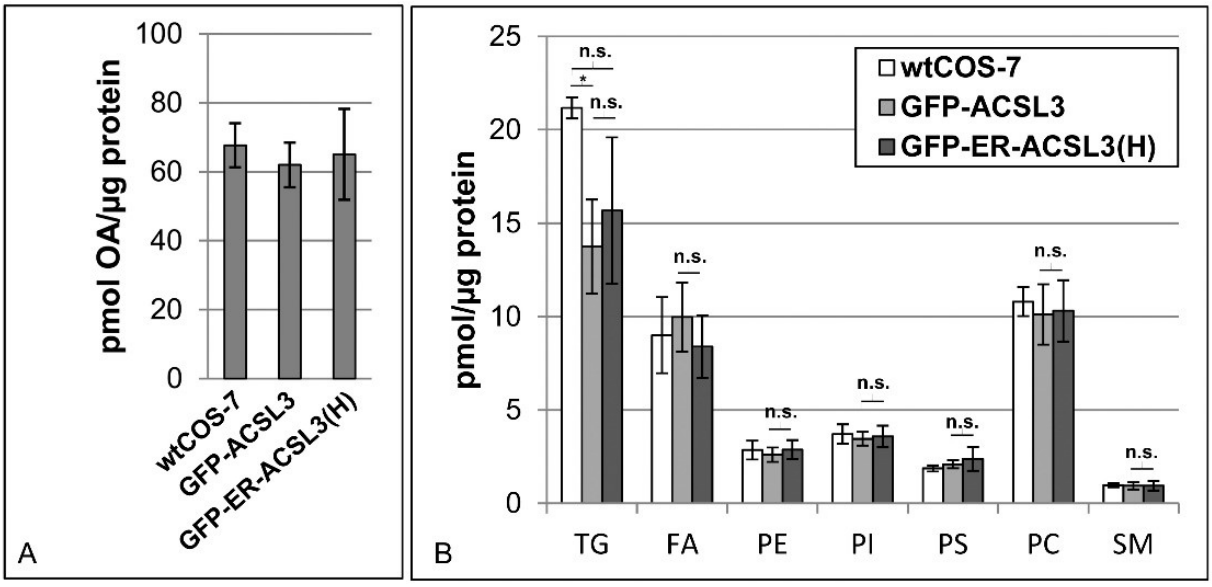

***Fig. 16*: ^{14}C-OA labelling of intracellular lipids in starved cells after LD induction.** The cells were starved for 24 h and then incubated with 600 µM ^{14}C-OA labelling mix for 20 min. The lipids were extracted by Folch extraction and analyzed by TLC. TG, triglycerides; FA, non-esterified fatty acids; PE, phosphatidylethanolamine; PI, phosphatidylinositol; PS, phosphatidylserine; PC, phosphatidylcholine; SM, sphingomyelin. Statistical analysis was performed using the Student's T-Test for unequal variances. The level of significance is indicated as follows: $p < 0.05$ (*), not significant (n.s.). n = 3 independent experiments; error bars are SD. Please note, that the cell lines were stably transduced with the lipid droplet marker A3Nt-mcherry for this experiment and have the corresponding cell line numbers C239 (wtCOS-7), C241 (GFP-ACSL3) and C244 (GFP-ER-ACSL3(H)). These data were generated in cooperation with Cassian Afting (medical doctoral candidate).

The LD biogenesis experiment was repeated with 60 min OA incubation instead of 20 min in order to investigate, if the difference between the GFP-ACSL3 and GFP-ER-ACSL3(H) cells

is valid for the early stages of LD formation or if it remains for a longer period of time. Representative images and the diagram of the LD quantification is shown in *figure 17*. After 1 h OA incubation there was no significant difference in LD number between wtCOS-7, GFP-ACSL3 and GFP-ER-ACSL3(H) cells.

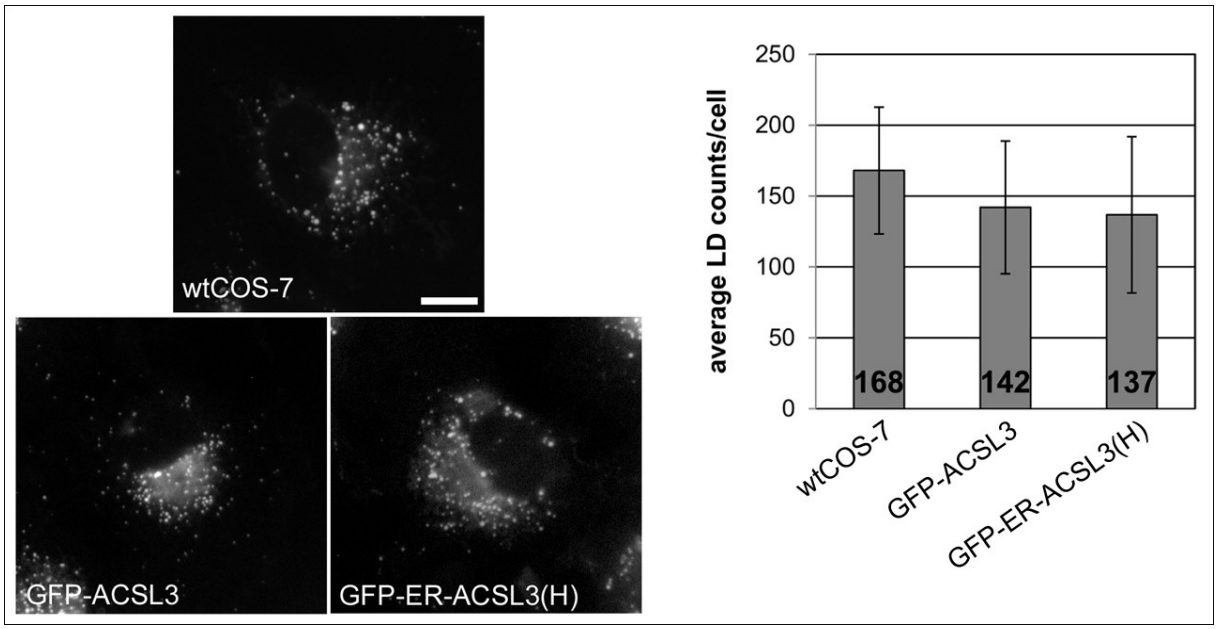

***Fig. 17*: LD biogenesis in starved cell after 60 min OA incubation.** The cells were starved for 24 h and then incubated with 600 µM OA labelling for 60 min. 60x objective. Scale bar 10 µm. n = 1 independent experiment including 10 cells. Statistical analysis was performed using the Student's T-Test for unequal variances. There was no significant difference in LD number between the cell lines. Please note, that the cell lines were stably transduced with the lipid droplet marker A3Nt-mcherry for this experiment and have the corresponding cell line numbers C239 (wtCOS-7), C241 (GFP-ACSL3) and C244 (GFP-ER-ACSL3(H)).

5.2.2.5 Lipid synthesis from endogenously synthesized fatty acids

The cells were incubated with radiolabelled ^{14}C-acetate in order to obtain information about the metabolism of endogenously synthesized fatty acids in the cell lines. In principle, acetate is intracellularly metabolized to malonyl-CoA that serves as a substrate for the fatty acid synthase complex catalyzing fatty acid synthesis. The experiment was performed in two approaches: the cells were either pre-incubated in standard growth medium only or with 600 µM OA to examine the influence of fatty acid supplementation on endogenous fatty acid synthesis and metabolism in the GFP_A3ko and GFP-AA-ACSL3 expressing cells. Regarding the GFP-ACSL3 and GFP-ER-ACSL3 expressing cells, the OA pre-incubation was relevant to increase potential differences between these cell lines, because GFP-ER-ACSL3 is not able to translocate to the lipid droplets under OA supplementation like GFP-ACSL3 does.

^{14}C-acetate labelling in the GFP_A3ko and GFP-AA-ACSL3 cells

Regarding the wtCOS-7, GFP_A3ko and GFP-AA-ACSL3 cells, the total acetate incorporation under standard growth was not significantly different between the cell lines. After OA pre-incubation, the acetate incorporation was still comparable between the cell lines, but was significantly decreased by 51-63 % compared to the standard growth conditions (*figure 18A*). TLC revealed that, under both conditions, the GFP_A3ko and GFP-AA-ACSL3 cells cells were likewise able to synthesize TG, CH, various phospholipids like PC, PE and SM and were not significantly different in intracellular non-esterified fatty acids (*figure 18B* and *C*). However, both cell lines were significantly reduced in TG synthesis compared to the wtCOS-7 cells. TG synthesis in the GFP_A3ko cells amounted to 47 % of the TG synthesis in wtCOS-7 cells under standard growth conditions and 56 % after OA pre-incubation. TG in the GFP-AA-ACSL3 cells was slightly higher with 54 % of wtCOS-7 under standard growth conditions and 61 % after OA pre-incubation. Concerning phospholipid synthesis under standard growth conditions, the GFP_A3ko and the GFP-AA-ACSL3 cells were increased. The increase was particularly prominent for PC and SM. PC and SM synthesis were increased by 49 % and 70 % in the GFP_A3ko cells compared to wtCOS-7. In the GFP-AA-ACSL3 the increase in PC and SM synthesis was 73 % and 63 % compared to wtCOS-7. After OA pre-incubation, the phospholipid synthesis was brought more in line with the wtCOS-7 cells, but was still significatly increased, except SM synthesis in the GFP_A3ko cells. The PC and SM synthesis in OA-treated GFP_A3ko cells was increased by 30 % and 21 % compared to wtCOS-7. The PC and SM synthesis in OA-treated GFP-AA-ACSL3 cells was increased by 39 % and 34 % compared to wtCOS-7. The GFP_A3ko were not significantly different in FA levels compared to wtCOS-7 cells although the levels were increased by 33 % under standard growth conditions and by 4 % after OA treatment, which is neglectable. The GFP-AA-ACSL3 were increased in FA levels by 52 % under standard growth conditions and 12 % after OA treatment compared to wtCOS-7, though the difference was only significant for standard growth conditions.

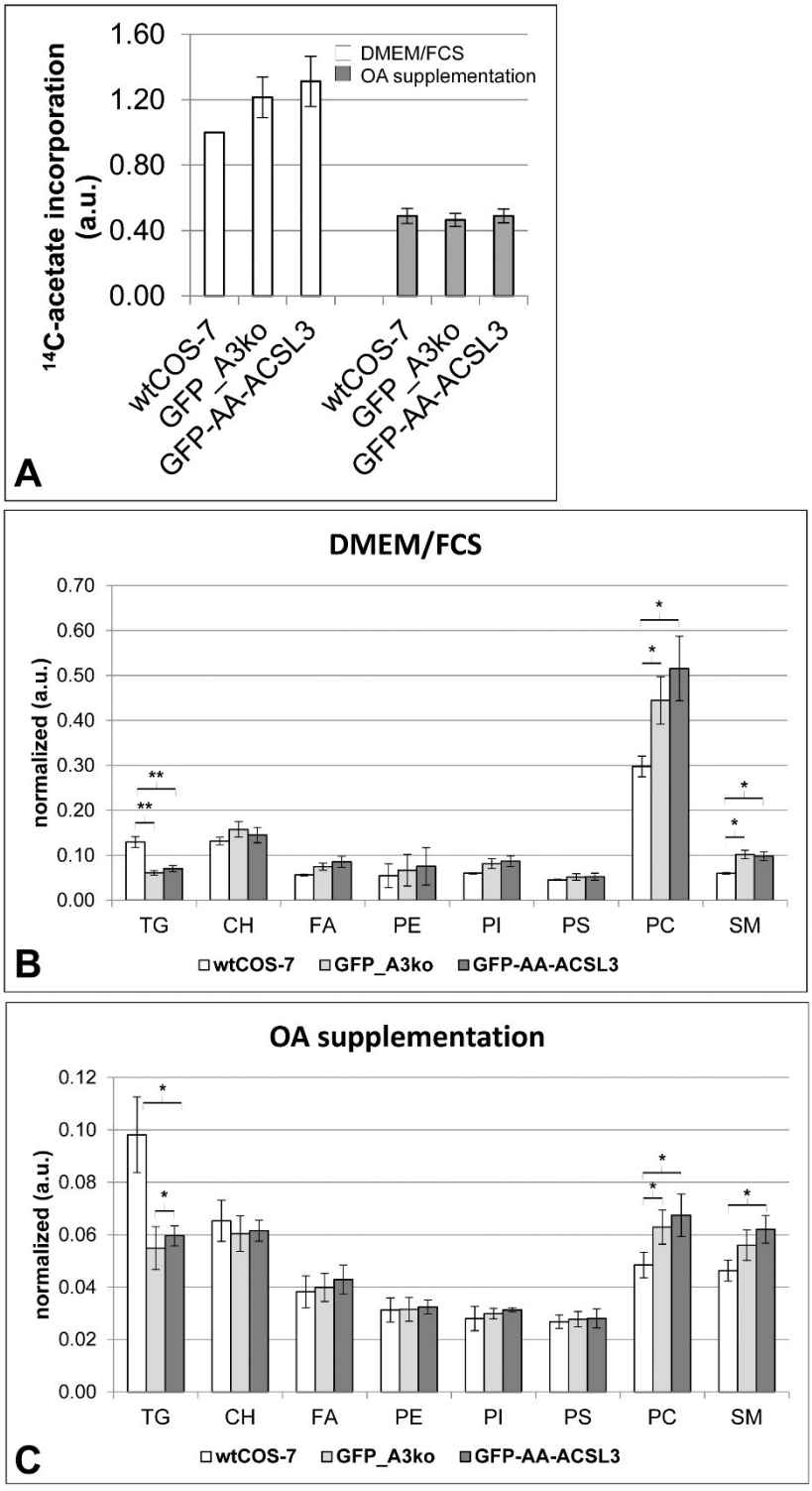

***Fig. 18*: Metabolism of endogenously synthesized fatty acids in the GFP_A3ko and GFP-AA-ACSL3 cells.** The cells were either pre-incubated in standard growth medium (DMEM/FCS) or 600 µM OA bound to 100 µM BSA (OA supplementation) for 16 h. The synthesized lipids were labelled by incubation in 5 µM ^{14}C-acetate for 6 h. Intracellular lipids were extracted by Folch lipid extraction and lipid species were identified and quantified by thin layer chromatography. **(A)** Total cellular ^{14}C-acetate incorporation was normalized to the wtCOS-7 by dividing the acetate incorporation of each cell line (pmol/µg protein) by the incorporation of the wtCOS-7 cells under standard growth condition (pmol/µg protein). The normalization was done individually for each experiment and then the mean of all experiments was calculated. The total incorporation of ^{14}C-acetate into the cells was significantly decreased comparing standard conditions and OA supplementation, but there were no significant differences between the cell lines. **(B)** shows the synthesis of various lipid species under standard growth conditions. Normalization was done by dividing the absolute quantities of each lipid species (pmol/µg protein) by the ^{14}C-acetate incorporation of the wtCOS-7 cells under standard growth condition (pmol/µg protein). The normalization was done individually for each experiment and then the mean of all experiments was calculated. **(C)** shows the synthesis of various lipid species after OA pre-incubation. Normalization was done likewise to (B). TG, triglycerides; CH, cholesterol; FA, non-esterified fatty acids; PE, phosphatidylethanolamine; PI, phosphatidylinositol; PS, phosphatidylserine; PC, phosphatidylcholine; SM, sphingomyelin. Statistical analysis was performed using the Student's T-Test for unequal variances. The level of significance is indicated as follows: $p < 0.05$ (*), $p < 0.01$ (**). n = 3 independent experiments; error bars are SD. These data were generated in cooperation with Cassian Afting (medical doctoral candidate).

^{14}C-acetate labelling in the GFP-ACSL3 and GFP-ER-ACSL3 cells

The results obtained from ^{14}C-acetate labelling in the GFP-ER-ACSL3 expressing cell lines and the GFP-ACSL3 cells are given in *figure 19*. The OA pre-incubation was assumed to augment the differences between the GFP-ER-ACSL3 cell lines and the GFP-ACSL3 cells observed under standard growth conditions. Surprisingly, the OA pre-incubation inverted the directions of the trends observed, i.e. what was increased in the GFP-ER-ACSL3 expressing cell lines under standard growth conditions became decreased after OA treatment and the other way round. After OA pre-incubation, the total acetate incorporation was not significantly different between the GFP-ACSL3 and GFP-ER-ACSL3 expressing cell lines, though was slightly decreased in the GFP-ER-ACSL3 cells by 19 % in the low and by 12 % in the high expressing cell line. Under standard growth conditions, acetate incorporation was significantly increased in the GFP-ER-ACSL3 cells by 16 % in the low and 32 % in the high expressing cell line compared to the GFP-ACSL3 cells. Similar to the GFP_A3ko and the GFP-AA-ACSL3 cells the acetate incorporation was reduced significantly by OA pre-incubation (*figure 19A*). In *table 8* the differences in lipid species synthesis in the GFP-ER-ACSL3 expressing cell lines compared to the GFP-ACSL3 cells are summarized. After OA pre-incubation, the TG synthesis in the GFP-ER-ACSL3 expressing cell lines was decreased by 21.1 % in the low and 24.2 % in the high expressing cell line compared to the GFP-ACSL3 cells, though not significantly. Compared to wtCOS-7, TG synthesis was significantly decreased by approximately 40 % in the GFP-ER-ACSL3 cell lines. Phospholipid synthesis was decreased in the GFP-ER-ACSL3 cell lines compared to the GFP-ACSL3 cells, most strikingly for PC and SM. PC and SM synthesis were significantly decreased by 37.0 % and 37.9 % in the low expressing cell line. For the high expressing cell line, PC and SM were decreased by 34.3 % and 34.2 %, though not significantly. Under standard growth conditions, the GFP-ER-ACSL3 cell lines were significantly increased in lipid synthesis, particularly for TG, PC and SM. In the low expressing cell line TG, PC and SM synthesis were increased by 26.5 %, 30.1 % and 16.4 %. In the high expressing cell line TG, PC and SM synthesis were increased by 38.3 %, 34.7 % and 30.8 %. The difference for PC and SM was significant for both cell lines. Surprisingly, CH synthesis was highly increased by 31.2 % in the low and by 43.2 % in the high expressing GFP-ER-ACSL3 cell line compared to GFP-ACSL3. Independent from the culture conditions, the high expressing cell line appeared to be superior over the low expressing cell line in the synthesis of the measured lipid species, except for TG after OA supplementation (*figure 19B* and *C*).

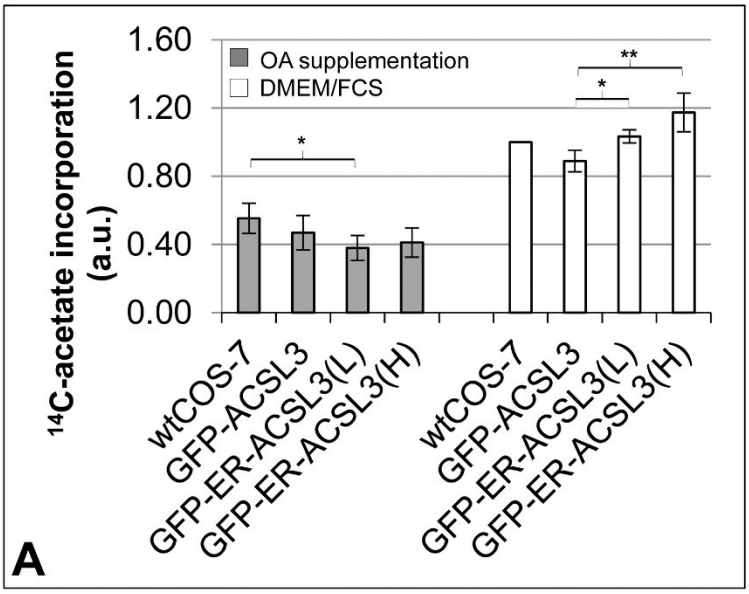
1.60
1.20
0.80
0.40
0.00
OA supplementation
DMEM/FCS
^{14}C-acetate incorporation (a.u.)
wtCOS-7
GFP-ACSL3
GFP-ER-ACSL3(L)
GFP-ER-ACSL3(H)
A

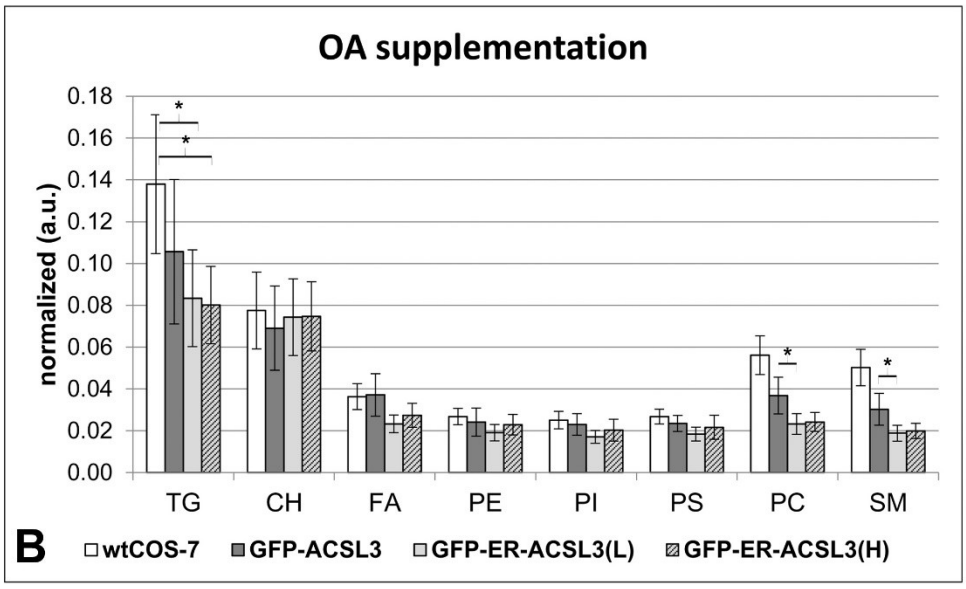
OA supplementation
normalized (a.u.)
0.18
0.16
0.14
0.12
0.10
0.08
0.06
0.04
0.02
0.00
TG
CH
FA
PE
PI
PS
PC
SM
B
wtCOS-7
GFP-ACSL3
GFP-ER-ACSL3(L)
GFP-ER-ACSL3(H)

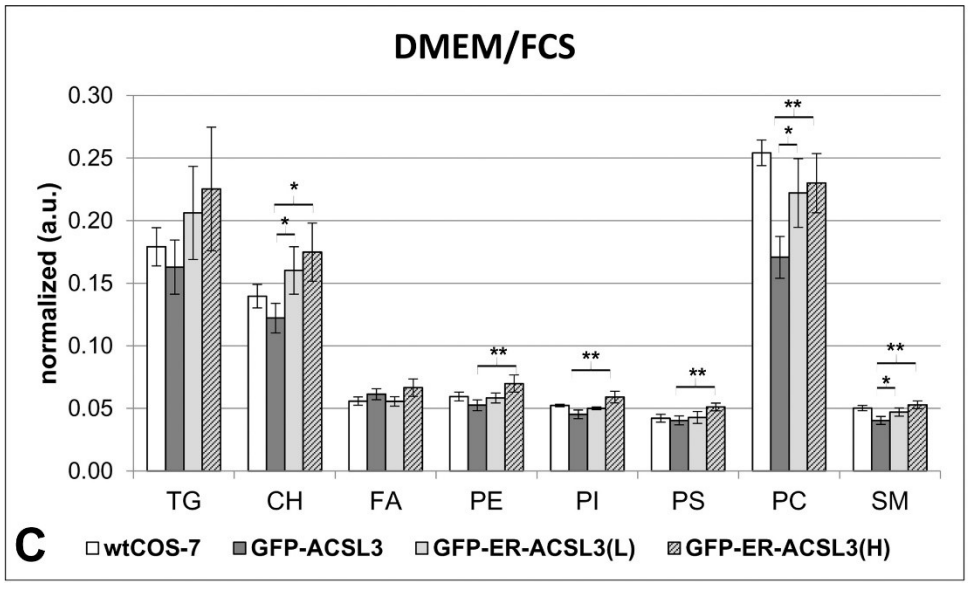
DMEM/FCS
normalized (a.u.)
0.30
0.25
0.20
0.15
0.10
0.05
0.00
TG
CH
FA
PE
PI
PS
PC
SM
C
wtCOS-7
GFP-ACSL3
GFP-ER-ACSL3(L)
GFP-ER-ACSL3(H)

***Fig. 19*: Metabolism of endogenously synthesized fatty acids in the rescue cell lines.** The cells were either pre-incubated in standard growth medium (DMEM/FCS) or 600 µM OA bound to 100 µM BSA (OA supplementation) for 16 h. The synthesized lipids were labelled by incubation in 5 µM ^{14}C-acetate for 6 h. Intracellular lipids were extracted by Folch lipid extraction and lipid species were identified and quantified by TLC. **(A)** Total cellular ^{14}C-acetate incorporation was normalized to the wtCOS-7 by dividing the acetate incorporation of each cell line (pmol/µg protein) by the incorporation of the wtCOS-7 cells under standard growth condition (pmol/µg protein). The normalization was done individually for each experiment and then the mean of all experiments was calculated. **(B)** shows the synthesis of various lipid species under standard growth conditions. Normalization was done by dividing the absolute quantities of each lipid species (pmol/µg protein) by the ^{14}C-acetate incorporation of the wtCOS-7 cells under standard growth condition (pmol/µg protein). The normalization was done individually for each experiment and then the mean of all experiments was calculated. **(C)** shows the synthesis of various lipid species after OA pre-incubation. Normalization was done likewise to (B). TG, triglycerides; CH, cholesterol; FA, non-esterified fatty acids; PE, phosphatidylethanolamine; PI, phosphatidylinositol; PS, phosphatidylserine; PC, phosphatidylcholine; SM, sphingomyelin. Statistical analysis was performed using the Student's T-Test for unequal variances. The level of significance is indicated as follows: $p < 0.05$ (*), $p < 0.01$ (**), not significant (n.s.). n = 4 independent experiments; error bars are SD. These data were generated in cooperation with Cassian Afting (medical doctoral candidate).

***Tab. 8*: The differences in lipid species synthesis from endogenously synthesized fatty acids between the GFP-ER-ACSL3 expressing cell lines and the GFP-ACSL3 cells.**

Lipid species	OA pre-incubation		Standard growth conditions	
	GFP-ER-ACSL3(L)	GFP-ER-ACSL3(H)	GFP-ER-ACSL3(L)	GFP-ER-ACSL3(H)
TG	-21.1 (n.s.)	-24.2 (n.s.)	26.5 (n.s.)	38.3 (n.s.)
CH	7.6 (n.s.)	8.2 (n.s.)	31.2 (*)	43.2 (*)
FA	-37.3 (n.s.)	-26.3 (n.s.)	-9.4 (n.s.)	8.5 (n.s.)
PE	-20.9 (n.s.)	-5.2 (n.s.)	11.0 (n.s.)	33.1 (**)
PI	-25.9 (n.s.)	-11.8 (n.s.)	10.7 (n.s.)	30.5 (**)
PS	-21.6 (n.s.)	-7.8 (n.s.)	5.9 (n.s.)	26.5 (**)
PC	-37.0 (*)	-34.3 (n.s.)	30.1 (*)	34.7 (**)
SM	-37.9 (*)	-34.2 (n.s.)	16.4 (*)	30.8 (**)

The difference between the GFP-ER-ACSL3 expressing cell lines and the GFP-ACSL3 cells was calculated from the data shown in figure 18B and 18C and given as percentage. Increased lipid synthesis in the GFP-ER-ACSL3 expressing cell lines is highlighted in green and decreased lipid synthesis is highlighted in orange and labelled with a minus (-). Statistical analysis was performed using the Student's T-Test for unequal variances. The level of significance is given in brackets and indicated as follows: $p < 0.05$ (*), $p < 0.01$ (**), not significant (n.s.). TG, triglycerides; CH, cholesterol; FA, non-esterified fatty acids; PE, phosphatidylethanolamine; PI, phosphatidylinositol; PS, phosphatidylserine; PC, phosphatidylcholine; SM, sphingomyelin.

5.2.2.6 Lipid synthesis from exogenously supplied oleate

The cells were incubated with radiolabelled ^{14}C-OA in order to study lipid synthesis from exogenously supplied fatty acid. As specified for the acetate labelling assay, the cells were pre-incubated in standard growth medium or medium supplemented with 600 µM OA for 16 h. The latter is especially relevant for the comparison of the GFP-ACSL3 and the GFP-ER-ACSL3

cells, because the translocation of GFP-ACSL3 but not GFP-ER-ACSL3 to the lipid droplets increases the potential differences between the cell lines.

^{14}C-OA labelling in the GFP_A3ko and GFP-AA-ACSL3 cells

The results of the ^{14}C-OA labelling in the GFP_A3ko and the GFP-AA-ACSL3 cells are summarized in *figure 20*. The ^{14}C-OA incorporation was slightly decreased in GFP_A3ko and GFP-AA-ACSL3 cells. Under standard growth conditions, it was significantly reduced by 33 % in the GFP_A3ko and by 31 % in the GFP-AA-ACSL3 cells. After OA pre-incubation, the GFP_A3ko and the GFP-AA-ACSL3 cells also incorporated slightly less ^{14}C-OA, but the difference was not significant. Thin layer chromatography revealed that under both conditions, the synthesis of TG and the phospholipids PE, PI, PS, PC and SM was comparable between the GFP_A3ko and the GFP-AA-ACSL3 cell lines. Under both conditions, TG synthesis in the GFP_A3ko and GFP-AA-ACSL3 cells was significantly reduced to approximately half the TG synthesis of the wtCOS-7 cells. The level of non-esterified fatty acids was highly elevated in the GFP_A3ko and the GFP-AA-ACSL3 cells, although not significantly due to high standard deviation.

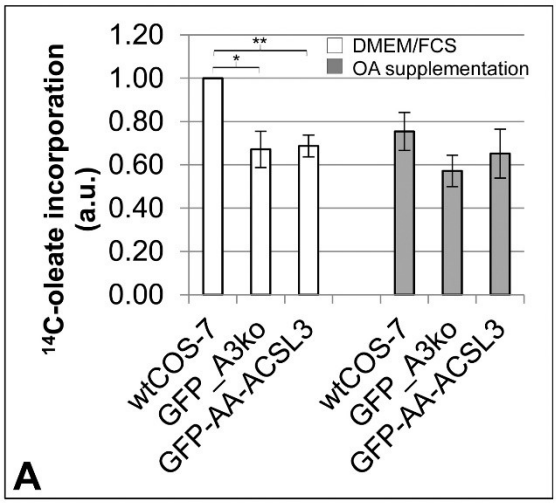

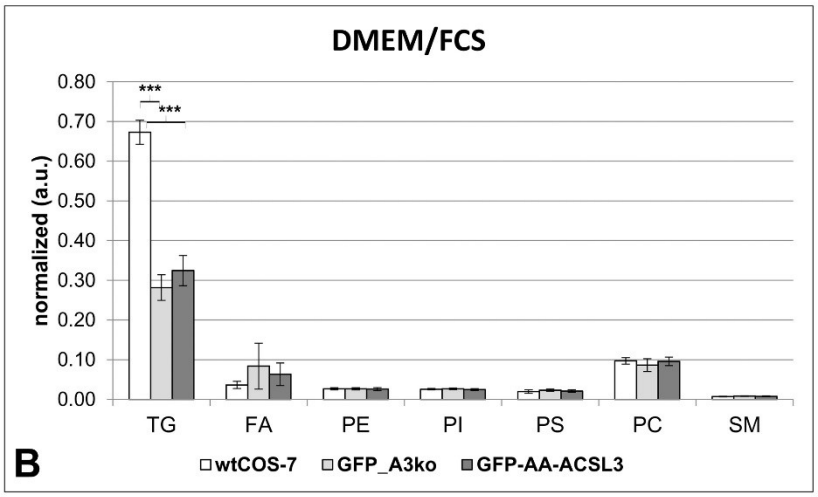

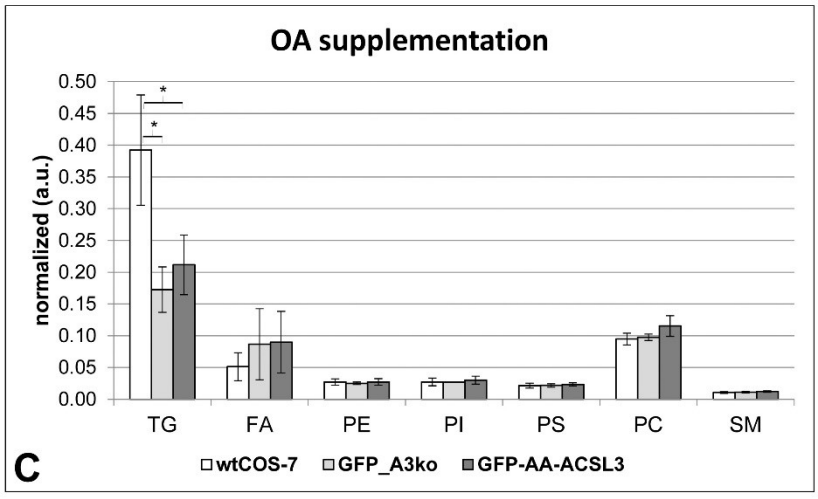

***Fig. 20*: Metabolism of exogenously supplied OA in GFP_A3ko and GFP-AA-ACSL3 cells.** The cells were either pre-incubated in standard growth medium (standard) or 600 µM OA bound to 100 µM BSA (OA supplementation) for 16 h. The synthesized lipids were labelled by incubation in 180 µM ^{14}C-OA for 3 h. Intracellular lipids were extracted by Folch lipid extraction and lipid species were identified and quantified by TLC. **(A)** Total cellular ^{14}C-OA incorporation was normalized to the wtCOS-7 by dividing the acetate incorporation of each cell line (pmol/µg protein) by the incorporation of the wtCOS-7 cells under standard growth condition (pmol/µg protein). The normalization was done individually for each experiment and then the mean of all experiments was calculated. **(B)** shows the synthesis of various lipid species under standard growth conditions. Normalization was done by dividing the absolute quantities of each lipid species (pmol/µg protein) by the ^{14}C-acetate incorporation of the wtCOS-7 cells under standard growth condition (pmol/µg protein). The normalization was done individually for each experiment and then the mean of all experiments was calculated. **(C)** shows the synthesis of various lipid species after OA pre-incubation. Normalization was done likewise to (B). TG, triglycerides; FA, non-esterified fatty acids; PE, phosphatidylethanolamine; PI, phosphatidylinositol; PS, phosphatidylserine; PC, phosphatidylcholine; SM, sphingomyelin. Statistical analysis was performed using the Student's T-Test for unequal variances. The level of significance is indicated as follows: $p < 0.01$ (**), $p < 0.001$ (***), not significant (n.s.). n = 3 independent experiments; error bars are SD. These data were generated in cooperation with Cassian Afting (medical doctoral candidate).

^{14}C-OA labelling in the GFP-ACSL3 and the GFP-ER-ACSL3 cell line

The results of the ^{14}C-OA labelling in the GFP-ACSL3 and GFP-ER-ACSL3 cell lines are summarized in *figure 21*. The OA incorporation in the GFP-ER-ACSL3 cells was slightly increased compared to GFP-ACSL3 cells under both conditions, though only significantly for the high-expressing cell line under standard growth conditions. *Table 9* gives the differences in lipid species synthesis between the GFP-ER-ACSL3 expressing cell lines and the GFP-ACSL3 cells as percentage.

TG synthesis was augmented in the GFP-ER-ACSL3 cell lines compared to the GFP-ACSL3 cells. The increase was distinct after OA pre-incubation and amounted to 31.7 % in the low expressing cell line and 35.9 % in the high expressing cell line. Under standard growth conditions the difference was smaller with 13.2 % and 23.0 %. Regarding the summarized values these differences are only significant for the high expressing GFP-ER-ACSL3 cell line under standard growth conditions, but regarding the individual experiments, the differences were clearer, especially after OA pre-incubation. TG synthesis was significantly elevated in three of three assays in the low expressing cell lines and in two of three assays in the high expressing cell line. Under standard growth conditions, TG synthesis was significantly augmented in the high expressing cell line in three of three assays, whereas for the low expressing cell line the findings were not clear. The level of non-esterified fatty acids was decreased in the GFP-ER-ACSL3 cell lines, most notably for the low expressing cell line with a decrease of 50.1 % (*) after OA treatment and 41.7 % (n.s.) under standard growth conditions. Regarding phospholipid synthesis the results were heterogenous. PE and PI synthesis were increased, whereas PS, PC and SM synthesis were slightly decreased, most notably after OA pre-incubation (*table 9*).

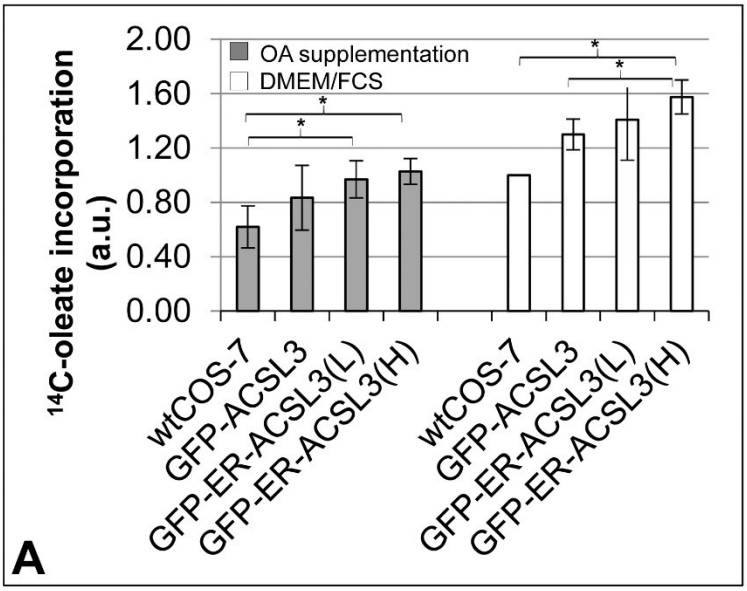
2.00
1.60
1.20
0.80
0.40
0.00
14C-oleate incorporation (a.u.)
OA supplementation
DMEM/FCS
*
*
*
*
wtCOS-7
GFP-ACSL3
GFP-ER-ACSL3(L)
GFP-ER-ACSL3(H)
wtCOS-7
GFP-ACSL3
GFP-ER-ACSL3(L)
GFP-ER-ACSL3(H)
A

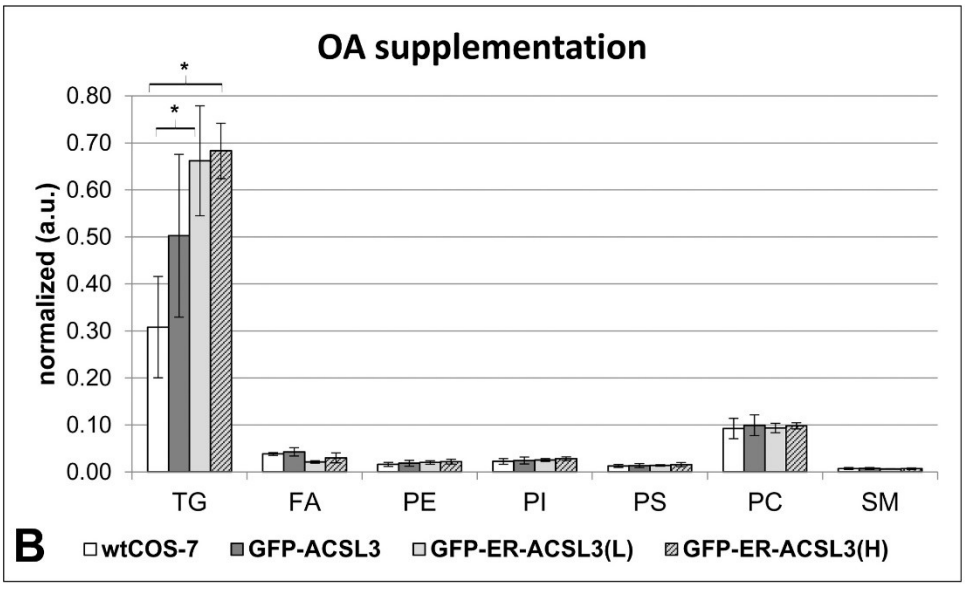
OA supplementation
normalized (a.u.)
0.80
0.70
0.60
0.50
0.40
0.30
0.20
0.10
0.00
*
*
TG
FA
PE
PI
PS
PC
SM
B
wtCOS-7
GFP-ACSL3
GFP-ER-ACSL3(L)
GFP-ER-ACSL3(H)

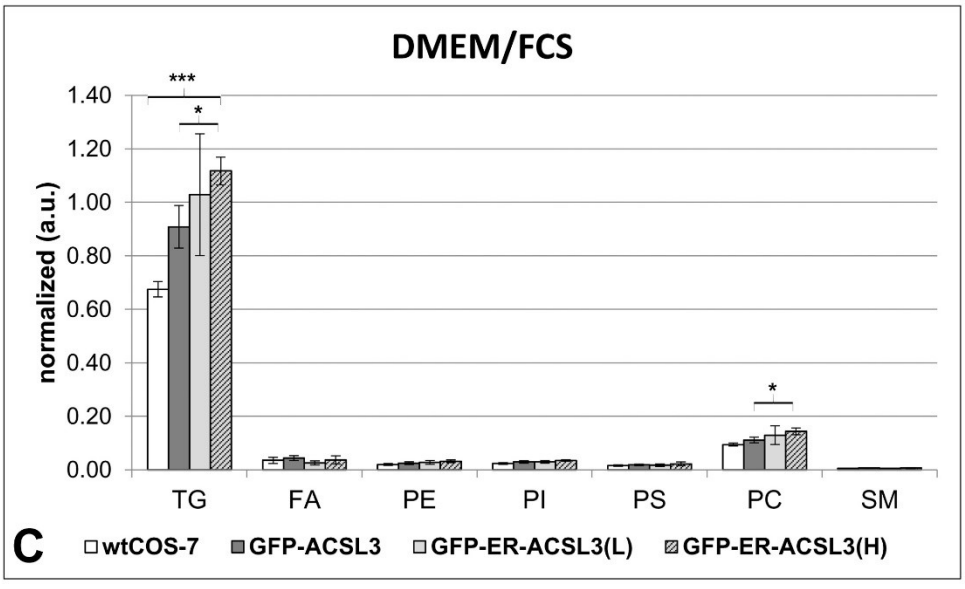
DMEM/FCS
normalized (a.u.)
1.40
1.20
1.00
0.80
0.60
0.40
0.20
0.00
***
*
*
TG
FA
PE
PI
PS
PC
SM
C
wtCOS-7
GFP-ACSL3
GFP-ER-ACSL3(L)
GFP-ER-ACSL3(H)

***Fig. 21*: Metabolism of exogenously supplied OA in rescue cell lines.** The cells were either pre-incubated in standard growth medium (standard) or 600 µM OA bound to 100 µM BSA (OA supplementation) for 16 h. The synthesized lipids were labelled by incubation in 180 µM ^{14}C-OA for 3 h. Intracellular lipids were extracted by Folch lipid extraction and lipid species were identified and quantified by TLC. **(A)** Total cellular ^{14}C-OA incorporation was normalized to the wtCOS-7 by dividing the acetate incorporation of each cell line (pmol/µg protein) by the incorporation of the wtCOS-7 cells under standard growth condition (pmol/µg protein). The normalization was done individually for each experiment and then the mean of all experiments was calculated. **(B)** shows the synthesis of various lipid species after OA pre-incuation. Normalization was done by dividing the absolute quantities of each lipid species (pmol/µg protein) by the ^{14}C-acetate incorporation of the wtCOS-7 cells under standard growth condition (pmol/µg protein). The normalization was done individually for each experiment and then the mean of all experiments was calculated. **(C)** shows the synthesis of various lipid species under standard growth conditions. Normalization was done likewise to (B). TG, triglycerides; FA, non-esterified fatty acids; PE, phosphatidylethanolamine; PI, phosphatidylinositol; PS, phosphatidylserine; PC, phosphatidylcholine; SM, sphingomyelin. Statistical analysis was performed using the Student's T-Test for unequal variances. The level of significance is indicated as follows: $p < 0.05$ (*), $p < 0.01$ (**), not significant (n.s.). n = 3 independent experiments; error bars are SD. These data were generated in cooperation with Cassian Afting (medical doctoral candidate).

***Table 9*: The differences in lipid species synthesis from exogenously supplied OA between the GFP-ER-ACSL3 expressing cell lines and the GFP-ACSL3 cells.**

Lipid species	OA pre-incubation		Standard growth conditions	
	GFP-ER-ACSL3(L)	GFP-ER-ACSL3(H)	GFP-ER-ACSL3(L)	GFP-ER-ACSL3(H)
TG	31.7 (n.s.)	35.9 (n.s.)	13.2 (n.s.)	23.0 (*)
FA	-50.1 (*)	-29.9 (n.s.)	-41.7 (n.s.)	-15.3 (n.s.)
PE	8.9 (n.s.)	18.6 (n.s.)	11.4 (n.s.)	26.6 (n.s.)
PI	4.7 (n.s.)	15.2 (n.s.)	0.1 (n.s.)	16.7 (n.s.)
PS	1.1 (n.s.)	16.3 (n.s.)	-6.1 (n.s.)	19.7 (n.s.)
PC	-6.1 (n.s.)	-1.3 (n.s.)	16.4 (n.s.)	29.1 (*)
SM	-13.6 (n.s.)	-8.5 (n.s.)	-13.5 (n.s.)	2.1 (n.s.)

The difference between the GFP-ER-ACSL3 expressing cell lines and the GFP-ACSL3 cells was calculated and given as percentage. Increased lipid synthesis in the GFP-ER-ACSL3 expressing cell lines is highlighted in green and, decreased lipid synthesis is highlighted in orange and labelled with a minus (-). The level of significance is given in brackets and indicated as follows: $p < 0.05$ (*), $p < 0.01$ (**), not significant (n.s.). TG, triglycerides; FA, non-esterified fatty acids; PE, phosphatidylethanolamine; PI, phosphatidylinositol; PS, phosphatidylserine; PC, phosphatidylcholine; SM, sphingomyelin.

5.2.2.7 Basal lipolysis

ACSL3 was hypothesized to counteract lipolysis by re-esterification of fatty acids liberated during lipolysis. GFP_A3ko cells were compared to wtCOS-7 cells to assess, if the ACSL3-knockout according to the hypothesis increases the loss of stored lipids. Comparison of GFP_A3ko cells with GFP-AA-ACSL3 cells was supposed to show if the presence of ACSL3 on LD influences the lipolytic rate by e. g. shielding the TG core from lipases. GFP-ACSL3

and GFP-ER-ACSL3 expressing cells were compared to obtain information about the relevance of ACSL3 localization for re-esterification of fatty acids during lipolysis.

Lipolysis was assessed by feeding the cells with ^{14}C-OA to label the synthesized lipid species. Subsequently, the cells were exposed to nutrient-poor medium to achieve basal lipolysis. The degradation of the initial lipid species levels were studied over the course of starvation by extracting and quantifying the remaining lipids in mock-treated cells at different time points of starvation and performing TLC for quantification. The focus was especially put on the change of intracellular TG levels, since these are preferentially hydrolyzed during starvation. There were no remarkable findings regarding phospholipid levels (data not shown).

Lipolysis in the GFP_A3ko and the GFP-AA-ACSL3 cells

The initial TG levels were supposed to be comparable between the cell lines to allow a reliable interpretation of the data. The ^{14}C-OA labelling assay revealed that the GFP_A3ko and GFP-AA-ACSL3 cells were decreased in TG synthesis compared to wtCOS-7, when incubated with the same OA concentration like the wtCOS-7 cells (see section 5.2.2.6). Therefore in this experiment, the OA concentration was increased to 600 µM for the GFP_A3ko and GFP-AA-ACSL3 cells, whereas the wtCOS-7 cells were incubated in 120 µM, 60 µM and 20 µM OA. This approach was supposed to push the OA incorporation in the GFP_A3ko and GFP-AA-ACSL3 cells and obtain matching levels of synthesized TG. *Figure 22A* and *B* depict the ^{14}C-OA uptake and the incorporation into different lipid species after labelling prior to starvation. The OA incorporation and initial TG levels in the GFP_A3ko and the GFP-AA-ACSL3 was comparable to wtCOS-7 cells 120 µM. The GFP_A3ko and GFP-AA-ACSL3 cells were not significantly different in OA incorporation or initial TG levels. *Figure 22C* and *D* illustrate the development of intracellular TG levels over the course of lipolysis. The intracellular TG levels decreased with extended duration of starvation. In the GFP_A3ko and the GFP-AA-ACSL3 cells the intracellular TG levels decreased to a higher extent, since there was no significant difference to wtCOS-7 120 µM at the beginning, but after 6 h starvation, the TG levels were significantly decreased by 46 % in the GFP_A3ko cells and by 33 % in the GFP-AA-ACSL3 cells. This was rather noticeable in the last interval of lipolysis between 3h and 6h starvation, where the curve for the TG loss proceeds steeper than in the first hours of starvation (*figure 22D*). This behaviour of the GFP_A3ko and GFP-AA-ACSL3 cells became even more obvious in comparison with the wtCOS-7 cells incubated in 60 µM OA. Initially, the TG levels in the GFP_A3ko and GFP-AA-ACSL3 cells were significantly increased and after 6 h starvation, the TG levels were significantly decreased compared in the GFP_A3ko and not significantly

different in the GFP-AA-ACSL3 cells. Surprisingly, the TG levels measured in the GFP-AA-ACSL3 showed a slightly smaller decrease than the GFP_A3ko cells. The trend in TG decrease was identical during the first hour of starvation, but then the curve of the GFP-AA-ACSL3 cells flattened whereas the curve of the GFP_A3ko cells exhibited a steeper decline resulting in significant decreased TG levels after 6 h of starvation (*figure 22D*). The difference in intracellular TG levels between the GFP_A3ko and the GFP-AA-ACSL3 cells after 6 h of starvation amounted to 24 %. Through normalization of the intracellular TG to the initial TG of wtCOS-7 cells incubated at 120 µM OA, the differences in initial TG levels between wtCOS-7120 µM and GFP-AA-ACSL3 became significant, wheras the difference between wtCOS-7 120 µM and GFP_A3ko remained not significant (*figure 22D*). Moreover, through normalization of the intracellular TG to the initial TG of wtCOS-7 cells incubated at 120 µM OA, the difference between the GFP_A3ko and the GFP-AA-ACSL3 cells after 6 h starvation becomes not significant (*figure 22D*).

Comparing the curve of TG degradation in the wtCOS-7 cells, it is striking, that the extent of TG hydrolysis appeared to be dependent on the initial TG levels present in the cells. The wtCOS-7 cells incubated in 120 µM OA had the highest initial TG levels of 112 pmol/µg protein. After 6 h of starvation, the TG levels amounted to 49 pmol/µg protein corresponding to a decrease of 56 %. The wtCOS-7 cells incubated with 20 µM OA had the lowest initial TG levels of 30 pmol/µg protein. After 6 h of starvation, the TG levels amounted to 14 pmol/µg protein corresponding to a decrease of 53 %. The relative decrease was comparable, but the absolute loss of TG was highly reduced in the wtCOS-7 incubated in 20 µM OA. After 6 h of starvation, the normalized TG levels of the GFP_A3ko and the GFP-AA-ACSL3 cells were still significantly decreased compared to wtCOS-7 120 µM, but the difference between the GFP_A3ko and the GFP-AA-ACSL3 cells became not significant (*figure 22D*).

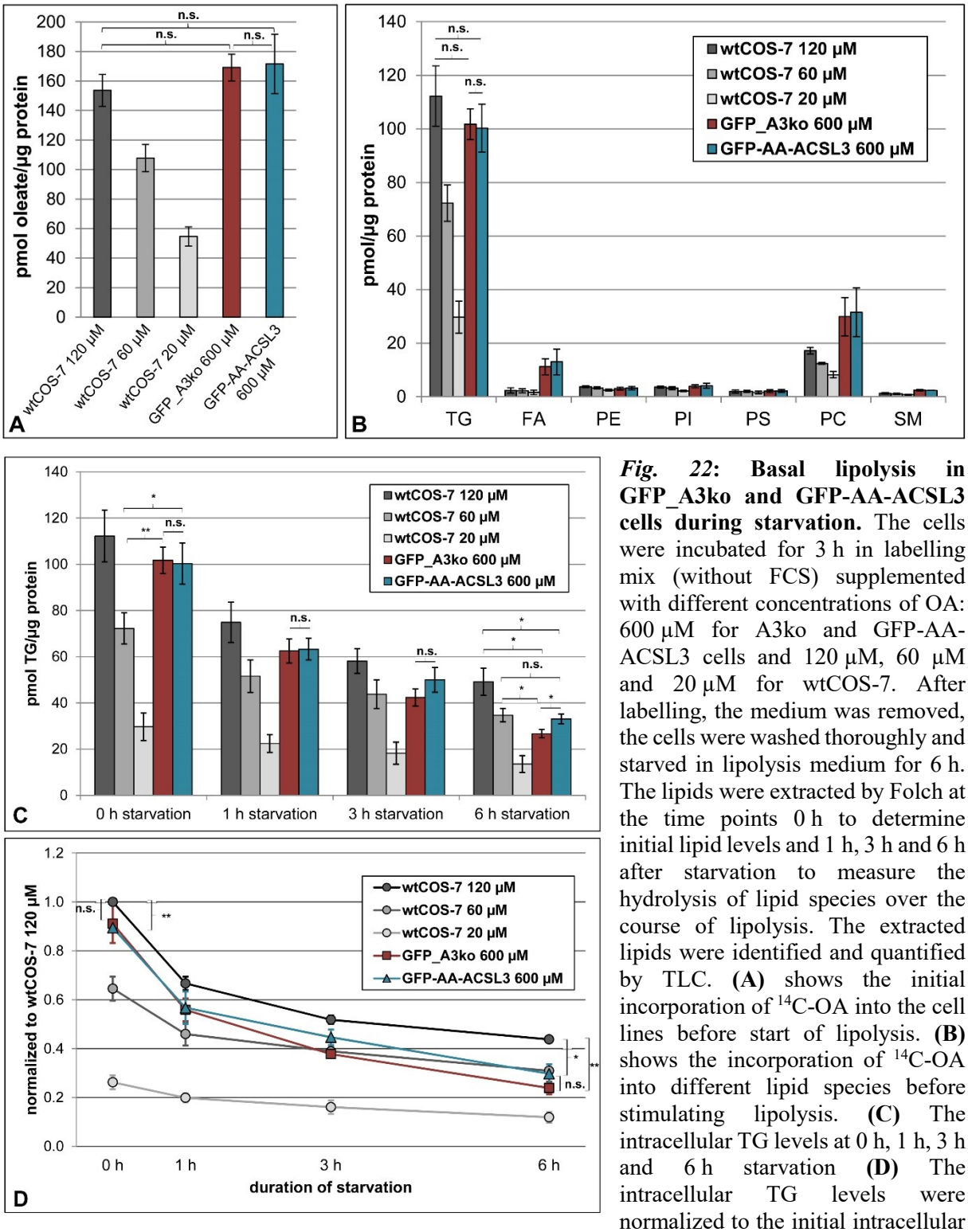

***Fig. 22*: Basal lipolysis in GFP_A3ko and GFP-AA-ACSL3 cells during starvation.** The cells were incubated for 3 h in labelling mix (without FCS) supplemented with different concentrations of OA: 600 µM for A3ko and GFP-AA-ACSL3 cells and 120 µM, 60 µM and 20 µM for wtCOS-7. After labelling, the medium was removed, the cells were washed thoroughly and starved in lipolysis medium for 6 h. The lipids were extracted by Folch at the time points 0 h to determine initial lipid levels and 1 h, 3 h and 6 h after starvation to measure the hydrolysis of lipid species over the course of lipolysis. The extracted lipids were identified and quantified by TLC. **(A)** shows the initial incorporation of ^{14}C-OA into the cell lines before start of lipolysis. **(B)** shows the incorporation of ^{14}C-OA into different lipid species before stimulating lipolysis. **(C)** The intracellular TG levels at 0 h, 1 h, 3 h and 6 h starvation **(D)** The intracellular TG levels were normalized to the initial intracellular TG levels of wtCOS-7 120 µM for each individual experiment and then the mean and SD was calculated for all experiments. Statistical analysis was performed using the Student's T-Test for unequal variances. The level of significance is indicated as follows: $p < 0.05$ (*), $p < 0.01$ (**), not significant (n.s.). n = 3 independent experiments; error bars are SD.

Lipolysis in the GFP-ACSL3 and GFP-ER-ACSL3 expressing cell lines

Figure 23 depicts the ^{14}C-OA uptake and the incorporation into different lipid species after labelling and the intracellular TG levels over the course of starvation measured in the GFP-ACSL3 and GFP-ER-ACSL3 expressing cell lines. When applied the same OA concentration of 120 µM for all cell lines, the initial TG levels in the GFP-ER-ACSL3 expressing cell lines was increased by 54 % in the GFP-ER-ACSL3(L) and 71 % in the GFP-ER-ACSL3(H) cells compared to the GFP-ACSL3 cells. Therefore the GFP-ACSL3 cells were additionally incubated in 300 µM and 450 µM OA to achieve comparable levels of initial TG. The labelling efficiency was not significantly different between the cell lines (*figure 23A*). The small difference in OA incorporation between the GFP-ACSL3 cells incubated at 120 µM, 300 µM and 450 µM OA suggest an unproportional relation between the OA concentration in the environment and the amount of OA incorporated in the cells. The initial TG levels of the the GFP-ACSL3 cells incubated at 300 µM and 450 µM were closest to the GFP-ER-ACSL3 expressing cell lines. All cell lines showed a degradation of intracellular TG over the course of starvation. The TG loss ranged from 39-54 % comparing initial TG levels and TG levels after 6 h starvation. The intracellular TG levels were not significantly different between the cell lines at any time of measurement. The GFP-ACSL3 cells incubated at 450 µM OA slightly gained TG between 1 h and 3 h starvation.

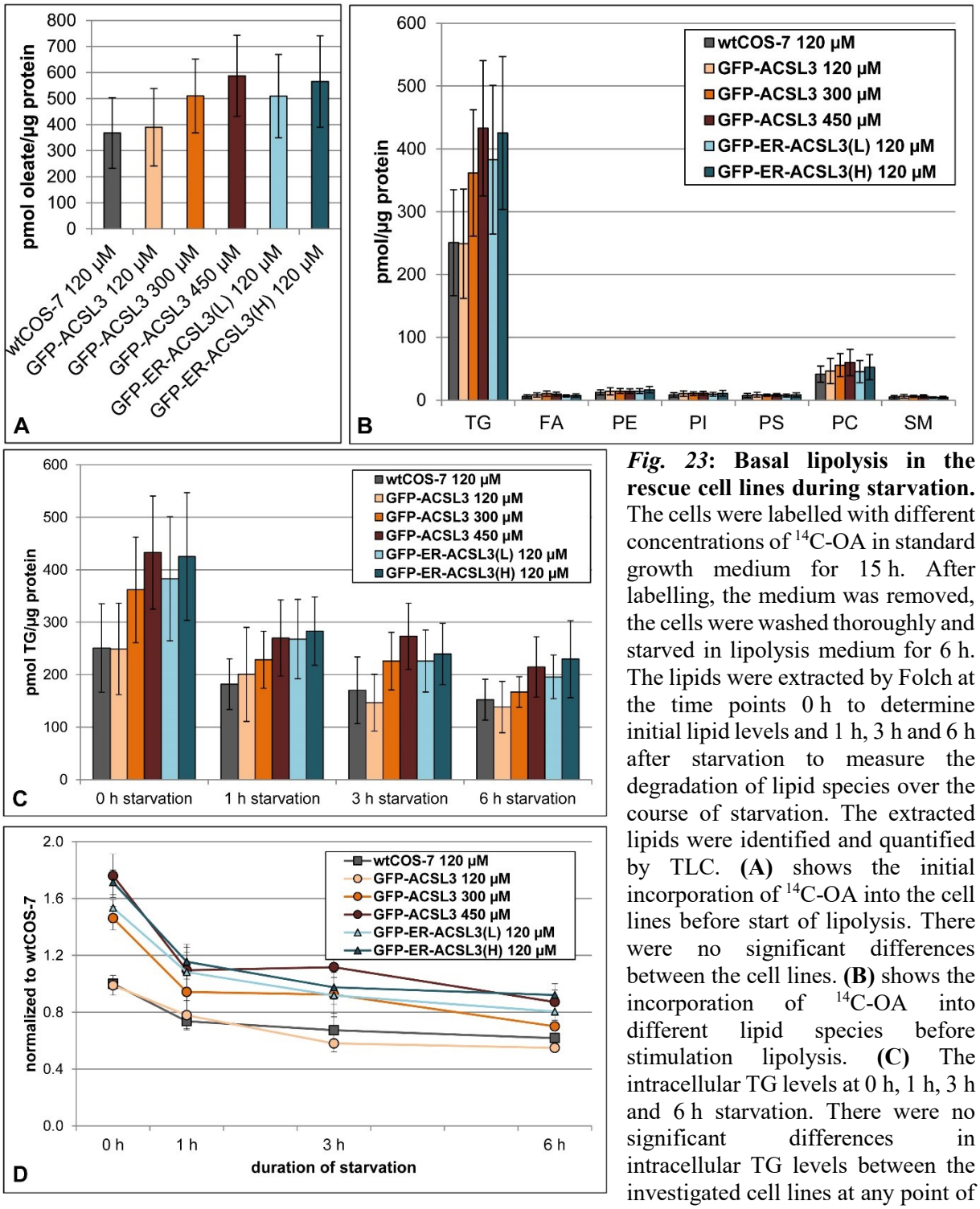

***Fig. 23*: Basal lipolysis in the rescue cell lines during starvation.** The cells were labelled with different concentrations of ^{14}C-OA in standard growth medium for 15 h. After labelling, the medium was removed, the cells were washed thoroughly and starved in lipolysis medium for 6 h. The lipids were extracted by Folch at the time points 0 h to determine initial lipid levels and 1 h, 3 h and 6 h after starvation to measure the degradation of lipid species over the course of starvation. The extracted lipids were identified and quantified by TLC. **(A)** shows the initial incorporation of ^{14}C-OA into the cell lines before start of lipolysis. There were no significant differences between the cell lines. **(B)** shows the incorporation of ^{14}C-OA into different lipid species before stimulation lipolysis. **(C)** The intracellular TG levels at 0 h, 1 h, 3 h and 6 h starvation. There were no significant differences in intracellular TG levels between the investigated cell lines at any point of measurement. **(D)** The intracellular TG levels were normalized to the initial intracellular TG levels of wtCOS-7 120 µM for each individual experiment and then the mean and SD was calculated for all experiments. Statistical analysis was performed using the Student's T-Test for unequal variances. There were no significant differences between the cell lines concerning OA incorporation and lipid levels at any time of measurement. n = 3 independent experiments; error bars are SD.

5.3 Metabolic capacity of lipid droplet-associated ACSL3 in A431 cells

5.3.1 Subcellular fractionation in A431 cells

The aim of the subcellular fractionation was to evaluate the importance of LD-localized ACSL3 for lipid droplet growth in A431 cells as a human cell line. The hypothesis was that LD-associated ACSL3 might create a hot spot for fatty acid activation on the lipid droplets pushing TG synthesis and driving lipid droplet growth. This experiment was supposed to show, if the amount and enzymatic activity of LD-associated ACSL3 significantly contributes to local TG synthesis and lipid droplet growth.

Prior to the subcellular fractionation in a sucrose gradient, A431 cells were grown in standard growth medium or in medium supplemented with 600 µM OA for 24 h to achieve considerable lipid droplet growth and translocation of ACSL3 from the ER to the LD. The flotation of LD under these conditions was based on previous work (Moessinger et al., 2011). In general, the LD were contained in fraction 1 (most upper fraction). Fraction 3 and 4 contained the cytosolic and membrane components. The partitioning of the fractions was verified by determination of calnexin as an ER marker and PLIN-3/Tip47 as a lipid droplet marker. Western blotting of the obtained fractions allowed to determine the amounts of ACSL3 in the fractions by densitometry (see *figure 24*). Without OA supplementation, ACSL3 was found in the bottom fractions 3 and 4, where the ER is found. In OA-treated cells, 25 % of ACSL3 translocated to the LD contained in fraction 1.

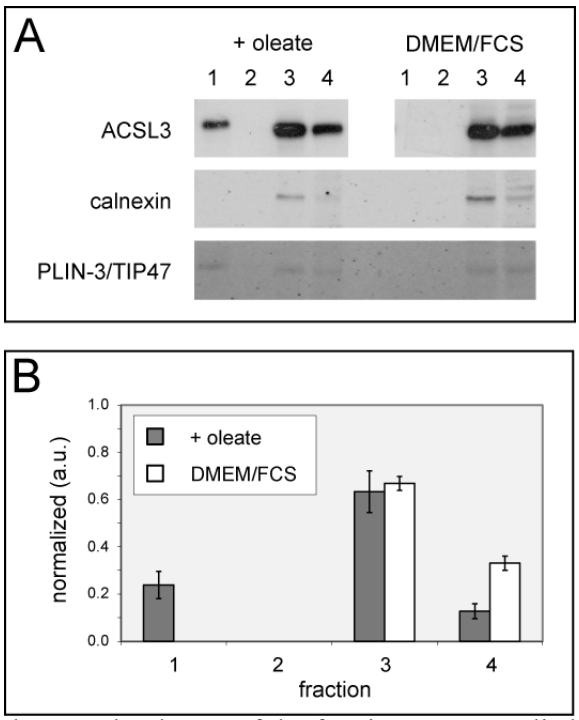

***Fig. 24*: Distribution of ACSL3 in subcellular fractions of A431 cells.** A431 cells were incubated with 600 µM OA (+oleate) or in standard culture medium (DMEM/FCS) for 24 h. Cells were homogenized by shearing using a G22 needle, and centrifuged at 1,000 x g for 5 min. The postnuclear supernatant was adjusted to 1.1 M sucrose and overlayed with an equal volume of buffer solution. After 3 h at 100,000 x g, four fractions were collected from top (F1) to bottom (F4). **(A)** Western blotting of ACSL3, calnexin (ER marker protein) and Plin3/TIP47 (LD marker). Representative blots from three independent experiments are shown. Note that the ACSL3 bands are from the same blot (but no free lane was used between the two conditions). Fractions 3 and 4 contained non-LD membranes as well as cytosolic proteins (Plin3/TIP47 is also localized in the cytosol). **(B)** ACSL3 bands were quantified by densitometry using ImageJ and normalized to total cellular ACSL3. n = 3 independent experiments; error bars are SD. Note that the four fractions had the same size (1.0 ml) and that equal volumes of the fractions were applied for western blotting. Some of the Western Blots were carried out by Fadil Minden (medical doctoral candidate). Published in Poppelreuther et al. (2018) (shared first authorship).

The subcellular fractionation was repeated with OA-treated cells. The ACSL3 amount and the ACS activity in the fractions was determined to investigate, if the ACS activity of LD-associated ACSL3 is changed compared to ER-associated ACSL3 and if this could influence TG synthesis. *Figure 25* depicts how much of total cellular ACSL3 and ACS activity was found in each fraction. Densitometry of the fluorescence signals obtained from Western Blot revealed that the major part of total ACSL3 protein (78.7 %) was still found in the membrane fraction, mainly ER, although the cells were fed with OA. In this experiment, ACSL3 was found in fraction 1 and additionally in fraction 2. It is unclear, why ACSL3 was found in fraction 2 in this experiment in contrast to the subcellular fractionation shown in *figure 24*, however, it does not effect the conclusion, because only a percentage of 21.3 % was found in the LD fractions 1 and 2. The contribution to total cellular ACS activity was 13.4 % for the LD fractions and 86.6 % for the membrane fraction.

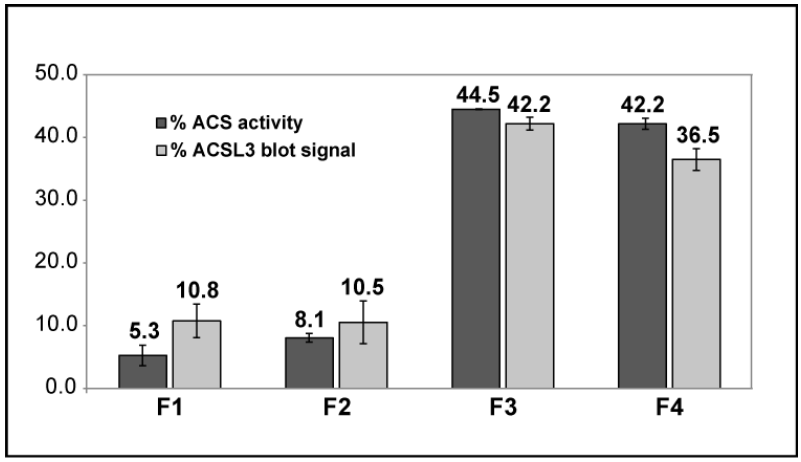

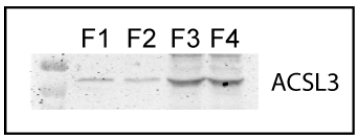

***Fig. 25*: ACS activity and ACSL3 quantity in subcellular fractions of OA-treated A431 cells.** The major portion of cellular ACSL3 protein and ACS activity was found in the non-LD membrane and cytosolic fractions (F3 and F4). An amount of 21.3 % of total cellular ACSL3 and 13.4 % of total cellular ACS activity were found in the LD fractions (F1 and F2). A431 cells were cultured in standard tissue culture medium supplemented with 600 µM OA for 24 h. Subcellular fractions were generated like described in section 4.3.3.7 . Oleoyl-CoA synthetase activity was determined as described in section 4.3.3.2, except that 50 µl of subcellular fraction were used instead of 10 µl Tx-100 cell lysate. 30 µl aliquots were separated by SDS-PAGE, incubated with mouse polyclonal anti human ACSL3 (Abnova H00002181-B01P) and LI-COR secondary antibodies, and scanned by an Odyssey Classic 900. LI-COR Image Studio 4.0.21 was used for the quantification of the ACSL3 blot signal. Two independent fractionation experiments were performed, with each experiment comprising triplicate samples for the determination of the enzyme activity. Error bars are SD. Published in Poppelreuther et al. (2018) (shared first authorship).

5.3.2 Molar quantification of ACSL3 in A431 cells

In order to draw conclusions concerning the metabolic capacity of ACSL3 on LD, the average amount of ACSL3 per cell was assessed. Recombinant GST-ACSL3 was generated from bacteria and quantified by applying a dilution series of BSA in a Western Blot analysis (*figure 26A*). Subsequently, a dilution series of the recombinant ACSL3 was prepared as a standard and analysed by Western Blot together with total cell lysates of A431 cells (*figure 26B*). By means of regression analysis the amount of endogenous ACSL3 in A431 cells was calculated. Considering the differences in molecular weight between GST-ACSL3 and endogenous ACSL3 the average amount of ACSL3 in A431 cells was 0.19 pg/cell. Taking into account the molecular weight of ACSL3 (80.42 g/mol) and the Avogadro constant (≈$6.02*10^{23}$ molecules/mol) the average number of ACSL3 molecules was 1.45 million molecules/cell.

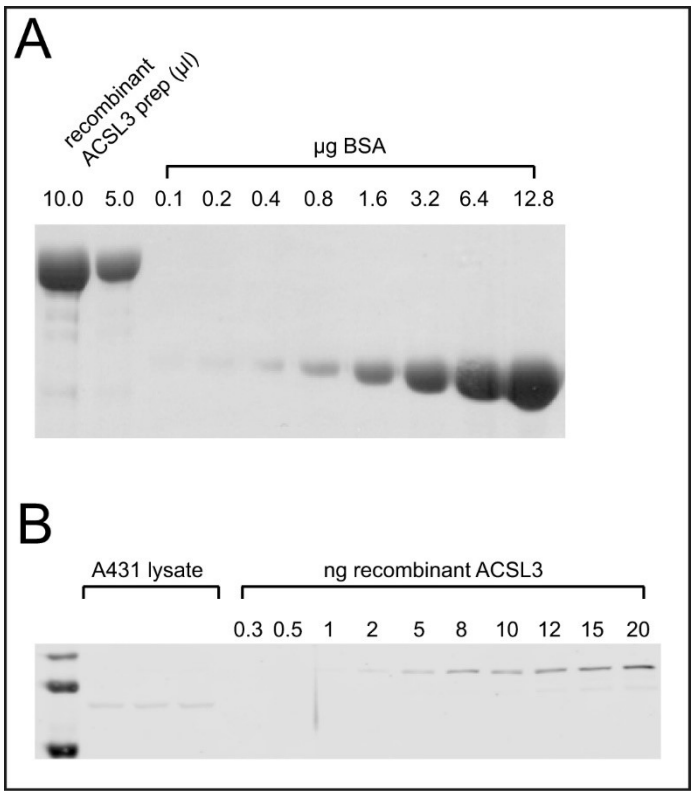

***Fig. 26*: Quantification of endogenous ACSL3 by comparison to recombinant protein. (A)** GST-ACSL3 was isolated from overexpressing bacteria. The concentration of recombinant GST-ACSL3 in the preparation was quantified by comparing the signal to different amounts of BSA after Coomassie brilliant blue R250 staining. Densitometry was performed by analysis with ImageJ version 2.0.0. **(B)** Aliquots of A431 total cell lysates and a dilution series of the recombinant GST-ACSL3 were analyzed by Western Blotting. Immunodetection was performed with a polyclonal mouse αACSL3 antibody (J059d). Quantification of ACSL3 in the A431 was done by densitometry using ImageJ version 2.0.0. n = 3 independent experiments. Published in Poppelreuther et al. (2018) (shared first authorship).

The molar quantification of ACSL3 was the basis to determine the metabolic capacity of LD-associated ACSL3 for LD growth by local triglyceride synthesis. Data from subcellular fractionation experiments (see section 5.3.1), cellular fatty acid incorporation and LD quantification by microscopy (data not shown, experiments performed by other students) were included for the calculation. The calculated LD parameters are summarized in *table 10*. We calculated, that the turnover for each ACSL3 molecule was 3.1 OA molecules per second during the OA incubation for 3 h. A number of 680 ACSL3 molecules was found on an average LD with a surface of 1.4 µm^2 and a diameter of 0.66 µm containing up to 95 million triglyceride molecules. The total TG synthesis in an A431 cell was compared to the amount of ACSL3 molecules existent on LDs. It was estimated that the contribution of LD-associated ACSL3 to cellular TG synthesis was only 3.3 %. See Poppelreuther et al. (2018) for details of the processed data and calculations.

***Tab. 10*: Summary of the calculated LD parameters.**

	+ oleate		DMEM/FCS	
ACSL3 molecules (total)	1,450,000	/cell	1,450,000	/cell
% ACSL3 on LDs	25.0	%	2.10	%
ACSL3 molecules on LDs	362,000	/cell	30,000	/cell
number of LDs per cell	533	/cell	44.4	/cell
total LD surface/cell	810	µm²	60.9	µm²
total LD volume/cell	82.8	µm³	6.71	µm³
avg diameter of LD	0.663	µm	0.661	µm
LD surface	1.38	µm²	1.37	µm²
LD volume	0.152	µm³	0.151	µm³
ACSL3 molecules per LD	680	/LD	680	/LD
LD surface occupied by ACSL3	1.26	%	1.27	%
TG molecules per LD	94,900,000	/LD	93,900,000	/LD

Molar quantification of ACSL3 in A431 cells was carried out using recombinant ACSL3. There was no difference in ACSL3 amount between OA-treated and untreated cells. The percentage of ACSL3 was calculated based on subcellular fractionation experiments. LD number and volume was determined based on analysis of image obtained from confocal microscopy (carried out by Tarik Exner, medical doctoral candidate). Published in Poppelreuther et al. (2018) (shared first authorship).

5.3.3 Indirect immunofluorescence of ACSL3 in A431 cells

Standard wide-field microscopy after immunofluorescence staining demonstrated that under standard growth conditions, ACSL3 was localized in the LD surrounding membrane and the tubular network of the ER (*figure 27A*). However, after OA treatment, only lipid droplet staining pattern was visible pretending that all cellular ACSL3 translocated to the LDs. This finding is divergent with the results obtained from subcellular fractionation estimating that the majority of ACSL3 is localized in the ER even after OA supplementation. In order to elucidate this discrepancy arising through limits in spatial resolution of conventional microscopy, dSTORM was performed. High-resolution images acquired by dSTORM confirmed ACSL3 staining on the LDs as well as in the cytoplasmic surrounding. The ACSL3-knockout cells showed minor background spots and were devoid of stained lipid droplets (*figure 27B*).

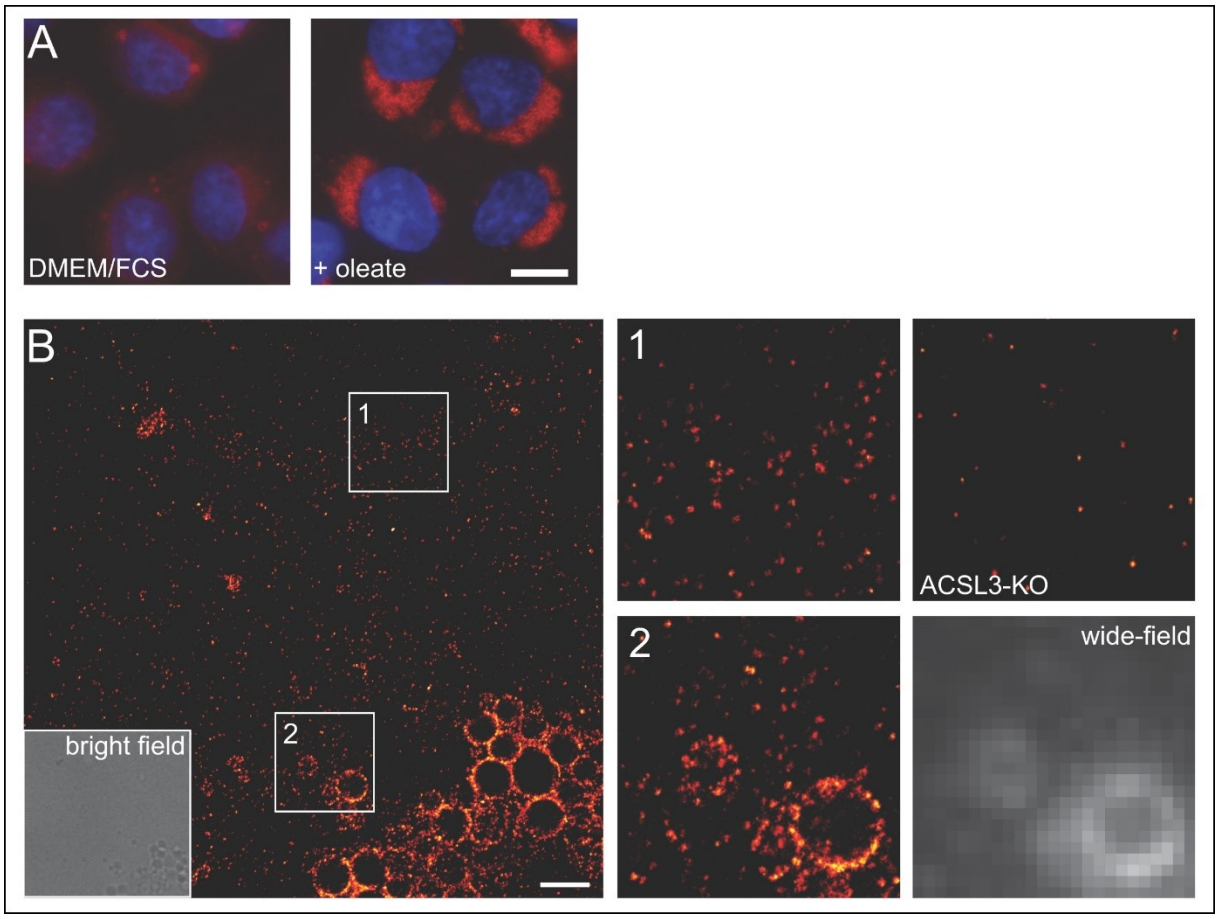

***Fig. 27*: dSTORM shows cytoplasmic localization of ACSL3. (A)** Conventional wide-field microscopy of ACSL3 immunofluorescence staining in A431 cells cultured under standard growth conditions and 600 µM OA supplementation for 24 h. ACSL3 was stained using polyclonal mouse αACSL3 antibody (J059d) and Cy3-conjugated αmouse antibody (J101). The nuclei were stained with Hoechst dye. Objective 60x. Scale bar 10 µm. **(B)** dSTORM of a section of an A431 cell treated with OA. Scale bar 2 µm. Inset 1 (4x4 µm) shows ACSL3 staining in the cytoplasmic area. A431 cells comprising an ACSL3-knockout (ACSL3-KO) were used as a negative control. Inset 2 (4x4 µm) depicts LD-localized ACSL3 with additional staining in the cytoplasmic periphery. A wide-field image clearly illustrated the gain in resolution obtained by dSTORM. Published in Poppelreuther et al. (2018). These data were generated in collaboration with Marina Dietz and Mike Heilemann from the Institute for Physical and Theoretical Chemistry at Goethe-University Frankfurt.

6. Discussion

6.1 ACSL3 is the dominant acyl-CoA synthetase in COS-7 cells

The ACSL3-knockout of the GFP_A3ko cells led to a decrease of ACS activity by 93 %. A similar decrease of 96 % was measured in the GFP-AA-ACSL3 expressing cells, as the transduced enzyme variant contained a mutation in the AMP-binding site and was not able to catalyze the esterification of fatty acids to CoA. This was also reflected by the decreased ^{14}C-OA incorporation and the increased levels of non-esterified fatty acids measured in the lipid extracts after labelling with ^{14}C-OA and ^{14}C-acetate (*figure 18* and *20*). The residual cellular ACS activity was imparted by other ACS family members. Conclusively, ACSL3 is the dominant ACS enzyme in COS-7 cells, which has been also shown for A431 cells (Poppelreuther et al., 2018).

Interestingly, in cell lines overexpressing ACSL3 the ACS activity did not increase proportionally to the expression level. The GFP-ACSL3 expression in the GFP-ACSL3 rescue cell lines was 10.2-fold increased compared to wtCOS-7, whereas the ACS activity was increased only by 2.7-fold (*figure 10* and *11*). This suggests that the reaction for esterification of fatty acids is not only dependent on the amount of available ACS enzyme, but also other rate-limiting factors, like e.g. GPAT (glycerol-3-phosphate acyltransferase), which is the rate-limiting enzyme for TG synthesis (Wang et al., 2017; Wendel et al., 2009). Accumulation of activated fatty acids might lead to a deceleration of the catalyzed reaction through substrate inhibition. When the activated fatty acids are not metabolized in subsequent pathways and accumulate, a negative feedback loop might downregulate the ACS enzymes and slow down the rate of fatty acid activation. Substrate inhibition has been described for many enzymes, e. g. the phosphofructokinase, acetylcholinesterase and the DNA methyltransferase (Reed et al., 2010).

6.2 Lipid species synthesis from endogenously synthesized fatty acids and exogenously supplied oleate

The GFP_A3ko and the GFP-AA-ACSL3 cells were expected to be impaired in lipid synthesis, because they were lacking endogenous ACSL3, which is the dominant ACS family member. The ACS enzymes are crucial for metabolizing fatty acids because they enable fatty acids to enter lipogenic pathways by esterifying fatty them with CoA. Since the cells are probably slowed down in metabolizing synthesized fatty acids due to a reduced ACS enzymatic capacity, non-esterified fatty acids were expected to accumulate in the cells.

The GFP-ER-ACSL3 expressing cell lines were expected to be increased in total substrate incorporation and thus lipid synthesis, because elevated amounts of GFP-ER-ACSL3 in the ER might increase the rate of fatty acid esterification. The activated fatty acids synthesized from acetyl-CoA might be rapidly used for synthesis of various lipid species. Due to a higher amount of enzyme in the high expressing cell line (GFP-ER-ACSL3(H)), the substrate incorporation and thus lipid synthesis was assumed higher compared to the low expressing cell line (GFP-ER-ACSL3(L)) due to metabolic trapping.

6.2.1 Depletion of ACSL3 by RNA interference or CRISPR knockout decreases triglyceride synthesis favouring phospholipid synthesis

The knockout of endogenous ACSL3 in the GFP_A3ko and the GFP-AA-ACSL3 cells led to a significant decrease in TG synthesis compared to wtCOS-7 cells. This was obvious in labelling experiments using ^{14}C-acetate and ^{14}C-OA and suggests that the impairment in TG synthesis was independent of the provided substrate (*figure 7*, *18* and *20*). These findings lead to the conclusion, that ACSL3 is essential to acquire cellular fat stores helping the cells during periods of nutrient deprivation. Other studies support these findings and demonstrate that a lack of ACSL3 or inhibition of ACSL3 by Triacsin C resulted in a decreased incorporation of radiolabelled OA into TG (Brasaemle et al., 2000; Igal and Coleman, 1996; Kassan et al., 2013; Muoio et al., 2000). In addition, the results are in line with studies of Bu et al. (2009), who report that the knockdown of ACSL3 in hepatocytes reduced ^{14}C-acetate incorporation in TG by 40 %.

The marked decrease in capacity for activation of fatty acids was expected to result in a clear decrease in overall lipid synthesis, because the reaction required for the fatty acids to enter pathways of lipid synthesis could not occur to a proper extent. However, the A3-RNAi cells, GFP_A3ko and GFP-AA-ACSL3 cells were characterized by a shift from TG synthesis to phospholipid synthesis when lipid synthesis from endogenously synthesized fatty acids was investigated (*figure 7* and *18*). The increased rate in phospholipid synthesis provided the substrates for enhanced cell proliferation observed in A3-RNAi cells (*figure 6*). It is interesting, that cells being impaird in lipid metabolism by ACSL3 depletion would prefer spending the available resources on cell proliferation rather than building up fat stores to ensure survival. Overexpression of the ACS family member FATP4 in A3-RNAi cells was able to downregulate phospholipid synthesis to the level of control cells, but was not able to compensate for the reduction in TG synthesis (*figure 7*). Therefore ACSL3 can be assumed as a protein regulating

deeply anchored mechanism equipping the cells with sufficient energy stores for survival and that this function is probably unique among the ACS enzyme family members.

6.2.2 GFP-ER-ACSL3 was more efficient in lipid synthesis than GFP-ACSL3

It was presumed that OA pre-incubation before labelling would augment potential differences between the GFP-ACSL3 and the GFP-ER-ACSL3 expressing cell lines, because GFP-ER-ACSL3, in contrast to GFP-ACSL3, was excluded from the lipid droplets. Especially the data from acetate labelling show an inversion of trends between the cell lines comparing the two growth conditions and lead to the conclusion, that lipid synthesis was more complex than pretended (*table 8*).

After OA pre-incubation, TG synthesis from endogenously synthesized fatty acids in the GFP-ER-ACSL3 cell lines tended to be reduced, as well as as phospholipid synthesis, especially PC and SM synthesis. Both were increased under standard growth conditions. Since phospholipid synthesis was increased in the GFP_A3ko cells, which are completely lacking ACSL3, the relative decrease in PC synthesis can not be simply explained by the situation that ACSL3 in the GFP-ER-ACSL3 cell lines was absent from lipid droplets, but might involve other factors like ACS activity and potential interaction with other regulatory proteins. More likely the differences in lipid species quantities simply reflect the differences in acetate incorporation, which was slightly decreased after OA pre-incubation and slightly increased under standard growth conditions. The finding that the relative proportions of lipid species distribution (data not shown) did not indicate any preferred lipid species for the GFP-ER-ACSL3 cell lines substantiates the assumption, that GFP-ER-ACSL3 does not channel endogenously fatty acids into certain lipid species but that the differences might be caused by different labelling efficiencies (*figure 19*). Using exogenously supplied OA as a substrate for lipid synthesis, the GFP-ER-ACSL3 cell lines synthesized more TG compared to the GFP-ACSL3 cells especially after OA pre-incubation (+31.7 % for the low expressing cell line; +35.9 % for the high expressing cell line). Phospholipid synthesis was marginally affected. Under standard growth conditions the TG synthesis in the GFP-ER-ACSL3 cell lines was closer to the GFP-ACSL3 cells but was still increased by 13.2 % and 23.0 % (*table 9*). Again, this differences are likely to result from the increased OA incorporation in the GFP-ER-ACSL3 cells.

The ACS activity was decreased by 60 % in the low expressing GFP-ER-ACSL3 cell line and by 34 % in the high expressing cell line compared to the GFP-ACSL3 cells (*figure 11*). Since this gradation in ACS activity was not reflected in lipid synthesis like the model of metabolic

trapping suggests, GFP-ER-ACSL3 appears to be superior over GFP-ACSL3 in substrate incorporation and lipid synthesis. By its localization in the ER, GFP-ER-ACSL3, independent from ACS activity, was more efficient in activation of fatty acids and delivering substrates for lipid synthesis. However, both ^{14}C-acetate and ^{14}C-OA labelling demonstrate that the high expressing GFP-ER-ACSL3 cell line tended to be superior in lipid synthesis than the low expressing cell line though mostly not significantly. Therefore it is reasonable to assume, that the level of ACS activity influences lipid synthesis at least to a small extent.

Regarding the entire magnitude of data obtained from the labelling experiments a substantial importance of ACSL3 localization for lipid synthesis is hard to conclude. The results do not always enable clear-cut interpretation and the high standard deviations impede a reliable statistical analysis of the data. However, GFP-ER-ACSL3 appears to be superior in fatty acid activation making lipid synthesis more efficient. This effect is presumably less dependent on ACS activity, because the effect was also observed for the low expressing GFP-ER-ACSL3 cells, which contained less than half the ACS activity of the GFP-ACSL3 cells (*figure 11*). Moreover, differences observed in phospholipid synthesis might have tremendous consequences with higher impact on ER membrane composition and lipid droplet nucleation (discussed in section 6.3.3).

6.2.3 ER-associated ACSL3 rather than lipid droplet-associated ACSL3 mediated lipid droplet growth by cellular triglyceride synthesis

^{14}C-acetate and ^{14}C-OA labelling assays showed that ACSL3 is essential for TG synthesis (*figure 7*, *18* and *20*). It has been hypothesized, that particularly LD-associated ACSL3 drives LD growth by local synthesis of TG due to its spatial proximity to LD. The idea of local TG synthesis on LD by ACSL3 becomes feasible, as at least one member of the enzyme families required for de novo synthesis, GPAT4, AGPAT3, PAP and DGAT2, has been reported to be present on cytosolic LDs (Pol et al., 2014). LD-associated ACSL3 might increase the local concentration of fatty acyl-CoAs and thus provide substrates for lipid synthesis. By subcellular fractionation in A341 cells LD-associated and ER-associated ACSL3 were separated and collected in different fractions. Quantification of ACSL3 protein and determination of ACS activity in the fractions was done to assess whether LD-associated ACSL3 is more potent in TG synthesis than ER-associated ACSL3. However, even after OA supplementation, the majority of total cellular ACSL3 protein and ACS activity was found in the membrane/cytosolic fraction, containing mainly the ER. Only 21.3 % of ACSL3 protein and 13.4 % of total ACS activity were contained in the LD fraction. It is not reasonable, that such a small percentage of

ACSL3 in the LD fraction might significantly contribute to LD expansion. And also the fact that the percentage of total ACS activity in the LD fraction was smaller than the ACSL3 protein content, suggest that ACS activity is not increased by translocation of ACSL3 to the LD but rather decreased. In addition, we provided a molecular model for a LD based on LD morphometrics, dSTORM microscopy, molar quantification of ACSL3 and LD counting in confocal images. It has been estimated, that LD-associated ACSL3 accounts for 3.3 % of total cellular TG synthesis. The data from subcellular fractionation are in accordance with studies in Huh7 cells, where 40 % of ACSL3 were found in the LD fraction (Fujimoto et al., 2007; Fujimoto et al., 2004). Differences in the applied biological system might account for the small discrepancy in the percentage. Kassan et al. (2013) suggested a 'complete redistribution of ACSL3 from the ER into LDs', which is a vague statement in view of a missing validated quantification. Taking all these data together, the metabolic capacity of ACSL3 on LD is assumed to be insufficient to solely drive by LD growth by local TG synthesis. Instead it is suggested that the neutral lipid transfer from the ER to the LD accounts for a higher amount of LD growth (Poppelreuther et al., 2018). The transfer of lipids might occur through LD-ER-membrane bridges already described for protein transfer. Emerging LDs were found out to be devoid of DGAT2 substantiating the assumption that local TG synthesis does not occur to an adequate extent at least in early stages of LD growth (Kassan et al., 2013).

6.3 Lipid droplet biogenesis

ACSL3 has been shown to translocate from the ER to nascent LD suggesting a role for ACSL3 in LD biogenesis (Kassan et al., 2013; Poppelreuther et al., 2012). In order to compare the capability of the cell lines to generate lipid droplets, the cells were starved and then incubated with 600 µM OA for a short time of 20 min. The LD were labelled by the transduced marker protein A3Nt-mcherry that efficiently translocates to the LD (Poppelreuther et al., 2012) and microscopic pictures were analyzed by an automated algorithm in ImageJ to determine the LD number in each cell. The time of 20 min was sufficient to see the newly synthesized lipid droplets under the microscope, but was short enough to allow distinction between recently generated LD and LD that were remained in the cells in spite of starvation. So to speak 'starvation resistant' LD were bigger than early LD and showed a fluorescence pattern surrounding the LD since the neutral lipid core is not labelled by A3Nt-mcherry. Cells containing such LD were excluded from the analysis. The newly synthesized LD were recognized as fluorescing dots, since the microscopic resolution was not high enough to separate LD membrane and the neutral lipid core. LD emerging during biogenesis can be

already detected after 5-7 min (Kassan et al., 2013). A longer LD-induction time of 20 min in this experiment was considered suitable to increase and detect the differences in LD biogenesis between the cell lines more easily.

The GFP_A3ko and the GFP-AA-ACSL3 cells were expected to be reduced in lipid droplet biogenesis, because they were depleted from ACS enzymatic capacity due to the ACSL3-knockout. Therefore activation of OA and TG synthesis might be slowed down and impaired. In the GFP-ER-ACSL3(H) cells the whole portion of GFP-ER-ACSL3 was localized in the ER, because it was not able to translocate to the LD like GFP-ACSL3. This feature was assumed to be a potential advantage in LD biogenesis, because GFP-ER-ACSL3 might enhance the activation of fatty acids feeding the lipogenic machinery, which is harboured at the ER, with substrates. Therefore, the GFP-ER-ACSL3(H) cells were expected to have an increased LD biogenesis.

6.3.1 ACSL3-knockout cells and rescue cell lines were comparable in sensitivity to starvation

The LD number in starved cells was not significantly different between the cell lines, suggesting there were no differences in sensitivity to starvation (*figure 15A*). Although not statistically significant, the average LD number in starved GFP-ER-ACSL3(H) cells was doubled compared to the GFP-ACSL3 cells. However, the impression during microscopy did not ascertain a higher number of LD in starved GFP-ER-ACSL3(H) cells suggesting that the automated quantification had higher susceptibility to false-positive counting in these cells. One possible reason for that might be, that a higher A3Nt-mcherry expression in the GFP-ER-ACSL3(H) cells caused the formation of small fluorescing aggregates in the ER. These aggregates, which are common phenomena in overexpressing cells, might be wrongly identified as LD, since the automated quantification identified fluorescence intensity maxima. Yet this assumption is unlikely, because only cells with a moderate A3Nt-mcherry expression were included in the analysis. This was done by selecting cells with optimal imaging properties at an exposition time in a range of 100-700 ms.

6.3.2 ACSL3 was essential for an abundant lipid droplet biogenesis in starved COS-7 cells

The wtCOS-7 and the GFP-ACSL3 likewise increased their LD number to approximately 5-fold of the starvation control indicating that GFP-ACSL3 could rescue LD biogenesis in these

cell lacking endogenous ACSL3. The GFP_A3ko and GFP-AA-ACSL3 cells were both heavily impaired in LD biogenesis demonstrating that the capability to generate LD is depending on the level of cellular ACS activity (*figure 15B*). The GFP_A3ko and GFP-AA-ACSL3 cells could not efficiently metabolize the OA due to diminished activation. These findings confirm former investigations showing that depletion of ACSL3 by siRNA or ACSL3 inhibition with Triacsin C significantly reduced LD formation (Herms et al., 2013; Kassan et al., 2013). Compensation of ACSL3-knockdown in COS-1 cells with ACSL1 and ACSL4 did not rescue LD formation indicating that ACSL3 has probably a unique role in LD biogenesis among the ACS family members (Kassan et al., 2013).This essential role of ACSL3 in TG synthesis was also revealed in previous experiments investigating TG synthesis in well-nourished cells by ^{14}C-acetate and ^{14}C-OA labelling (*figure 18* and *20*). These data show that the endogenous ACSL3-knockout led to a heavy impairment in fatty acid metabolism beginning already at the early stages of lipid droplet formation.

6.3.3 Lipid droplet biogenesis was impaired in GFP-ER-ACSL3(H) cells

Unexpectedly, the GFP-ER-ACSL3(H) cells were significantly reduced in LD biogenesis. The lipid droplet number was not even doubled during lipid droplet induction and compared to the GFP-ACSL3 cells, the lipid droplet number was significantly reduced by 54 % after 20 min of OA incubation (*figure 15B*). Taking into account the higher rate of false-positive counts in this cell line, the LD number of 46 in OA-treated GFP-ER-ACSL3(H) cells might be even overestimated. Moreover, the protein expression was quantified by analysis of the cellular GFP fluorescence. That there was no correlation between GFP fluorescence and LD number was probably due to a small sample size and the selection of cells with a moderate GFP fluorescence. If the range of flurescence intensity was extended and sample size increased, it would be very likely to find a correlation as the number of emerging lipid droplets very well increased with increasing levels of ACSL3 protein in former studies (Kassan et al., 2013). The LD number would probably increase with increasing ACSL3 protein content until a plateau is reached marking the saturation level of the enzymatic activity. The GFP-fluorescence in the GFP-ER-ACSL3(H) cells was increased by 55 % compared to the GFP-ACSL3 cells (*figure 15C*). Therefore, a lower expression level of GFP-ER-ACSL3 and thus lower cellular ACS activity can be excluded as a reason for the reduced number of LD in the GFP-ER-ACSL3(H) cells. In order to get deeper insight into the cellular TG synthesis under these conditions, the biochemistry of the cells was investigated by labelling the starved cells with ^{14}C-OA during LD induction. Subsequent TLC of the extracted cellular lipids did not reveal differences in the

synthesis of TG or phospholipids between GFP-ACSL3 and GFP-ER-ACSL3(H) cells. TG synthesis of the GFP-ER-ACSL3(H) cells was yet increased by 14 %, although not significantly (*figure 16*). Apparently, the GFP-ER-ACSL3(H) cells were not impaired in TG synthesis, but they were not able to put these into LD. Probably the TG accumulated between the two ER leaflets without forming growing lipid lenses and being released into the cytosol as lipid droplets. This phenotype is surprising and leads to the conclusion, that ACSL3 is not only essential for TG synthesis, but also the formation of nascent lipid droplets.

The de novo biogenesis of LD is described to occur in three steps: 1) Synthesis and accumulation of neutral lipids between the two leaflets of the ER. 2) Lense formation as the neutral lipid concentration reached a crucial threshold. 3) ER bilayer deformation and budding of the nascent LD into the cytosol (Wilfling et al., 2014a). TG synthesis was not impaired in the GFP-ER-ACSL3 expressing cells which suggests that the cells might be affected in lense formation. Thiam and Foret (2016) extensively explain the biophysics of lense formation during LD biogenesis. Before lense formation, the TG move freely within the ER phospholipid bilayer. Lense formation, i.e. nucleation, occurs as event of spontaneous demixing of the hydrophobic TG and the hydrophilic phospholipids contained in the membrane. This phase separation takes place when the nucleation barrier is surmounted, i.e. under conditions where the energy cost for the interaction of a TG and a phospholipid molecule exceeds the energy required for the interaction between two TG molecules. There are different mechanisms facilitating nucleation by lowering the nucleation barrier, e.g. membrane curvature and curvature-inducing proteins, TG synthesis resulting in high local TG concentrations and components interacting with TG like proteins and other lipids (Thiam and Foret, 2016).

The intrinsic shape of lipids, which is characterized by the size of their headgroups, length and saturation of their fatty acyl chains, influences the shape of the lipid bilayer and packaging of lipids in the bilayer. PC and PS have been shown to form flat monolayers due to their cylindrical shape. PE, diacylglycerols or cardiolipins are conical shaped and cause a negative, i.e. inwardly, curvature. Sterols improve the packaging of sphingolipids in the bilayer, which compromises spontaneous membrane curvature (McMahon and Boucrot, 2015). Acetate labelling showed that under steady state conditions, the endogenous synthesis of PC, PS, PE and CH was significantly increased by 35 %, 27 %, 33 % and 43 % in the GFP-ER-ACSL3(H) cells compared to the GFP-ACSL3 cells (*figure 19C, table 8*). Also OA labelling demonstrated an increase in PC, PS and PE synthesis in the GFP-ER-ACSL3 cell lines though slightly smaller (PC +29 %, PS +20 %, PE +27 %; *figure 22C, table 9*). This might lead to a change in ER

membrane composition and shape causing impairment in LD nucleation by mechanisms given above. However, to confirm this assumption, the lipid synthesis and ER membrane composition should be assessed in starved cells, as the specified data from the labelling experiments were obtained from cells grown under standard growth conditions or OA supplementation. Another aspect might be, that LD-associated ACSL3 could influence ER membrane lipid composition curvature by promoting LD-ER-bridges and supporting transfer of certain lipid species. In addition to the influence originating from the membrane lipids per se, the change in membrane lipid compositition might increase membrane curvature by recruitment of curvature-inducing proteins. (McMahon and Gallop, 2005).

Moreover, it has been reported, that the insertion of amphipathic helices into lipid bilayers increases membrane curvature. This has been demonstrated for proteins like epsin, amphophysin and endophilins containing amphipathic helices (McMahon and Gallop, 2005; Shen et al., 2012). ACSL3 also contains an amphipatic helix at its N-terminus (Pataki et al., 2018; Poppelreuther et al., 2012). As the N-terminus of the GFP-ER-ACSL3 construct is modified and the amphipathic helix motif is missing, the observed phenotype in LD biogenesis might not result from differences in protein localization, but from the modification of the protein structure.

After incubation in OA for 1 h after 24 h starvation (*figure 17*), under steady state conditions (*figure 12*) and after OA treatment (*figure 13*) the GFP-ACSL3 and GFP-ER-ACSL3 expressing cells were comparable in LD number and size. This suggests that the observed phenotype in the GFP-ER-ACSL3 cells is valid for the early stages of LD biogenesis and the cells catch up in later stages. Probably, nucleation occurs to an increasing degree, when the capacity for TG accumulation between the ER leaflets is exploited. The limit for TG solubility in phospholipid membranes amounts to approximately 3 % (w/w), depending on the cell type and subcellular compartment (Khandelia et al., 2010).

6.4 Basal lipolysis

Under fasting conditions, TG stored in the adipose tissue are hydrolyzed into free fatty acids and glycerol. The free fatty acids are used as substrates for β-oxidation to cover the demand for energy. However, not all fatty acids liberated during lipolysis are oxidized. It has been estimated, that 30 % of fatty acids are re-esterified back to triglycerides (Reshef et al., 2003). ACSL3, as it translocates to LD, might regulate lipolysis by re-esterification of the liberated fatty acids. Therefore, the GFP_A3ko cells were hypothesized to be elevated in lipolysis

because they are lacking ACSL3 that could re-esterify the liberated fatty acids. In addition to the ACS activity, ACSL3 might also counteract lipolysis by other means. ACSL3 by its presence on LD could inhibit lipolysis by forming a protective shell around the TG and prevent immediate accecss of lipases to the LD. Recruitment of other antilipogenic factors is also imaginable. Interaction of ACSL3 with other proteins has been verified for ancient ubiquitous protein 1 (AUP1) and spartin, which are involved in LD turnover, size and number (Eastman et al., 2009; Klemm et al., 2011; Milewska et al., 2009; Spandl et al., 2011). These functions independent from ACS activity were supposed to be investigatied in the GFP-AA-ACSL3 cell line, which might be assumed to show alleviated lipolysis compared to the GFP_A3ko cells. The localization of ACSL3 might also be relevant for lipolysis. Assuming that the presence of ACSL3 on LD has a protective function, the GFP-ER-ACSL3 expressing cells might show elevated lipolysis compared to the GFP-ACSL3 cells, because GFP-ER-ACSL3 was excluded from the LD. However, the higher proportion of GFP-ER-ACSL3 in the ER might increase lipid synthesis by channeling activated fatty acids towards the responsible enzymatic machinery, which is mainly harboured in the ER.

6.4.1 Triglyceride synthesis did not increase proportionally with the concentration of supplemented oleate

Comparison of the cell lines regarding lipolysis necessitated the establishment of initial situations that are as equal as possible, i. e. similar levels of intracellular TG after labelling with OA. When the cell lines differed in initial intracellular TG levels at equal OA concentrations, the OA concentration was increased in the cells that had lower TG levels to push OA incorporation and TG synthesis. That was especially necessary for the comparison of the GFP_A3ko and GFP-AA-ACSL3 cells with wtCOS-7 cells, but also for the comparison of the GFP-ACSL3 and GFP-ER-ACSL3 cells. WtCOS-7 cells were incubated in 20 µM, 60 µM and 120 µM OA to match the TG synthesis of the GFP_A3ko and GFP-AA-ACSL3 cells incubated in 600 µM OA. Comparing the wtCOS-7 cells, the initial TG levels were 29.6 pmol/µg protein at 20 µM OA, 72.2 pmol/µg protein at 60 µM OA and 112.2 pmol/µg protein at 120 µM OA (*figure 22B*). The increase in TG synthesis from 20 µM to 60 µM was not 3-fold but 2.4-fold. The TG synthesis from 60 µM to 120 µM was not doubled but increased by 1.6-fold. The GFP-ACSL3 cells were incubated at 120 µM, 300 µM and 450 µM OA to match the TG synthesis of the GFP-ER-ACSL3 cell lines incubated at 120 µM OA. The initial TG levels in the GFP-ACSL3 cells were 249.1 pmol/µg protein at 120 µM OA, 361.7 pmol/µg protein at 300 µM OA and 432.8 pmol/µg protein at 450 µM OA (see *figure 23B*). The increase in TG synthesis from

120 µM to 300 µM was not 2.5-fold but 1.5-fold. The increase in TG synthesis from 300 µM to 450 µM was not 1.5-fold but 1.2-fold. Taken together, the relative increase in TG synthesis achieved by an increase in OA concentration was smaller than expected. This suggests that the correlation between OA concentration and TG synthesis is not linear but logarithmic, reaching a plateau at high OA concentrations due to a saturation of enzymes involved in TG synthesis. Since the plateau was not reached in the current experiments, the saturation concentration for wtCOS-7 was higher than 120 µM and higher than 450 µM for GFP-ACSL3 cells. Estimating from the available data, the saturation would be probably reached between the range of 500-600 µM OA.

6.4.2 The lipolytic rate was dependent on initital intracellular level of triglycerides and acyl-CoA synthetase activity

WtCOS-7 cells were radiolabelled with 120 µM, 60 µM and 20 µM OA. This resulted in different levels of intracellular TG with the highest values in the cells treated with 120 µM OA and the lowest values in the cells treated with 20 µM OA. This confirms, that the OA incorporation is dependent on the OA concentration in the medium and that OA incorporation can be pushed by elevating the OA concentration in the medium (Alsabeeh et al., 2017). Comparing the cells incubated in 120 µM and 20 µM, the relative loss of TG over the course of starvation is approximately 50 % for both cell lines. Calculating the absolute loss of TG, the value is much higher for the cells treated with 120 µM OA. In the cells incubated in 20 µM OA, the lipolytic rate was downregulated (*figure 22*). Apparently, cells that are well-provided with energy stores are not as keen to maintain these stores under starving conditions. When the cells are poorer in energy stores in the form of lipids, their metabolism might be more strictly regulated also under nutrient-depletion to ensure cell survival. Lipolysis might be downregulated by energy-sensors inhibiting lipolytic enzymes when intracellular TG levels are low. A protein that could mediate such effect is AMPK, which is discussed to be the key sensor in cellular energy and an important player in the regulation of lipolysis together with PKA (Djouder et al., 2010). This involves numerous proteins on several levels of cell biological processes, like ATGL, HSL, CGI-58, G0S2, justifying the assumption, that an energy-sensor might downregulate lipolytic activity, when intracellular TG stores are small.

The initial intracellular TG levels measured in the GFP_A3ko and GFP-AA-ACSL3 cells were comparable to the wtCOS-7 cells treated with 120 µM OA and significantly higher than in the wtCOS-7 cells incubated in 60 µM OA. After 6 h of starvation, the intracellular TG levels in

the GFP_A3ko and GFP-AA-ACSL3 cells were significantly decreased compared to the wtCOS-7 cell at 120 µM. Compared to wtCOS-7 at 60 µM after 6 h starvation, the TG levels were significantly decreased in the GFP_A3ko cells and not significantly different in the GFP-AA-ACSL3 cells (*figure 22*). Obviously, the GFP_A3ko and GFP-AA-ACSL3, both depleted in ACS activity, had a higher lipolytic rate suggesting that ACSL3 indeed counteracts lipolysis. This effect is probably dependent on re-esterification of fatty acids deliberated during lipolysis, since GFP_A3ko and GFP-AA-ACSL3 were both highly affected.

6.4.3 The ACSL3 membrane anchor was protective against basal lipolysis

In addition to the inhibition of lipolysis by re-esterification, the ACSL3 membrane anchor per se might counteract lipolysis. This effect was observed comparing the GFP_A3ko and the GFP-AA-ACSL3 cells. Within the first hour of starvation, both cell lines, that did not differ in initial intracellular TG levels, were equivalent in TG loss. Afterwards, the lipolytic rate in the GFP-AA-ACSL3 cells slowed down resulting in significantly higher intracellular TG levels after 6 h starvation. After 3 h of starvation, the intracellular TG level in the GFP-AA-ACSL3 was increased by 18 % compared to the GFP_A3ko cells and after 6 h the percentage was 24 % (*figure 22C*). It would be interesting to investigate the development of TG levels over a longer period of starvation. The difference between the cell lines might outweigh over time or the advantage of the GFP-AA-ACSL3 cells over the GFP_A3ko cells might become even more pronounced due to a higher stability of intracellular TG levels or even higher cell survival under nutrient deprivation.

Since both cell lines are lacking ACS activity, the presence of ACSL3 alone is likely to be responsible for that difference. The effect might be explained by a shielding function of ACSL3 on LD, restricting access of lipases to the TG. One example for proteins with a shielding function is PLIN1 that has been reported to protect LD from cytosolic lipases with its amino and carboxyl termini (Garcia et al., 2004). The recent model, however, suggests a scaffolding role for PLIN1 which binds CGI-58, when lipolysis is suppressed and thus inhibits lipolysis (Konige et al., 2014). Moreover, the percentage of LD surface covered by ACSL3 in A431 cells has been estimated to 1.3 % (Poppelreuther et al., 2018). This density appears to low to mediate suffient shielding of TG by ACSL3. Alternatively, ACSL3 might recruit antilipolytic proteins to the LD inhibiting lipolysis. GFP-AA-ACSL3 is also localized in the ER, therefore an effect arising from there should also be considered. However, it is unlikely, that a GFP-AA-ACSL3 on the ER imparts a repressive effect on lipolysis. Recruitment of proteins could only influence

lipolysis by indirect cell signaling pathways due to the spatial distance to the LD. Therefore, an action implemented directly on the LD is more likely.

6.4.4 The localization of ACSL3 did not impact cellular lipolysis

Investigation of basal lipolysis did not reveal significant differences between the GFP-ACSL3 and GFP-ER-ACSL3 expressing cell lines. Like observed in the wtCOS-7 cells, different OA concentrations applied for the GFP-ACSL3 cells resulted in different levels in TG synthesis. The OA concentration had to be elevated to 300 and 450 µM in the GFP-ACSL3 cells to obtain comparable initial intracellular TG levels to the GFP-ER-ACSL3 expressing cell lines. This goes in line with the data obtained from the OA labelling assay, where the GFP-ER-ACSL3 expressing cell lines were increased in TG synthesis when incubated with the same OA concentration like the GFP-ACSL3 cells (*figure 21B*). The ACS activity was the highest in the GFP-ACSL3 cells and the lowest in the low-expressing GFP-ER-ACSL3 cell line (f*igure 11*) but there were no major differences in lipolytic rate between the cell lines. The high-expressing GFP-ER-ACSL3 cell line was increased in ACS activity by 62 % compared to the low-expressing cell line but differences in intracellular TG levels during starvation were only marginal (*figure 23*). These findings indicate that ACS activity in these cell lines did not impact cellular processes of basal lipolysis. It is suprising, that the intracellular TG levels were so much increased in the GFP-ER-ACSL3 cell lines compared to GFP-ACSL3 at 120 µM OA. Likewise to the OA labelling assay, where the increased TG synthesis in the GFP-ER-ACSL3 (*figure 21B*) was presumed to be a consequence of the increased OA incorporation (*figure 21A*), the increased TG synthesis in the GFP-ER-ACSL3 cells could also be caused by an increased OA incorporation in the lipolysis experiment. Though not significantly, the OA incorporation was increased by 31% in the low-expressing GFP-ER-ACSL3 cell line and by 45 % in the high expressing cell line compared to the GFP-ACSL3 cell line incubated at 120 µM OA (*figure 23A*). Passage numbers of the cell lines used for the experiments were similiar and in a range considered appropriate. In addition, microscopy confirmed that the GFP-ACSL3 was still present and intact in the cells (data not shown). Therefore the increased TG synthesis at 120 µM OA in the GFP-ER-ACSL3 cells compared to GFP-ACSL3 was probably not conditioned by a perturbation in the biological system. This might suggest a superior capability of GFP-ER-ACSL3 in TG synthesis due to the higher availablility of ACSL3 enzyme activity at the ER, which harbours the enzyme machinery for TG synthesis.

The observation that the GFP-ACSL3 cells incubated at 450 µM OA very slightly increased in TG between 1 h and 3 h starvation is most likely not a physiological finding, but a consequence from variation in the experimental procedure, because the values were not established in the same cells, but in mock-treated cells (*figure 23C* and *D*).

6.5 Benefits and drawbacks of the biological system

Most of this work was done in COS-7 cells which were genetically modified by the CRISPR/Cas9 method and retroviral transduction. An ACSL3-knockout was generated using CRISPR/Cas9 that is a tool for genetic engineering increasingly applied in various fields of life sciences. The endogenous knockout means a complete depletion of the cellular ACSL3 protein and therefore outplays former techniques achieving a knockdown and thus bearing the risk of unexpected upregulation of residual enzymatic activity. Although the effort of CRISPR/Cas9 is manageable and the experimental benefit is huge, most previous work included knockdown of ACSL3 by RNA interference (Ansari et al., 2017; Bu et al., 2009; Kageyama et al., 2013; Kassan et al., 2013; Padanad et al., 2016; Poppelreuther et al., 2012; Poppelreuther et al., 2018) or inhibition of ACSL3 with Triacsin C (Brasaemle et al., 2000; Herms et al., 2013; Igal and Coleman, 1996; Kassan et al., 2013; Muoio et al., 2000). Therefore, this work is of high interest and importance. The ACSL3-knockout cells were rescued with the ACSL3 enzyme variants GFP-ER-ACSL3 and GFP-AA-ACSL3. Studies with the GFP-ER-ACSL3 expressing cells were supposed to deliver insight into the relevance of ACSL3 localization. This approach is unique until now and holds the potential to provide answers for the fundamental question about ACSL3 function on LD. By means of GFP-AA-ACSL3 lacking ACS activity the functions of ACSL3 independent from ACS activity were supposed to be investigated. Also this approach is new and can help to identify unexpected functions of ACSL3 influencing different fields of cellular biology.

The generation of genetic modifications by CRISPR/Cas9 always holds the risc to hit off-targets and induce unrequested alterations in the organism or cell line. If these off-targets effect genes involved in cell morphology, growth, formation of structural elements, damaged cell lines can be spotted during work of cell culture routine or characterization of the cell lines. Off-target effects modifying genes involved in pathways being subject of investigation can have a tremendous influence on the obtaind results. The CRISPR direct tool, which has been used to design the guide RNA for the ACSL3-knockout, screens the genomic data and defines potential off-target sites for every proposed guide RNA. The off-target evaluation does not only include

target sites perfectly matching the guide RNA, but also ‘seed sequences’, i.e. where not the complete, but parts of the guide RNA, 8 or 12 nucleotides, are complementary to the genome. This kind of evaluation covers the vast majority of potential risks and gives a reliable estimation of which guide RNA is efficient and specific. The guide RNA contained in the CRISPR plasmid A3-ex4 was highly specific without potential off-targets for the complete target sequence and the seed sequence of 12 nucleotides. The guide RNA-contained in the CRISPR plasmid A3-ex2 comprised ten potential off-target sites for the seed sequence of 12 nucleotides. The probability to generate a double strand break in a seed sequence is rather low, because perfect complementary base-pairing is not possible. Each three clones, inconspicuous in cell morphology and behaviour, raised from transfection with the CRISPR plasmids were pooled to level out potential off-target effects. Therefore, the vulnerability to off-target effects having significant impact on the obtained data is estimated to be quite low.

However, this biological system holds some weaknesses that have to be considered interpreting the data obtained from the experiments. ACS activity mediated by the ACSL enzymes can impact fatty acid uptake by metabolic trapping (Füllekrug et al., 2012; Watkins, 2008). Metabolic trapping has been previously shown for FATP4 and ACSL1 (Milger et al., 2006; Schneider et al., 2014). Fatty acid uptake yet directly impacts the lipid synthesis, because the relative substrate deficit or excess are metabolized differently in cells. Considering this model, the expression level of GFP-ACSL3 and GFP-ER-ACSL3 should be equal to draw reliable conclusions from the data. Identical expression levels were not achieved by retroviral transduction. One strategy managing this situation was to include GFP-ER-ACSL3 cells with a high and a low expression level to monitor, if the expression level and thus cellular ACS activity influences the cellular metabolism. However, the ACS activity might be more dynamic and dependent on various factors like cell density, passage number, nutrient availability, culture conditions. Possible changes of ACS activity under variation of conditions had not been elaborately assessed and should be investigated in detail in future studies to provide a reliable fundament for the interpretation of the data.

7. Conclusions and Outlook

Summarizing the current data, ACSL3 can be concluded as the dominant ACS family member in COS-7 cells. The knockout of ACSL3 reduced ^{14}C-OA incorporation and heavily impaired TG synthesis. Thus, ACSL3 is required for efficient TG synthesis by activation of fatty acids to fatty acyl-CoA and has an important role to provide sufficient energy reservoirs in periods of nutrient deprivation. Studies with the GFP_A3ko and GFP-AA-ACSL3 cells revealed that lipid synthesis is related to the ACS activity mediated by ACSL3. The GFP-AA-ACSL3 cells expressing an ACSL3 mutant variant lacking ACS activity did not differ in incorporation of substrates or lipid species synthesis compared to the GFP_A3ko cells.

ACSL3 is not only involved in lipid synthesis but also maintains intracellular lipid stores by counteracting lipolysis. The GFP_A3ko and GFP-AA-ACSL3 cells exhibited a higher lipolytic rate compared to wtCOS-7 cells. Both cell lines were lacking ACSL3 functional as ACS enzyme suggesting that endogenous ACSL3 counteracts lipolysis possibly by re-esterification of the liberated fatty acids. Surprisingly, the GFP-AA-ACSL3 cells were slightly slowed down in basal lipolysis indicating that the presence of ACSL3 on LD might counteract lipolysis independent from ACS activity. Further studies are needed to reveal the precise mechanism as ACSL3 density on LD surface is too low to convincingly promote a shielding of lipids from cytosolic lipases. Scaffolding and recruitment of other antilipolytic proteins is another possible mechanism which requires further investigations. LD-ACSL1, a construct generated in the lab by Kathrin Seeburger (medical doctoral candidate), is ACSL1 containing the N-terminus of ACSL3 and therefore localized on LD. This might be beneficial to resolve the question, if simply the presence of a protein integrated in the LD membrane inhibits lipolysis or if ACSL3 has a unique function by recruiting other antilipolytic proteins. For this purpose, GFP_A3ko cells can be transduced with LD-ACSL1 and compared to GFP_A3ko and GFP-AA-ACSL3 cells in LD biogenesis.

Moreover, ACSL3 plays an important role in LD biogenesis by activation of fatty acids but also maybe by regulation of the nucleation sites in the ER. In this aspect, the localization of ACSL3 on the LD appears crucial as ER-associated ACSL3 in the experiments was heavily impaired in initial LD biogenesis. The GFP-ER-ACSL3 cells were not decreased in cellular TG synthesis indicating the phenotype was caused by an impaired nucleation of LD. However, the mechanism how LD-associated ACSL3 might influence nucleation at the ER is unclear. The change in lipid composition of the ER membrane was discussed, as the synthesis of lipid species

constraining membrane curvature (PC, PS, PE, CH) were increased in the GFP-ER-ACSL3 cells. Another tentative explanation addresses the N-terminal amphipathic helix, which advantages LD nucleation by promoting membrane curvature (McMahon and Gallop, 2005; Shen et al., 2012). The N-terminal amphipathic helix was missing in the GFP-ER-ACSL3 construct to exclude the protein from LD localization. Therefore, it needs to be elucidated, if the observed phenotype in the GFP-ER-ACSL3 expressing cell lines was really a consequence of protein localization or if it was an artefact caused by the genetic modification of the protein. In order to resolve this question, GFP_A3ko cells could be rescued with other ACS family members and compared in LD biogenesis with the GFP-ACSL3 and GFP-ER-ACSL3 cells. However, naturally occurring ACS family members complying with the requirements as possible candidates are missing. In order to draw final conclusions, an ACSL3 protein only localized on the LD or an ACSL3 protein containing an N-terminal amphipathic helix without being localized on the LD would be necessary. The challenge for the design of an ACSL3 protein that is only localized on the LD is the dynamic metabolism of LD that shrink and grow depending on the nutritional status. Wildtype ACSL3 translocates to the ER when LD disappear due to lipolysis. A protein only localized to LD would have to be degraded directly after dissociation from the LD which underlies complex regulation processes and has only been shown for adipophilin (Masuda et al., 2006; Pauloin et al., 2016). A construct comprising an N-terminal amphipathic helix and exclusively localized to the ER would give information about the relevance of the N-terminus for LD nucleation, but the generation of such a construct is impossible, because the N-terminal amphipathic helix is the reason why ACSL3 can be targeted to the LD in addition to the ER (Poppelreuther et al., 2012).

ER-localized ACSL3 was more efficient in lipid synthesis, especially TG synthesis. This effect was probably independent from ACS activity and maybe caused by the proximity to the lipogenic enzyme machinery, which is harboured in the ER. ER-ACSL3 probably increases lipid synthesis by activating fatty acids and deliver them to the enzymes required for lipid synthesis. This goes in line with the data obtained from model calculations based on molar quantification and subcellular fractionation of ACSL3 in A431 cells. This model showed convincingly, that neither the ACS activity nor the ACSL3 protein amount of LD-associated ACSL3 sufficiently contribute to the growth of LD. Therefore, the hypothesis of local TG synthesis on LD mediated by ACSL3 has to be refused and the transfer of lipids from the ER to the LD assumed as the main source for LD growth. Regarding catabolic lipid metabolism, GFP-ACSL3 and GFP-ER-ACSL3 cells were not significantly different, suggesting that re-

esterification of liberated fatty acids on the LD was as good as in the ER. The proximity of GFP-ER-ACSL3 to the lipogenic enzymes harboured in the ER was not beneficial for efficient re-esterification.

Comparison of the GFP-ACSL3 cell line with the high and the low expressing GFP-ER-ACSL3 cell line were supposed to clarify the interpretation of the obtained data and help to distinguish between metabolic effects caused by protein localization and effects caused by metabolic trapping. Experiments investigating lipid synthesis and basal lipolysis did not show evidence for a significant influence of protein expression and ACS activity on the obtained results. Still, the ACS activity is an important feature of the cells with a high potential to impact the data. Therefore, prior to further experiments ACS activity should be investigated regarding consistency over a wide range of passage numbers and possible dynamic changes depending on culture conditions and nutritional status. Establishment of a cell line with an inducible gene expression system would enable to adjust the expression of the enzyme variants in different cell lines and thus eliminate misleading results caused by metabolic trapping. A promising approach would be tetracycline-controlled transcriptional activation, a system using doxycycline to induce expression of the target gene (W. and C., 2002).

Besides performing studies concerning the lipid metabolism, the GFP-AA-ACSL3 cell line is an appropriate system to investigate other fields of cellular biology, where ACSL3 might fulfill ACS activity-independent functions. Previous studies have shown that ACSL3 acts as a regulator of transcription factors and that ACSL5 is involved in the modulation of apoptosis in enterocytes (Bu et al., 2009; Gassler et al., 2007), suggesting that ACS enzymes are involved in cellular metabolic pathways unrelated or not directly related to lipid metabolism.

The GFP-ER-ACSL3 construct holds great potential to further study the interplay between function and translocation of ACSL3. One aspect might be the investigation of putative phosphorylation sites of ACSL3. According to PhosphoSitePlus, a tool for the study of protein post-translational modifications (https://www.phosphosite.org/homeAction.action) (Hornbeck et al., 2015), amino acids assigned as phosphorylation sites in human ACSL3 are tyrosine at position 591 (29 references), serine at position 683 (16 references) and threonine at position 688 (33 references). Investigation of these phosphorylation sites in GFP-ER-ACSL3 and GFP-ACSL3 cells might reveal if the posttranslational modification of ACSL3 triggers differences in subcellular localization or regulation of enzyme activity.

ACSL3 is a key player in LD metabolism and its functional mechanisms as well as interactions with other cellular proteins need to be assessed in future studies to advance understanding of lipid metabolism and the development of therapeutics against lipid metabolism-related diseases.

8. Literature

Addgene (2016). CRISPR 101: A desktop resource, 1 edn (Addgene).

Alsabeeh, N., Chausse, B., Kakimoto, P.A., Kowaltowski, A.J., and Shirihai, O. (2017). Cell culture models of fatty acid overload: Problems and solutions. Biochim Biophys Acta *1863*, 143-151.

Ansari, I.H., Longacre, M.J., Stoker, S.W., Kendrick, M.A., O'Neill, L.M., Zitur, L.J., Fernandez, L.A., Ntambi, J.M., and MacDonald, M.J. (2017). Characterization of Acyl-CoA synthetase isoforms in pancreatic beta cells: Gene silencing shows participation of ACSL3 and ACSL4 in insulin secretion. Arch Biochem Biophys *618*, 32-43.

Barbosa, A.D., and Siniossoglou, S. (2017). Function of lipid droplet-organelle interactions in lipid homeostasis. Biochim Biophys Acta Mol Cell Res *1864*, 1459-1468.

Beilstein, F., Carriere, V., Leturque, A., and Demignot, S. (2016). Characteristics and functions of lipid droplets and associated proteins in enterocytes. Exp Cell Res *340*, 172-179.

Berg, J.M., Tymoczko, J.L., and Stryer, L. (2013). Biochemie, 7 edn (Springer-Verlag Berlin Heidelberg). Bersuker, K., and Olzmann, J.A. (2017). Establishing the lipid droplet proteome: Mechanisms of lipid droplet protein targeting and degradation. Biochim Biophys Acta *1862*, 1166-1177.

Bersuker, K., and Olzmann, J.A. (2018). In Close Proximity: The Lipid Droplet Proteome and Crosstalk With the Endoplasmic Reticulum. Contact (Thousand Oaks) *1*.

Black, P.N., and DiRusso, C.C. (2003). Transmembrane Movement of Exogenous Long-Chain Fatty Acids: Proteins, Enzymes, and Vectorial Esterification. Microbiology and Molecular Biology Reviews *67*, 454-472.

Borlinghaus, R.T., Eggert, D., Hamers, C., Reimer, R., and van den Boom, F. (2015). Hochauflösende Mikroskopie. 43-61.

Bozza, P.T., Bakker-Abreu, I., Navarro-Xavier, R.A., and Bandeira-Melo, C. (2011). Lipid body function in eicosanoid synthesis: an update. Prostaglandins Leukot Essent Fatty Acids *85*, 205-213.

Bradford, M.M. (1976). A rapid and sensitive method for the quantitation of microgram quantities of protein utilizing the principle of protein-dye binding. Analytical Biochemistry *72*, 248-254.

Brasaemle, D.L., Dolios, G., Shapiro, L., and Wang, R. (2004). Proteomic analysis of proteins associated with lipid droplets of basal and lipolytically stimulated 3T3-L1 adipocytes. The Journal of biological chemistry *279*, 46835-46842.

Brasaemle, D.L., Rubin, B., Harten, I.A., Gruia-Gray, J., Kimmel, A.R., and Londos, C. (2000). Perilipin A increases triacylglycerol storage by decreasing the rate of triacylglycerol hydrolysis. The Journal of biological chemistry *275*, 38486-38493.

Brown, R.J., Araujo-Vilar, D., Cheung, P.T., Dunger, D., Garg, A., Jack, M., Mungai, L., Oral, E.A., Patni, N., Rother, K.I.*, et al.* (2016). The Diagnosis and Management of Lipodystrophy Syndromes: A Multi-Society Practice Guideline. J Clin Endocrinol Metab *101*, 4500-4511.

Bu, S.Y., Mashek, M.T., and Mashek, D.G. (2009). Suppression of long chain acyl-CoA synthetase 3 decreases hepatic de novo fatty acid synthesis through decreased transcriptional activity. The Journal of biological chemistry *284*, 30474-30483.

Cermelli, S., Guo, Y., Gross, S.P., and Welte, M.A. (2006). The lipid-droplet proteome reveals that droplets are a protein-storage depot. Curr Biol *16*, 1783-1795.

Chakravarty, B., Gu, Z., Chirala, S.S., Wakil, S.J., and Quiocho, F.A. (2004). Human fatty acid synthase: structure and substrate selectivity of the thioesterase domain. Proc Natl Acad Sci U S A *101*, 15567-15572.

Choudhary, V., Ojha, N., Golden, A., and Prinz, W.A. (2015). A conserved family of proteins facilitates nascent lipid droplet budding from the ER. The Journal of cell biology *211*, 261-271.

Cronin, J., Zhang, X.-Y., and Reiser, J. (2005). Altering the tropism of lentiviral vectors through pseudotyping. Curr Gene Ther *5*, 387-398.

Digel, M., Ehehalt, R., Stremmel, W., and Füllekrug, J. (2009). Acyl-CoA synthetases: fatty acid uptake and metabolic channeling. Mol Cell Biochem *326*, 23-28.

Djouder, N., Tuerk, R.D., Suter, M., Salvioni, P., Thali, R.F., Scholz, R., Vaahtomeri, K., Auchli, Y., Rechsteiner, H., Brunisholz, R.A.*, et al.* (2010). PKA phosphorylates and inactivates AMPKalpha to promote efficient lipolysis. EMBO J *29*, 469-481.

Dong, B., Kan, C.F., Singh, A.B., and Liu, J. (2013). High-fructose diet downregulates long-chain acyl-CoA synthetase 3 expression in liver of hamsters via impairing LXR/RXR signaling pathway. J Lipid Res *54*, 1241-1254.

DSMZ (Deutsche Sammlung von MIkroorganismen und Zellkulturen GmbH).

Eastman, S.W., Yassaee, M., and Bieniasz, P.D. (2009). A role for ubiquitin ligases and Spartin/SPG20 in lipid droplet turnover. The Journal of cell biology *184*, 881-894.

Ellis, J.M., Frahm, J.L., Li, L.O., and Coleman, R.A. (2010). Acyl-coenzyme A synthetases in metabolic control. Curr Opin Lipidol *21*, 212-217.

Fraisl, P., Tanaka, H., Forss-Petter, S., Lassmann, H., Nishimune, Y., and Berger, J. (2006). A novel mammalian bubblegum-related acyl-CoA synthetase restricted to testes and possibly involved in spermatogenesis. Arch Biochem Biophys *451*, 23-33.

Fujimoto, Y., Itabe, H., Kinoshita, T., Homma, K.J., Onoduka, J., Mori, M., Yamaguchi, S., Makita, M., Higashi, Y., Yamashita, A.*, et al.* (2007). Involvement of long chain acyl-CoA synthetase in local synthesis of neutral lipids in cytoplasmic lipid droplets in human hepatocyte HuH7. J Lipid Res *48*, 1280-1292.

Fujimoto, Y., Itabe, H., Sakai, J., Makita, M., Noda, J., Mori, M., Higashi, Y., Kojima, S., and Takano, T. (2004). Identification of major proteins in the lipid droplet-enriched fraction isolated from the human hepatocyte cell line HuH7. Biochim Biophys Acta *1644*, 47-59.

Fujino, T., Kang, M.-J., Suzuki, H., Iijima, H., and Yamamoto, T. (1996). Molecular Characterization and Expression of Rat Acyl-CoA Synthetase 3. J Biol Chem *271*, 16748-16752.

Füllekrug, J., Ehehalt, R., and Poppelreuther, M. (2012). Outlook: Membrane junctions enable the metabolic trapping of fatty acids by intracellular acyl-CoA synthetases. Frontiers in Physiology *3*.

Fullekrug, J., and Poppelreuther, M. (2016). Measurement of Long-Chain Fatty Acyl-CoA Synthetase Activity. Methods Mol Biol *1376*, 43-53.

Gao, Q., and Goodman, J.M. (2015). The lipid droplet-a well-connected organelle. Front Cell Dev Biol *3*, 49.

Garcia, A., Subramanian, V., Sekowski, A., Bhattacharyya, S., Love, M.W., and Brasaemle, D.L. (2004). The amino and carboxyl termini of perilipin a facilitate the storage of triacylglycerols. The Journal of biological chemistry *279*, 8409-8416.

Gassler, N., Roth, W., Funke, B., Schneider, A., Herzog, F., Tischendorf, J.J., Grund, K., Penzel, R., Bravo, I.G., Mariadason, J.*, et al.* (2007). Regulation of enterocyte apoptosis by acyl-CoA synthetase 5 splicing. Gastroenterology *133*, 587-598.

Gemmink, A., Goodpaster, B.H., Schrauwen, P., and Hesselink, M.K.C. (2017). Intramyocellular lipid droplets and insulin sensitivity, the human perspective. Biochim Biophys Acta *1862*, 1242-1249.

Goodman, J.M. (2018). Understanding the Lipid Droplet Proteome and Protein Targeting. Dev Cell *44*, 1-2.

Graham, F.L., and van der Eb, A.J. (1973). A new technique for the assay of infectivity of human adenovirus 5 DNA. Virology *52*, 456-467.

Hamilton, J.A., Guo, W., and Kamp, F. (2002). Mechanism of cellular uptake of long-chain fatty acids: Do we need cellular proteins? Mol Cell Biochem *239*, 17-23.

Hegyi, G., Kardos, J., Kovács, M., Málnási-Csizmadia, A., Nyitray, L., Pál, G., Radnai, L., Rényi, A., and Venekei, I. (2013). Introduction to practical biochemistry (ELTE Faculty of Natural Sciences, Institute of Biology).

Herms, A., Bosch, M., Ariotti, N., Reddy, B.J., Fajardo, A., Fernandez-Vidal, A., Alvarez-Guaita, A., Fernandez-Rojo, M.A., Rentero, C., Tebar, F.*, et al.* (2013). Cell-to-cell heterogeneity in lipid droplets suggests a mechanism to reduce lipotoxicity. Curr Biol *23*, 1489-1496.

Hodges, B.D., and Wu, C.C. (2010). Proteomic insights into an expanded cellular role for cytoplasmic lipid droplets. J Lipid Res *51*, 262-273.

Hornbeck, P.V., Zhang, B., Murray, B., Kornhauser, J.M., Latham, V., and Skrzypek, E. (2015). PhosphoSitePlus, 2014: mutations, PTMs and recalibrations. Nucleic Acids Res *43*, D512-520.

Igal, R.A., and Coleman, R.A. (1996). Acylglycerol Recycling from Triacylglycerol to Phospholipid, Not Lipase Activity, Is Defective in Neutral Lipid Storage Disease Fibroblasts. The Journal of biological chemistry *271*, 16644-16651.

Inoue, H., Nojima, H., and Okayama, H. (1990). High efficiency transformation of Escherichia coli with plasmids. Gene *96*, 23-28.

Kageyama, A., Matsui, H., Ohta, M., Sambuichi, K., Kawano, H., Notsu, T., Imada, K., Yokoyama, T., and Kurabayashi, M. (2013). Palmitic acid induces osteoblastic differentiation in vascular smooth muscle cells through ACSL3 and NF-kappaB, novel targets of eicosapentaenoic acid. PloS one *8*, e68197.

Kassan, A., Herms, A., Fernández-Vidal, A., Bosch, M., Schieber, N.L., Reddy, B.J.N., Fajardo, A., Gelabert-Baldrich, M., Tebar, F., Enrich, C.*, et al.* (2013). Acyl-CoA synthetase 3 promotes lipid droplet biogenesis in ER microdomains. The Journal of cell biology *203*, 985-1001.

Khandelia, H., Duelund, L., Pakkanen, K.I., and Ipsen, J.H. (2010). Triglyceride blisters in lipid bilayers: implications for lipid droplet biogenesis and the mobile lipid signal in cancer cell membranes. PloS one *5*, e12811.

Khor, V.K., Shen, W.J., and Kraemer, F.B. (2013). Lipid droplet metabolism. Current opinion in clinical nutrition and metabolic care *16*, 632-637.

Kimura, H., Arasaki, K., Ohsaki, Y., Fujimoto, T., Ohtomo, T., Yamada, J., and Tagaya, M. (2018). Syntaxin 17 promotes lipid droplet formation by regulating the distribution of acyl-CoA synthetase 3. J Lipid Res *59*, 805-819.

Klemm, E.J., Spooner, E., and Ploegh, H.L. (2011). Dual role of ancient ubiquitous protein 1 (AUP1) in lipid droplet accumulation and endoplasmic reticulum (ER) protein quality control. The Journal of biological chemistry *286*, 37602-37614.

Komor, A.C., Badran, A.H., and Liu, D.R. (2017). CRISPR-Based Technologies for the Manipulation of Eukaryotic Genomes. Cell *168*, 20-36.

Konige, M., Wang, H., and Sztalryd, C. (2014). Role of adipose specific lipid droplet proteins in maintaining whole body energy homeostasis. Biochim Biophys Acta *1842*, 393-401.

Kory, N., Farese, R.V., Jr., and Walther, T.C. (2016). Targeting Fat: Mechanisms of Protein Localization to Lipid Droplets. Trends Cell Biol *26*, 535-546.

Kremer, B.P., and Bannwarth, H. (2014). Einführung in die Laborpraxis - Basiskompetenzen für Laborneulinge, 3 edn (Springer-Verlag Berlin Heidelberg).

Küch, E.-M. (2012). Intrazelluläre Kanalisierung von Fettsäuren durch Acyl-CoA-Synthetasen. In Faculty of Biosciences (Heidelberg University).

Küch, E.-M., Vellaramkalayil, R., Zhang, I., Lehnen, D., Brügger, B., Stremmel, W., Ehehalt, R., Poppelreuther, M., and Füllekrug, J. (2014). Differentially localized acyl-CoA synthetase 4 isoenzymes mediate the metabolic channeling of fatty acids towards phosphatidylinositol. Biochimica et Biophysica Acta (BBA) - Molecular and Cell Biology of Lipids *1841*, 227-239.

Lagace, T.A., and Ridgway, N.D. (2013). The role of phospholipids in the biological activity and structure of the endoplasmic reticulum. Biochimica et Biophysica Acta (BBA) - Molecular Cell Research *1833*, 2499-2510.

Larsson, S., Resjo, S., Gomez, M.F., James, P., and Holm, C. (2012). Characterization of the lipid droplet proteome of a clonal insulin-producing beta-cell line (INS-1 832/13). J Proteome Res *11*, 1264-1273.

Li, Z., Thiel, K., Thul, P.J., Beller, M., Kuhnlein, R.P., and Welte, M.A. (2012). Lipid droplets control the maternal histone supply of Drosophila embryos. Curr Biol *22*, 2104-2113.

Mashek, D.G., Khan, S.A., Sathyanarayan, A., Ploeger, J.M., and Franklin, M.P. (2015). Hepatic lipid droplet biology: Getting to the root of fatty liver. Hepatology, n/a-n/a.

Mashek, D.G., Li, L.O., and Coleman, R.A. (2006). Rat long-chain acyl-CoA synthetase mRNA, protein, and activity vary in tissue distribution and in response to diet. J Lipid Res *47*, 2004-2010.

Mashek, D.G., Li, L.O., and Coleman, R.A. (2007). Long-chain acyl-CoA synthetases and fatty acid channeling. Future Lipidology *2*, 465-476.

Masuda, Y., Itabe, H., Odaki, M., Hama, K., Fujimoto, Y., Mori, M., Sasabe, N., Aoki, J., Arai, H., and Takano, T. (2006). ADRP/adipophilin is degraded through the proteasome-dependent pathway during regression of lipid-storing cells. J Lipid Res *47*, 87-98.

McMahon, H.T., and Boucrot, E. (2015). Membrane curvature at a glance. Journal of Cell Science *128*, 1065-1070.

McMahon, H.T., and Gallop, J.L. (2005). Membrane curvature and mechanisms of dynamic cell membrane remodelling. Nature *438*, 590-596.

Milewska, M., McRedmond, J., and Byrne, P.C. (2009). Identification of novel spartin-interactors shows spartin is a multifunctional protein. Journal of Neurochemistry *111*, 1022-1030.

Milger, K., Herrmann, T., Becker, C., Gotthardt, D., Zickwolf, J., Ehehalt, R., Watkins, P.A., Stremmel, W., and Füllekrug, J. (2006). Cellular uptake of fatty acids driven by the ER-localized acyl-CoA synthetase FATP4. J Cell Sci *119*, 4678-4688.

Minekura, H., Fujino, T., Kang, M.-J., Fujita, T., Endo, Y., and Yamamoto, T.T. (1997). Human acyl-coenzyme A synthetase 3 cDNA and localization of its gene (ACS3) to chromosome band 2q34-q35. Genomics *42*, 180-181.

Moessinger, C., Kuerschner, L., Spandl, J., Shevchenko, A., and Thiele, C. (2011). Human lysophosphatidylcholine acyltransferases 1 and 2 are located in lipid droplets where they catalyze the formation of phosphatidylcholine. The Journal of biological chemistry *286*, 21330-21339.

Mosmann, T. (1983). Rapid colorimetric assay for cellular growth and survival: Application to proliferation and cytotoxicity assays. Journal of Immunological Methods *65*, 55-63.

Mühlhardt, C. (2009). Der Experimentator - Molekularbiologie/Genomics, 6 edn (Spektrum Akademischer Verlag Heidelberg).

Muoio, D.M., Lewin, T.M., Wiedmer, P., and Coleman, R.A. (2000). Acyl-CoAs are functionally channeled in liver: potential role of acyl-CoA synthetase. Am J Physiol Endocrinol Metab *279*, E1366–E1373.

Naito, Y., Hino, K., Bono, H., and Ui-Tei, K. (2015). CRISPRdirect: software for designing CRISPR/Cas guide RNA with reduced off-target sites. Bioinformatics *31*, 1120-1123.

Nolan, G.P. (2018). Retroviral Systems (https://web.stanford.edu/group/nolan/_OldWebsite/retroviral_systems/retsys.html) (Stanford University).

Ohsaki, Y., Suzuki, M., and Fujimoto, T. (2014). Open questions in lipid droplet biology. Chemistry & biology *21*, 86-96.

Omura, S. (1976). The Antibiotic Cerulenin, a Novel Tool for Biochemistry as an Inhibitor of Fatty Acid Synthesis. Bacteriological Reviews *40*, 681-697.

Onal, G., Kutlu, O., Gozuacik, D., and Dokmeci Emre, S. (2017). Lipid Droplets in Health and Disease. Lipids Health Dis *16*, 128.

Padanad, M.S., Konstantinidou, G., Venkateswaran, N., Melegari, M., Rindhe, S., Mitsche, M., Yang, C., Batten, K., Huffman, K.E., Liu, J.*, et al.* (2016). Fatty Acid Oxidation Mediated by Acyl-CoA Synthetase Long Chain 3 Is Required for Mutant KRAS Lung Tumorigenesis. Cell Rep *16*, 1614-1628.

Pataki, C.I., Rodrigues, J., Zhang, L., Qian, J., Efron, B., Hastie, T., Elias, J.E., Levitt, M., and Kopito, R.R. (2018). Proteomic analysis of monolayer-integrated proteins on lipid droplets identifies amphipathic interfacial α-helical membrane anchors. PNAS *115*, E8172–E8180.

Pauloin, A., Adenot, P., Hue-Beauvais, C., and Chanat, E. (2016). The perilipin-2 (adipophilin) coat of cytosolic lipid droplets is regulated by an Arf1-dependent mechanism in HC11 mouse mammary epithelial cells. Cell Biol Int *40*, 143-155.

Pol, A., Gross, S.P., and Parton, R.G. (2014). Biogenesis of the multifunctional lipid droplet: Lipids, proteins, and sites. The Journal of cell biology *204*, 635-646.

Poppelreuther, M., Rudolph, B., Du, C., Grossmann, R., Becker, M., Thiele, C., Ehehalt, R., and Füllekrug, J. (2012). The N-terminal region of acyl-CoA synthetase 3 is essential for both the localization on lipid droplets and the function in fatty acid uptake. J Lipid Res *53*, 888-900.

Poppelreuther, M., Sander, S., Minden, F., Dietz, M.S., Exner, T., Du, C., Zhang, I., Ehehalt, F., Knuppel, L., Domschke, S.*, et al.* (2018). The metabolic capacity of lipid droplet localized acyl-CoA synthetase 3 is not sufficient to support local triglyceride synthesis independent of the endoplasmic reticulum in A431 cells. Biochim Biophys Acta *1863*, 614-624.

Prevost, C., Sharp, M.E., Kory, N., Lin, Q., Voth, G.A., Farese, R.V., Jr., and Walther, T.C. (2018). Mechanism and Determinants of Amphipathic Helix-Containing Protein Targeting to Lipid Droplets. Dev Cell *44*, 73-86 e74.

Prinz, W.A. (2013). A bridge to understanding lipid droplet growth. Dev Cell *24*, 335-336.

Ran, F.A., Hsu, P.D., Wright, J., Agarwala, V., Scott, D.A., and Zhang, F. (2013). Genome engineering using the CRISPR-Cas9 system. Nature protocols *8*, 2281-2308.

Reed, M.C., Lieb, A., and Nijhout, H.F. (2010). The biological significance of substrate inhibition: a mechanism with diverse functions. Bioessays *32*, 422-429.

Rehner, G., and Daniel, H. (2010). Biochemie der Ernährung, 3 edn (Spektrum Akademischer Verlag Heidelberg).

Reshef, L., Olswang, Y., Cassuto, H., Blum, B., Croniger, C.M., Kalhan, S.C., Tilghman, S.M., and Hanson, R.W. (2003). Glyceroneogenesis and the triglyceride/fatty acid cycle. The Journal of biological chemistry *278*, 30413-30416.

Rosen, Evan D., and Spiegelman, Bruce M. (2014). What We Talk About When We Talk About Fat. Cell *156*, 20-44.

Ruggles, K.V., Turkish, A., and Sturley, S.L. (2013). Making, Baking, and Breaking: the Synthesis, Storage, and Hydrolysis of Neutral Lipids. Annual Review of Nutrition *33*, 413-451.

Salo, V.T., Belevich, I., Li, S., Karhinen, L., Vihinen, H., Vigouroux, C., Magre, J., Thiele, C., Holtta-Vuori, M., Jokitalo, E.*, et al.* (2016). Seipin regulates ER-lipid droplet contacts and cargo delivery. EMBO J *35*, 2699-2716.

Sander, J.D., and Joung, J.K. (2014). CRISPR-Cas systems for editing, regulating and targeting genomes. Nature biotechnology *32*, 347-355.

Sanders, M.A., Madoux, F., Mladenovic, L., Zhang, H., Ye, X., Angrish, M., Mottillo, E.P., Caruso, J.A., Halvorsen, G., Roush, W.R.*, et al.* (2015). Endogenous and Synthetic ABHD5 Ligands Regulate ABHD5-Perilipin Interactions and Lipolysis in Fat and Muscle. Cell Metab *22*, 851-860.

Schneider, H., Staudacher, S., Poppelreuther, M., Stremmel, W., Ehehalt, R., and Füllekrug, J. (2014). Protein mediated fatty acid uptake: Synergy between CD36/FAT-facilitated transport and acyl-CoA synthetase-driven metabolism. Archives of Biochemistry and Biophysics *546*, 8-18.

Schrader, M. (2001). Tubulo–Reticular Clusters of Peroxisomes in Living COS-7 Cells: Dynamic Behavior and Association with Lipid Droplets. J Histochem Cytochem *49*, 1421–1429.

Schreiber, R., Taschler, U., Preiss-Landl, K., Wongsiriroj, N., Zimmermann, R., and Lass, A. (2012). Retinyl ester hydrolases and their roles in vitamin A homeostasis. Biochim Biophys Acta *1821*, 113-123.

Schuck, S., Manninen, A., Honsho, M., Fullekrug, J., and Simons, K. (2004). Generation of single and double knockdowns in polarized epithelial cells by retrovirus-mediated RNA interference. PNAS *101*, 4912-4917.

Schuldiner, M., and Bohnert, M. (2017). A different kind of love - lipid droplet contact sites. Biochim Biophys Acta *1862*, 1188-1196.

Schweiger, M., Eichmann, T.O., Taschler, U., Zimmermann, R., Zechner, R., and Lass, A. (2014). Measurement of lipolysis. Methods Enzymol *538*, 171-193.

Shen, H., Pirruccello, M., and De Camilli, P. (2012). SnapShot: membrane curvature sensors and generators. Cell *150*, 1300, 1300 e1301-1302.

Shen, W.J., Azhar, S., and Kraemer, F.B. (2016). Lipid droplets and steroidogenic cells. Exp Cell Res *340*, 209-214.

Shi, Y., and Burn, P. (2004). Lipid metabolic enzymes: emerging drug targets for the treatment of obesity. Nat Rev Drug Discov *3*, 695-710.

Shyu, P., Jr., Wong, X.F.A., Crasta, K., and Thibault, G. (2018). Dropping in on lipid droplets: insights into cellular stress and cancer. Biosci Rep *38*.

Slaymaker, I.M., Gao, L., Zetsche, B., Scott, D.A., Yan, W.X., and Zhang, F. (2016). Rationally engineered Cas9 nucleases with improved specificity. Science *351*, 84-88.

Smith, M.E., Saraceno, G.E., Capani, F., and Castilla, R. (2013). Long-chain acyl-CoA synthetase 4 is regulated by phosphorylation. Biochem Biophys Res Commun *430*, 272-277.

Smith, P.K., Krohn, R.I., Hermanson, G.T., Mallia, A.K., Gartner, F.H., Provenzano, M.D., Fujimoto, E.K., Goeke, N.M., Olson, B.J., and Klenk, D.C. (1985). Measurement of protein using bicinchoninic acid. Analytical Biochemistry *150*, 76-85.

Spandl, J., Lohmann, D., Kuerschner, L., Moessinger, C., and Thiele, C. (2011). Ancient ubiquitous protein 1 (AUP1) localizes to lipid droplets and binds the E2 ubiquitin conjugase G2 (Ube2g2) via its G2 binding region. The Journal of biological chemistry *286*, 5599-5606.

Spicher, L., and Kessler, F. (2015). Unexpected roles of plastoglobules (plastid lipid droplets) in vitamin K1 and E metabolism. Curr Opin Plant Biol *25*, 123-129.

Steinberg, S.J., Morgenthaler, J., Heinzer, A.K., Smith, K.D., and Watkins, P.A. (2000). Very long-chain acyl-CoA synthetases. Human "bubblegum" represents a new family of proteins capable of activating very long-chain fatty acids. The Journal of biological chemistry *275*, 35162-35169.

Su, X., and Abumrad, N.A. (2009). Cellular fatty acid uptake: a pathway under construction. Trends Endocrinol Metab *20*, 72-77.

Suzuki, M., Shinohara, Y., Ohsaki, Y., and Fujimoto, T. (2011). Lipid droplets: size matters. J Electron Microsc (Tokyo) *60 Suppl 1*, S101-116.

Tang, Y., Zhou, J., Hooi, S.C., Jiang, Y.M., and Lu, G.D. (2018). Fatty acid activation in carcinogenesis and cancer development: Essential roles of long-chain acyl-CoA synthetases. Oncol Lett *16*, 1390-1396.

Tarnopolsky, M.A., Rennie, C.D., Robertshaw, H.A., Fedak-Tarnopolsky, S.N., Devries, M.C., and Hamadeh, M.J. (2007). Influence of endurance exercise training and sex on intramyocellular lipid and mitochondrial ultrastructure, substrate use, and mitochondrial enzyme activity. Am J Physiol Regul Integr Comp Physiol *292*, R1271-1278.

Thiam, A.R., and Beller, M. (2017). The why, when and how of lipid droplet diversity. J Cell Sci *130*, 315-324.

Thiam, A.R., and Foret, L. (2016). The physics of lipid droplet nucleation, growth and budding. Biochim Biophys Acta *1861*, 715-722.

Tomoda, H., Igarashi, K., and Omura, S. (1987). Inhibition of acyl-CoA synthetase by triacsins. Biochim Biophys Acta *921*, 595-598.

van de Linde, S., Sauer, M., and Heilemann, M. (2010). dSTORM: Hochauflösende Fluoreszenzmikroskopie. In BIOforum (Darmstadt: GIT VERLAG GmbH & Co. KG, Darmstadt), pp. 10-12.

W., H., and C., B. (2002). Tetracyclin-gesteuerte Genregulation: Vom bakteriellen Ursprung zum eukaryotischen Werkzeug. Bio-Spektrum.

Walther, T.C., and Farese Jr, R.V. (2012). Lipid Droplets and Cellular Lipid Metabolism. Annu Rev Biochem.

Wang, H., Airola, M.V., and Reue, K. (2017). How lipid droplets "TAG" along: Glycerolipid synthetic enzymes and lipid storage. Biochim Biophys Acta *1862*, 1131-1145.

Watkins, P.A. (2008). Very-long-chain Acyl-CoA Synthetases. J Biol Chem *283*, 1773-1777.

Welte, M.A., and Gould, A.P. (2017). Lipid droplet functions beyond energy storage. Biochim Biophys Acta *1862*, 1260-1272.

Wendel, A.A., Lewin, T.M., and Coleman, R.A. (2009). Glycerol-3-phosphate acyltransferases: rate limiting enzymes of triacylglycerol biosynthesis. Biochim Biophys Acta *1791*, 501-506.

Wilfling, F., Haas, J.T., Walther, T.C., and Jr, R.V. (2014a). Lipid droplet biogenesis. Curr Opin Cell Biol *29C*, 39-45.

Wilfling, F., Thiam, A.R., Olarte, M.J., Wang, J., Beck, R., Gould, T.J., Allgeyer, E.S., Pincet, F., Bewersdorf, J., Farese, R.V., Jr*., et al.* (2014b). Arf1/COPI machinery acts directly on lipid droplets and enables their connection to the ER for protein targeting. Elife *3*, e01607.

Yan, S., Yang, X.F., Liu, H.L., Fu, N., Ouyang, Y., and Qing, K. (2015). Long-chain acyl-CoA synthetase in fatty acid metabolism involved in liver and other diseases: an update. World journal of gastroenterology *21*, 3492-3498.

Yang, H.J., Hsu, C.L., Yang, J.Y., and Yang, W.Y. (2012). Monodansylpentane as a blue-fluorescent lipid-droplet marker for multi-color live-cell imaging. PloS one *7*, e32693.

Yao, H., and Ye, J. (2008). Long chain acyl-CoA synthetase 3-mediated phosphatidylcholine synthesis is required for assembly of very low density lipoproteins in human hepatoma Huh7 cells. The Journal of biological chemistry *283*, 849-854.

Zhang, C., and Liu, P. (2017). The lipid droplet: A conserved cellular organelle. Protein Cell *8*, 796-800.

9. Publications

Parts of this work are published in the following articles and posters:

Margarete Poppelreuther[1], **Simone Sander[1]**, Fadil Minden, Marina S. Dietz, Tarik Exner, Chen Du, Ingrid Zhang, Friedrich Ehehalt, Laura Knüppel, Susanne Domschke, Anna Badenhop, Sarah Staudachera Robert Ehehalt, Wolfgang Stremmel, Christoph Thiele, Mike Heilemann, Joachim Füllekrug (2018): The metabolic capacity of lipid droplet localized acyl-CoA synthetase 3 is not sufficient to support local triglyceride synthesis independent of the endoplasmic reticulum in A431 cells. *BBA - Molecular and Cell Biology of Lipids* 1863: 614–624.

[1] equal contribution.

Margarete Poppelreuther*, Leonard Fehring*, **Simone Sander***, Andrea Fernández-Vidal, Xuefeng Han, Robert Ehehalt, Wolfgang Stremmel, Albert Pol and Joachim Füllekrug: Depletion of ACSL3 specifically reduces triglyceride synthesis and lipid droplet biogenesis in COS-7 cells. *(manuscript submitted for publication)*

* equal contribution.

Joachim Füllekrug, Leonard Fehring, **Simone Sander**, Fadil Minden, Andrea Fernández-Vidal, Albert Pol, Xuefeng Han, Wolfgang Stremmel, Christoph Thiele , Margarete Poppelreuther: The acyl-CoA synthetase ACSL3 channels fatty acids towards triglyceride synthesis. FASEB conference ‚*Lipid Droplets: Dynamic Organelles in Metabolism and Beyond',* Snowmass, Colorado, 7/24/2016 - 7/29/2016.

Margarete Poppelreuther, **Simone Sander**, Leonard Fehring, Andrea Fernández-Vidal, Albert Pol, Joachim Füllekrug: Investigating the function of the lipid droplet localized acyl-CoA synthetase ACSL3. GRC conference: '*Lipids in Signaling and Metabolism*', Waterville Valley, New Hampshire, 7/30/2017 – 8/4/2017.

10. Appendix

10.1 CRISPR guide RNA design

10.1.1 CRISPR direct tool output for ACSL3 mRNA

Giving the ACSL3 mRNA (NCBI reference sequence number XM_007966443.1) as input for target sequence analysis by CRISPR direct tool delivered 213 entries. A selection is shown above highlighting the target sequences chosen for CRISPR guide RNA design (*figure 28*). In the column '20mer+PAM' the number of hits perfectly complementary for each target sequence is depicted. The number of hits shown in the columns '12mer+PAM' and '8mer+PAM' include target sites matching with the seed sequences. The numbers shown in the column 'number' of target sites include on-target and off-target sites, i. e. the target sequence used for the design of the CRISPR plasmid A3-ex4 is considered as highly specific, because the number for 20mer+PAM and 12mer+PAM is 1. The target sequence used for the design of the CRISPR plasmid A3-ex2 is not highly specific and has 10 potential off-targets for the 12mer seed sequence.

	position		target sequence	sequence information				number of target sites		
	start - end	+/-	20mer+PAM (total 23mer)	GC% of 20mer	Tm of 20mer	TTTT in 20mer	restriction sites	20mer +PAM	12mer +PAM	8mer +PAM
	509 - 531	-	ccgagtggatgatagctgcacag [gRNA]	50.00 %	72.74 °C	-		1 [detail]	8 [detail]	5251 [detail]
guide RNA A3-ex2	510 - 532	+	cgagtggatgatagctgcacagg [gRNA]	55.00 %	73.37 °C	-		1 [detail]	11 [detail]	4969 [detail]
	559 - 581	+	gttacattatatgctactctagg [gRNA]	30.00 %	62.14 °C	-		1 [detail]	24 [detail]	3830 [detail]
	562 - 584	+	acattatatgctactctaggagg [gRNA]	35.00 %	65.29 °C	-		1 [detail]	6 [detail]	3224 [detail]
	580 - 602	+	ggaggtccagccattgttcatgg [gRNA]	55.00 %	75.21 °C	-		1 [detail]	28 [detail]	5914 [detail]
	586 - 608	-	ccagccattgttcatggattaaa [gRNA]	35.00 %	64.53 °C	-		1 [detail]	27 [detail]	4495 [detail]
	590 - 612	-	ccattgttcatggattaaatgaa [gRNA]	25.00 %	58.94 °C	-		1 [detail]	49 [detail]	7492 [detail]
	597 - 619	+	tcatggattaaatgaaacagagg [gRNA]	30.00 %	60.43 °C	-		1 [detail]	53 [detail]	6700 [detail]
	623 - 645	-	ccaacatcattactagtaaagag [gRNA]	30.00 %	61.00 °C	-	SpeI	1 [detail]	17 [detail]	7021 [detail]
	645 - 667	+	gctcttacaaacaaagttgaagg [gRNA]	35.00 %	63.87 °C	-		1 [detail]	97 [detail]	7560 [detail]
	660 - 682	+	gttgaaggatatagtttctctgg [gRNA]	35.00 %	62.68 °C	-		0 [detail]	18 [detail]	8087 [detail]
	674 - 696	+	tttctctggtcccacgcctgcgg [gRNA]	60.00 %	77.27 °C	-		1 [detail]	19 [detail]	3186 [detail]
	684 - 706	-	cccacgcctgcggcacatcatca [gRNA]	60.00 %	78.38 °C	-		1 [detail]	3 [detail]	1754 [detail]
	685 - 707	-	ccacgcctgcggcacatcatcac [gRNA]	65.00 %	78.38 °C	-		1 [detail]	6 [detail]	1083 [detail]
	690 - 712	-	cctgcggcacatcatcactgttg [gRNA]	55.00 %	73.10 °C	-		1 [detail]	5 [detail]	970 [detail]
	694 - 716	+	cggcacatcatcactgttgatgg [gRNA]	50.00 %	71.02 °C	-		1 [detail]	27 [detail]	7373 [detail]
	710 - 732	+	ttgatggaaagccaccaacctgg [gRNA]	50.00 %	73.01 °C	-		1 [detail]	20 [detail]	4135 [detail]
	721 - 743	-	ccaacctggtccgagttcccc [gRNA]	65.00 %	79.00 °C	-		1 [detail]	43 [detail]	6498 [detail]
	724 - 746	-	ccaacctggtccgagttccccaa [gRNA]	60.00 %	79.00 °C	-		1 [detail]	2 [detail]	5519 [detail]
	726 - 748	+	aacctggtccgagttccccaagg [gRNA]	60.00 %	79.00 °C	-		1 [detail]	10 [detail]	5128 [detail]
	727 - 749	+	acctggtccgagttccccaagggg [gRNA]	60.00 %	79.00 °C	-		1 [detail]	13 [detail]	7249 [detail]
	728 - 750	+	cctggtccgagttccccaagggg [gRNA]	65.00 %	78.97 °C	-		1 [detail]	24 [detail]	5334 [detail]
	728 - 750	-	cctggtccgagttccccaaggggg [gRNA]	70.00 %	82.10 °C	-		1 [detail]	5 [detail]	750 [detail]
	729 - 751	+	ctggtccgagttccccaaggggg [gRNA]	65.00 %	78.97 °C	-		1 [detail]	22 [detail]	5171 [detail]
	734 - 756	-	ccgagttccccaaggggtcatc [gRNA]	60.00 %	78.72 °C	-		1 [detail]	39 [detail]	4822 [detail]
	741 - 763	-	cccaaggggtcatcgtgcata [gRNA]	55.00 %	75.20 °C	-		1 [detail]	13 [detail]	2772 [detail]
	742 - 764	-	ccaaggggtcatcgtgcatac [gRNA]	55.00 %	75.74 °C	-		1 [detail]	13 [detail]	2526 [detail]
	743 - 765	-	ccaaggggtcatcgtgcatacc [gRNA]	60.00 %	78.46 °C	-		1 [detail]	5 [detail]	2640 [detail]
guide RNA A3-ex4	747 - 769	+	gggggtcatcgtgcataccatgg [gRNA]	60.00 %	77.97 °C	-	BtgI NcoI	1 [detail]	1 [detail]	2021 [detail]

Fig. 28: **CRISPR direct tool ouput for possible ACSL3 target sequences.** The nucleotide sequence of the ACSL3 mRNA of Chlorocebus sabaeus was given as input and 'Green monkey (*Chlorocebus sabaeus*) genome, ChlSab1.1 (Mar, 2014)' was chosen for species selection. The output delivered 213 entries giving the position, GC-content, melting temperature, restriction sites and potential off-target sites for each target sequence. The target sequences applied for the CRISPR/Cas9 knockout are highlighted in red.

10.1.2 ACSL3 mRNA of *Chlorocebus sabaeus*

XM_007966443.1 (NCBI Reference Sequence of ACSL3 mRNA Chlorocebus sabaeus)
Chlorocebus sabaeus acyl-CoA synthetase long-chain family member 3 (ACSL3), mRNA

GATTCTCGCTGAAGTCTGTTAATTCTTTTTGAGTACTT**ATG**AATAACCACGTGTCTTCAAAACCATCTAC
CATGAAGCTAAAACATACCATCAACCCTATTCTTTTATATTTTATACATTTTCTAATATCACTTTATACT
ATTTTAACATACATTCCATTTTATTTTTTCTCTGAGTCAAGACAAGAAAAATCAAACCAAATTAAAGCAA
AGCCTGTAAATTCAAAACCTGATTCTGCATACAGATCTGTTAATAGTTTGGATGGTTTGGCTTCAGTATT
ATACCCTGGATGTGATACTCTAGATAAAGTTTTTACATATGCAAAAAACAAGTTTAAGAACAAAAGACTC
TTGGGAACACGTGAAGTTTTAAATGAGGAAGACGAAGTACAACCAAATGGAAAAATTTTTAAAAAGGTTA
TTCTTGGGCAGTATAATTGGCTTTCTTATGAAGATGTCTTCGTTCGAGCCTTGAATTTTGGGAATGGCTT
ACAGATGTTGGGCCAGAAACCAAAGACCAACATCGCCATCTTCTGTGAGACCAGGGCCGAGTGGATGATA
GCTGCACAGGCGTGTTTTATGTATAATTTTCAGCTTGTTACATTATATGCTACTCTAGGAGGTCCAGCCA
TTGTTCATGGATTAAATGAAACAGAGGTGACCAACATCATTACTAGTAAAGAGCTCTTACAAACAAAGTT
GAAGGATATAGTTTCTCTGGTCCCACGCCTGCGGCACATCATCACTGTTGATGGAAAGCCACCAACCTGG
TCCGAGTTCCCCAAGGGGGTCATCGTGCATACCATGGCTGCAGTGGAGGCCCTGGGAGCCAAGGCCAGCG
TGGAAAACCAACCTCATAGCAAACCATTGCCCTCAGATATTGCAGTAATCATGTACACAAGTGGATCCAC
AGGACTTCCAAAGGGAGTCATGATCTCACATAGTAACATTATTGCTGGTATAACTGGGATGGCAGAAAGG
ATTCCAGAACTGGGAGAGGAAGATGTCTACATTGGATATTTGCCTCTGGCCCATGTTCTAGAATTAAGTG
CTGAGCTTGTCTGTCTGTCTCACGGATGCCGCATTGGTTACTCTTCACCGCAGACTTTAGCAGATCAGTC
TTCAAAAATTAAAAAAGGAAGCAAAGGGGATACATCCATGTTGAAACCAACACTGATGGCAGCAGTTCCG
GAAATCATGGATCGGATCTACAAAAATGTCATGAATAAAGTGAATGAAATGAGTAGTTTTCAACGTAATC
TGTTTATTCTGGCTTATAATTACAAAATGGAACAGATTTCAAAAGGACGTAATACTCCACTGTGCAACAG
CTTTGTTTTCCGGAAAGTTCGAAGCTTGCTAGGGGGAAATATTCGTCTCCTGTTGTGTGGTGGCGCTCCT
CTTTCTGCAACTACGCAGCGGTTCATGAACATCTGTTTCTGCTGTCCTGTTGGTCAGGGATATGGACTCA
CTGAATCTGCTGGGGCCGGAACAATTACAGAAGTGTGGGACTACAATACTGGCAGAGTGGGAGCACCATT
AGTTTGCTGTGAAATCAAATTAAAAAACTGGGAGGAAGGTGGATACTTTAATACTGATAAACCACACCCC
AGGGGTGAAATTCTTATTGGGGGCCAAAATGTGACAATGGGATACTACAAAAATGAAGCAAAAACAAAAG
CTGATTTCTTTGAAGATGAAAATGGACAGAGGTGGCTCTGTACTGGGGATATTGGAGAGTTTGATCCTGA
TGGGTGCTTAAAGATTATTGATCGTAAAAAAGACCTTGTAAAACTACAGGCAGGAGAATATGTTTCTCTT
GGGAAAGTAGAGGCAGCTTTGAAGAATCTTCCACTAGTAGATAACATTTGTGCGTATGCAAACAGTTATC
ATTCTTATGTCATTGGATTTGTTGTGCCAAATCAAAAGGAACTAACTGAACTAGCTCGAAAGAAAGGACT
TAAAGGGACTTGGGAGGAGCTGTGCAACAGTTGTGAAATGGAAAATGAGGTACTGAAAGTGCTTTCCGAA
GCTGCTATTTCAGCAAGTCTGGAAAAGTTTGAAATTCCAGTAAAAATTCGTTTGAGCCCTGAACCGTGGA
CCCCTGAAACTGGTCTGGTGACAGATGCCTTCAAGCTGAAACGCAAAGAGCTTAAAACACATTACCAGGC
AGACATCGAGCGAATGTATGGAAGAAAATAATTACTCTCTTCTGGCATCAGTTTGCTACAGTGAGCTCAG
ATCAAATAGGAAAATACTTGAAATGCATGTCTCAAGCTGCGAGGCAAACTCCATTCCTCATATTAAACAT
TACTTCTCATGACGTCACCATTTTTAACTGACAGGATTAGTAAAACATTAAGACAGAAAACTTGTGTCTG
TCTCTTCTTTCGTTTTCCCCGCCACCAACTTCCTTTACCACCTATGACTGTACTTGTCAGTATGAGAATT
TTTCTGAATCATATTGGGGAAGCAGTGATTTTAAAACCTCAAGTTTTTAAACATGATTTATATGTTCTGT
ATAATGTTCAGTTTGTAACTTTTTAAAGTTTGGATGTATAGAGGGGTAAATAGGAAATATAAGAATTGGT
TATTTGGGGGCTTTTTTACTTACTGTATTTAAAAATACAAGGGTATTGATATGAAATTATGTAAATTTCA
AATGCTTGTGAATCAAATCATTGTTGAACAAAAGATTTGTTGCTGTGTAATTATTGTCTTGTATGCATTT
GAGAGAAATAAATATACCCGTACTTATGTTTTAAGAAATTGAGATCTTGTGAATATATGCCTGTCAGTGT
CTTCTTTATATATTTATTTTTTATTAGAAAAAATGAAGTTTGGTGATGCATGAAACAAAATAGCAAGAGA
GGGTTATAGTTTAATAGTAAGAGAGATAACACAGCACATTAGTCTCTAGTAGCTTACTATCAGAATGTTC
AATGAAGTCTTCTATTCAGCTGTTGAAACTAGAAAATGTCCAAACTTAAGTGGAAGCAATTCTGAAAGAG
AGGATAGAATTTAAAAAACAAGAGTATATAAAGTTATTCTTTGAATATTTCATTGCCTATATGTACATTG
AGTTATCTATATTTATAAACAAATTAGTCATGGAAAATTATTCTATCCCAAAGTCTCCTTTTAGTCTAGA
TAATCATATATCTCATTTGAAAATTAGTATTTTTCATAGTTTGCACTGATGCGTGTATGGATGTGTGTGA
GAGAGTCAGTGGTAGCTTATTTAAAAAGCACCTTATCCTTTCTACCATAACCTTTCTACACTAGAAAATG
AAATAATTTAGAATGCATTTGATAATAGCATTCTCACTAAGATACATGAAAATTTAACTTTATAACCATG
TGAGTTAAGATTTAATTTATAGGTTTTGATGTCAGTGTTGAAATTGTGAGTCAGAAACATTGCTTGTGTG
ATACATAGTAAGTCTCTTCATATGTTACTGCTTGTCTGTTGTTATTTCTGGATTATCAAAAGCGATAGTA
CACCAATTAAGATATGCTCAAATCAGGAGTTAAATCATAGGCACCACATTTTTCATGTCAGACTAGTTAT
TTCCTTGATTCTCAGTTACTGTAGGCATCAAAAGGCAATAAAAAGGAAAAAAAAAAAAAAA

The sequence shown above depicts the ACSL3 mRNA of Chlorocebus sabaeus with the reference sequence number XM_007966443.1 of NCBI, which was used for the guide RNA

design for the CRISPR knockout. The names of the nucleotides are abbreviated as adenine (A), guanine (G), cytosine (C), thymine (T). The start codon ATG is shown in bold red letters. The target sequence of the guide RNA of JF1052 is highlighted in green, the target sequence of the guide RNA of JF1053 is highlighted in blue. The PAM sequence is highlighted in grey.

10.2 Nucleotide and amino acid sequences of the transduced proteins

The names of the nucleotides in the DNA sequence are abbreviated as adenine (A), guanine (G), cytosine (C), thymine (T). The amino acids are shown in the 1-letter code (A: alanine; R: arginine; N: asparagine; D: aspartic acid; C: cysteine; E: glutamic acid; Q: glutamine; G: glycine; H: histidine; I: isoleucine; L: leucine; K: lysine; M: methionine; F: phenylalanine; P: proline; S: serine; T: threonine; W: tryptophane; Y: tyrosine; V: valine). The stop-codon in at the end of an amino acid sequence is designated by a star (*).

Plasmid JF623

The GFP-tag fused to the transduced proteins corresponds to the sequence data of enhanced GFP (eGFP) (NCBI Reference Sequence: NC_025025.1).

eGFP nucleotide sequence

```
ATGGTGAGCAAGGGCGAGGAGCTGTTCACCGGGGTGGTGCCCATCCTGGTCGAGCTGGACGGCGACGTAAACGGC
CACAAGTTCAGCGTGTCCGGCGAGGGCGAGGGCGATGCCACCTACGGCAAGCTGACCCTGAAGTTCATCTGCACC
ACCGGCAAGCTGCCCGTGCCCTGGCCCACCCTCGTGACCACCCTGACCTACGGCGTGCAGTGCTTCAGCCGCTAC
CCCGACCACATGAAGCAGCACGACTTCTTCAAGTCCGCCATGCCCGAAGGCTACGTCCAGGAGCGCACCATCTTC
TTCAAGGACGACGGCAACTACAAGACCCGCGCCGAGGTGAAGTTCGAGGGCGACACCCTGGTGAACCGCATCGAG
CTGAAGGGCATCGACTTCAAGGAGGACGGCAACATCCTGGGGCACAAGCTGGAGTACAACTACAACAGCCACAAC
GTCTATATCATGGCCGACAAGCAGAAGAACGGCATCAAGGTGAACTTCAAGATCCGCCACAACATCGAGGACGGC
AGCGTGCAGCTCGCCGACCACTACCAGCAGAACACCCCCATCGGCGACGGCCCCGTGCTGCTGCCCGACAACCAC
TACCTGAGCACCCAGTCCGCCCTGAGCAAAGACCCCAACGAGAAGCGCGATCACATGGTCCTGCTGGAGTTCGTG
ACCGCCGCCGGGATCACTCTCGGCATGGACGAGCTGTACAAGTAA
```

eGFP amino acid sequence (239 amino acids, 26941.48= 27 kDa)

```
MVSKGEELFTGVVPILVELDGDVNGHKFSVSGEGEGDATYGKLTLKFICTTGKLPVPWPTLVTTLTYGVQCFSRY
PDHMKQHDFFKSAMPEGYVQERTIFFKDDGNYKTRAEVKFEGDTLVNRIELKGIDFKEDGNILGHKLEYNYNSHN
VYIMADKQKNGIKVNFKIRHNIEDGSVQLADHYQQNTPIGDGPVLLPDNHYLSTQSALSKDPNEKRDHMVLLEFV
TAAGITLGMDELYK*
```

Plasmid JF825

The following sequence of GFP-ACSL3 is composed of GFP (highlighted in green) fused to the human ACSL3 (highlighted in purple; NCBI GenBank accession: BC041692.1) by a linker. The HA epitope tag at the C-terminus is highlighted in grey.

GFP-ACSL3 nucleotide sequence

ATGGTGAGCAAGGGCGAGGAGCTGTTCACCGGGGTGGTGCCCATCCTGGTCGAGCTGGACGGCGACGTAAACGGC
CACAAGTTCAGCGTGTCCGGCGAGGGCGAGGGCGATGCCACCTACGGCAAGCTGACCCTGAAGTTCATCTGCACC
ACCGGCAAGCTGCCCGTGCCCTGGCCCACCCTCGTGACCACCCTGACCTACGGCGTGCAGTGCTTCAGCCGCTAC
CCCGACCACATGAAGCAGCACGACTTCTTCAAGTCCGCCATGCCCGAAGGCTACGTCCAGGAGCGCACCATCTTC
TTCAAGGACGACGGCAACTACAAGACCCGCGCCGAGGTGAAGTTCGAGGGCGACACCCTGGTGAACCGCATCGAG
CTGAAGGGCATCGACTTCAAGGAGGACGGCAACATCCTGGGGCACAAGCTGGAGTACAACTACAACAGCCACAAC
GTCTATATCATGGCCGACAAGCAGAAGAACGGCATCAAGGTGAACTTCAAGATCCGCCACAACATCGAGGACGGC
AGCGTGCAGCTCGCCGACCACTACCAGCAGAACACCCCCATCGGCGACGGCCCCGTGCTGCTGCCCGACAACCAC
TACCTGAGCACCCAGTCCGCCCTGAGCAAAGACCCCAACGAGAAGCGCGATCACATGGTCCTGCTGGAGTTCGTG
ACCGCCGCCGGGATCACTCTCGGCATGGACGAGCTGTACAAGTCCGGACTCAGATCTCGAGCTCAAGCTTCGAAT
TCTGCAGTCGACGGTACCACCATGAATAACCACGTGTCTTCAAAACCATCTACCATGAAGCTAAAACATACCATC
AACCCTATTCTTTTATATTTTATACATTTTCTAATATCACTTTATACTATTTTAACATACATTCCGTTTTATTTT
TTCTCCGAGTCAAGACAAGAAAAATCAAACCGAATTAAAGCAAAGCCTGTAAATTCAAAACCTGATTCTGCATAC
AGATCTGTTAATAGTTTGGATGGTTTGGCTTCAGTATTATACCCTGGATGTGATACTTTAGATAAAGTTTTTACA
TATGCAAAAAACAAATTTAAGAACAAAAGACTCTTGGGAACACGTGAAGTTTTAAATGAGGAAGATGAAGTACAA
CCAAATGGAAAAATTTTTAAAAAGGTTATTCTTGGACAGTATAATTGGCTTTCCTATGAAGATGTCTTTGTTCGA
GCCTTTAATTTTGGAAATGGATTACAGATGTTGGGTCAGAAACCAAAGACCAACATCGCCATCTTCTGTGAGACC
AGGGCCGAGTGGATGATAGCTGCACAGGCGTGTTTTATGTATAATTTTCAGCTTGTTACATTATATGCCACTCTA
GGAGGTCCAGCCATTGTTCATGCATTAAATGAAACAGAGGTGACCAACATCATTACTAGTAAAGAACTCTTACAA
ACAAAGTTGAAGGATATAGTTTCTTTGGTCCCACGCCTGCGGCACATCATCACTGTTGATGGAAAGCCACCGACC
TGGTCCGAGTTCCCCAAGGGCATCATTGTGCATACCATGGCTGCAGTGGAGGCCCTGGGAGCCAAGGCCAGCATG
GAAAACCAACCTCATAGCAAACCATTGCCCTCAGATATTGCAGTAATCATGTACACAAGTGGATCCACAGGACTT
CCAAAGGGAGTCATGATCTCACATAGTAACATTATTGCTGGTATAACTGGGATGGCAGAAAGGATTCCAGAACTA
GGAGAGGAAGATGTCTACATTGGATATTTGCCTCTGGCCCATGTTCTAGAATTAAGTGCTGAGCTTGTCTGTCTT
TCTCACGGATGCCGCATTGGTTACTCTTCACCACAGACTTTAGCAGATCAGTCTTCAAAAATTAAAAAAGGAAGC
AAAGGGGATACATCCATGTTGAAACCAACACTGATGGCAGCAGTTCCGGAAATCATGGATCGGATCTACAAAAAT
GTCATGAATAAAGTCAGTGAAATGAGTAGTTTTCAACGTAATCTGTTTATTCTGGCCTATAATTACAAAATGGAA
CAGATTTCAAAAGGACGTAATACTCCACTGTGCGACAGCTTTGTTTTCCGGAAAGTTCGAAGCTTGCTAGGGGGA
AATATTCGTCTCCTGTTGTGTGGTGGCGCTCCACTTTCTGCAACCACGCAGCGATTCATGAACATCTGTTTCTGC
TGTCCTGTTGGTCAGGGATACGGGCTCACTGAATCTGCTGGGGCTGGAACAATTTCCGAAGTGTGGGACTACAAT
ACTGGCAGAGTGGGAGCACCATTAGTTTGCTGTGAAATCAAATTAAAAAACTGGGAGGAAGGTGGATACTTTAAT
ACTGATAAGCCACACCCCAGGGGTGAAATTCTTATTGGGGGCCAAAGTGTGACAATGGGGTACTATAAAAATGAA
GCAAAAACAAAAGCTGATTTCTTTGAAGATGAAAATGGACAAAGGTGGCTCTGTACTGGGGATATTGGAGAGTTT
GAACCCGATGGATGCTTAAAGATTATTGATCGTAAAAAGGACCTTGTAAAACTACAGGCAGGGGAATATGTTTCT
CTTGGGAAAGTAGAGGCAGCTTTGAAGAATCTTCCACTAGTAGATAACATTTGTGCATATGCAAACAGTTATCAT
TCTTATGTCATTGGATTTGTTGTGCCAAATCAAAAGGAACTAACTGAACTAGCTCGAAAGAAAGGACTTAAAGGG
ACTTGGGAGGAGCTGTGTAACAGTTGTGAAATGGAAAATGAGGTACTTAAAGTGCTTTCCGAAGCTGCTATTTCA
GCAAGTCTGGAAAAGTTTGAAATTCCAGTAAAAATTCGTTTGAGTCCTGAACCGTGGACCCCTGAAACTGGTCTG
GTGACAGATGCCTTCAAGCTGAAACGCAAAGAGCTTAAAACACATTACCAGGCGGACATTGAGCGAATGTATGGA
AGAAAATACCCATACGATGTTCCAGATTACGCTTGA

GFP-ACSL3 amino acid sequence (986 amino acids, 110187.56 = 110 kDa)

MVSKGEELFTGVVPILVELDGDVNGHKFSVSGEGEGDATYGKLTLKFICTTGKLPVPWPTLVTTLTYGVQCFSRY
PDHMKQHDFFKSAMPEGYVQERTIFFKDDGNYKTRAEVKFEGDTLVNRIELKGIDFKEDGNILGHKLEYNYNSHN
VYIMADKQKNGIKVNFKIRHNIEDGSVQLADHYQQNTPIGDGPVLLPDNHYLSTQSALSKDPNEKRDHMVLLEFV
TAAGITLGMDELYKSGLRSRAQASNSAVDGTTMNNHVSSKPSTMKLKHTINPILLYFIHFLISLYTILTYIPFYF
FSESRQEKSNRIKAKPVNSKPDSAYRSVNSLDGLASVLYPGCDTLDKVFTYAKNKFKNKRLLGTREVLNEEDEVQ
PNGKIFKKVILGQYNWLSYEDVFVRAFNFGNGLQMLGQKPKTNIAIFCETRAEWMIAAQACFMYNFQLVTLYATL
GGPAIVHALNETEVTNIITSKELLQTKLKDIVSLVPRLRHIITVDGKPPTWSEFPKGIIVHTMAAVEALGAKASM
ENQPHSKPLPSDIAVIMYTSGSTGLPKGVMISHSNIIAGITGMAERIPELGEEDVYIGYLPLAHVLELSAELVCL
SHGCRIGYSSPQTLADQSSKIKKGSKGDTSMLKPTLMAAVPEIMDRIYKNVMNKVSEMSSFQRNLFILAYNYKME
QISKGRNTPLCDSFVFRKVRSLLGGNIRLLLCGGAPLSATTQRFMNICFCCPVGQGYGLTESAGAGTISEVWDYN
TGRVGAPLVCCEIKLKNWEEGGYFNTDKPHPRGEILIGGQSVTMGYYKNEAKTKADFFEDENGQRWLCTGDIGEF
EPDGCLKIIDRKKDLVKLQAGEYVSLGKVEAALKNLPLVDNICAYANSYHSYVIGFVVPNQKELTELARKKGLKG
TWEELCNSCEMENEVLKVLSEAAISASLEKFEIPVKIRLSPEPWTPETGLVTDAFKLKRKELKTHYQADIERMYG
RKYPYDVPDYA*

Plasmid JF827

The following sequence of GFP-ER-ACSL3 is composed of GFP fused to amino acid 52-769 of the human ACSL3 (highlighted in purple; NCBI GenBank accession: BC041692.1) by a linker. The 51 amino acids starting from the N-terminus of ACSL3 are replaced with the transmembrane domain of the mouse FATP4 (highlighted in red; NCBI Reference Sequence: NM_011989.5). The HA epitope tag at the C-terminus is highlighted in grey.

GFP-ER-ACSL3 nucleotide sequence

```
ATGGTGAGCAAGGGCGAGGAGCTGTTCACCGGGGTGGTGCCCATCCTGGTCGAGCTGGACGGCGACGTAAACGGC
CACAAGTTCAGCGTGTCCGGCGAGGGCGAGGGCGATGCCACCTACGGCAAGCTGACCCTGAAGTTCATCTGCACC
ACCGGCAAGCTGCCCGTGCCCTGGCCCACCCTCGTGACCACCCTGACCTACGGCGTGCAGTGCTTCAGCCGCTAC
CCCGACCACATGAAGCAGCACGACTTCTTCAAGTCCGCCATGCCCGAAGGCTACGTCCAGGAGCGCACCATCTTC
TTCAAGGACGACGGCAACTACAAGACCCGCGCCGAGGTGAAGTTCGAGGGCGACACCCTGGTGAACCGCATCGAG
CTGAAGGGCATCGACTTCAAGGAGGACGGCAACATCCTGGGGCACAAGCTGGAGTACAACTACAACAGCCACAAC
GTCTATATCATGGCCGACAAGCAGAAGAACGGCATCAAGGTGAACTTCAAGATCCGCCACAACATCGAGGACGGC
AGCGTGCAGCTCGCCGACCACTACCAGCAGAACACCCCCATCGGCGACGGCCCCGTGCTGCTGCCCGACAACCAC
TACCTGAGCACCCAGTCCGCCCTGAGCAAAGACCCCAACGAGAAGCGCGATCACATGGTCCTGCTGGAGTTCGTG
ACCGCCGCCGGGATCACTCTCGGCATGGACGAGCTGTACAAGTCCGGACTCAGATCTCGAGCTCAAGCTTCGAAT
TCCATGCTACTTGGAGCATCTCTGGTGGGGGCGCTACTGTTCTCCAAGCTAGTGCTGAAGCTGCCCTGGACCCAG
GTGGGATTCTCCCTGTTGCTCCTGTACTTGGGGTCTGGTGGCTGGCGTTTCATCCGGGTCTTCATCTCAAGACAA
GAAAAATCAAACCGAATTAAAGCAAAGCCTGTAAATTCAAAACCTGATTCTGCATACAGATCTGTTAATAGTTTG
GATGGTTTGGCTTCAGTATTATACCCTGGATGTGATACTTTAGATAAAGTTTTTACATATGCAAAAAACAAATTT
AAGAACAAAAGACTCTTGGGAACACGTGAAGTTTTAAATGAGGAAGATGAAGTACAACCAAATGGAAAAATTTTT
AAAAAGGTTATTCTTGGACAGTATAATTGGCTTTCCTATGAAGATGTCTTTGTTCGAGCCTTTAATTTTGGAAAT
GGATTACAGATGTTGGGTCAGAAACCAAAGACCAACATCGCCATCTTCTGTGAGACCAGGGCCGAGTGGATGATA
GCTGCACAGGCGTGTTTTATGTATAATTTTCAGCTTGTTACATTATATGCCACTCTAGGAGGTCCAGCCATTGTT
CATGCATTAAATGAAACAGAGGTGACCAACATCATTACTAGTAAAGAACTCTTACAAACAAAGTTGAAGGATATA
GTTTCTTTGGTCCCACGCCTGCGGCACATCATCACTGTTGATGGAAAGCCACCGACCTGGTCCGAGTTCCCCAAG
GGCATCATTGTGCATACCATGGCTGCAGTGGAGGCCCTGGGAGCCAAGGCCAGCATGGAAAACCAACCTCATAGC
AAACCATTGCCCTCAGATATTGCAGTAATCATGTACACAAGTGGATCCACAGGACTTCCAAAGGGAGTCATGATC
TCACATAGTAACATTATTGCTGGTATAACTGGGATGGCAGAAAGGATTCCAGAACTAGGAGAGGAAGATGTCTAC
ATTGGATATTTGCCTCTGGCCCATGTTCTAGAATTAAGTGCTGAGCTTGTCTGTCTTTCTCACGGATGCCGCATT
GGTTACTCTTCACCACAGACTTTAGCAGATCAGTCTTCAAAAATTAAAAAAGGAAGCAAAGGGGATACATCCATG
TTGAAACCAACACTGATGGCAGCAGTTCCGGAAATCATGGATCGGATCTACAAAAATGTCATGAATAAAGTCAGT
GAAATGAGTAGTTTTCAACGTAATCTGTTTATTCTGGCCTATAATTACAAAATGGAACAGATTTCAAAAGGACGT
AATACTCCACTGTGCGACAGCTTTGTTTTCCGGAAAGTTCGAAGCTTGCTAGGGGGAAATATTCGTCTCCTGTTG
TGTGGTGGCGCTCCACTTTCTGCAACCACGCAGCGATTCATGAACATCTGTTTCTGCTGTCCTGTTGGTCAGGGA
TACGGGCTCACTGAATCTGCTGGGGCTGGAACAATTTCCGAAGTGTGGGACTACAATACTGGCAGAGTGGGAGCA
CCATTAGTTTGCTGTGAAATCAAATTAAAAAACTGGGAGGAAGGTGGATACTTTAATACTGATAAGCCACACCCC
AGGGGTGAAATTCTTATTGGGGGCCAAAGTGTGACAATGGGGTACTATAAAAATGAAGCAAAAACAAAAGCTGAT
TTCTTTGAAGATGAAAATGGACAAAGGTGGCTCTGTACTGGGGATATTGGAGAGTTTGAACCCGATGGATGCTTA
AAGATTATTGATCGTAAAAAGGACCTTGTAAAACTACAGGCAGGGGAATATGTTTCTCTTGGGAAAGTAGAGGCA
GCTTTGAAGAATCTTCCACTAGTAGATAACATTTGTGCATATGCAAACAGTTATCATTCTTATGTCATTGGATTT
GTTGTGCCAAATCAAAAGGAACTAACTGAACTAGCTCGAAAGAAAGGACTTAAAGGGACTTGGGAGGAGCTGTGT
AACAGTTGTGAAATGGAAAATGAGGTACTTAAAGTGCTTTCCGAAGCTGCTATTTCAGCAAGTCTGGAAAAGTTT
GAAATTCCAGTAAAAATTCGTTTGAGTCCTGAACCGTGGACCCCTGAAACTGGTCTGGTGACAGATGCCTTCAAG
CTGAAACGCAAAGAGCTTAAAACACATTACCAGGCGGACATTGAGCGAATGTATGGAAGAAAATACCCATACGAT
GTTCCAGATTACGCTTGA
```

GFP-ER-ACSL3 amino acid sequence (980 amino acids, 109213.73 Da = 109 kDa)

```
MVSKGEELFTGVVPILVELDGDVNGHKFSVSGEGEGDATYGKLTLKFICTTGKLPVPWPTLVTTLTYGVQCFSRY
PDHMKQHDFFKSAMPEGYVQERTIFFKDDGNYKTRAEVKFEGDTLVNRIELKGIDFKEDGNILGHKLEYNYNSHN
```

VYIMADKQKNGIKVNFKIRHNIEDGSVQLADHYQQNTPIGDGPVLLPDNHYLSTQSALSKDPNEKRDHMVLLEFV
TAAGITLGMDELYKSGLRSRAQASNSMLLGASLVGALLFSKLVLKLPWTQVGFSLLLLYLGSGGWRFIRVFISRQ
EKSNRIKAKPVNSKPDSAYRSVNSLDGLASVLYPGCDTLDKVFTYAKNKFKNKRLLGTREVLNEEDEVQPNGKIF
KKVILGQYNWLSYEDVFVRAFNFGNGLQMLGQKPKTNIAIFCETRAEWMIAAQACFMYNFQLVTLYATLGGPAIV
HALNETEVTNIITSKELLQTKLKDIVSLVPRLRHIITVDGKPPTWSEFPKGIIVHTMAAVEALGAKASMENQPHS
KPLPSDIAVIMYTSGSTGLPKGVMISHSNIIAGITGMAERIPELGEEDVYIGYLPLAHVLELSAELVCLSHGCRI
GYSSPQTLADQSSKIKKGSKGDTSMLKPTLMAAVPEIMDRIYKNVMNKVSEMSSFQRNLFILAYNYKMEQISKGR
NTPLCDSFVFRKVRSLLGGNIRLLLCGGAPLSATTQRFMNICFCCPVGQGYGLTESAGAGTISEVWDYNTGRVGA
PLVCCEIKLKNWEEGGYFNTDKPHPRGEILIGGQSVTMGYYKNEAKTKADFFEDENGQRWLCTGDIGEFEPDGCL
KIIDRKKDLVKLQAGEYVSLGKVEAALKNLPLVDNICAYANSYHSYVIGFVVPNQKELTELARKKGLKGTWEELC
NSCEMENEVLKVLSEAAISASLEKFEIPVKIRLSPEPWTPETGLVTDAFKLKRKELKTHYQADIERMYGRKYPYD
VPDYA*

Plasmid 844

The following sequence of GFP-AA-ACSL3 is composed of GFP (highlighted in green) fused to the human ACSL3 (highlighted in purple; NCBI GenBank accession: BC041692.1) by a linker. In the mutant variant of ACSL3 the serine at the positions 288 and 290 is replaced with alanine to diminish the ACS activity due to a functional mutation in the ATP-binding site of the enzyme (highlighted in red). The HA epitope tag at the C-terminus is highlighted in grey.

GFP-AA-ACSL3 nucleotide sequence

ATGGTGAGCAAGGGCGAGGAGCTGTTCACCGGGGTGGTGCCCATCCTGGTCGAGCTGGACGGCGACGTAAACGGC
CACAAGTTCAGCGTGTCCGGCGAGGGCGAGGGCGATGCCACCTACGGCAAGCTGACCCTGAAGTTCATCTGCACC
ACCGGCAAGCTGCCCGTGCCCTGGCCCACCCTCGTGACCACCCTGACCTACGGCGTGCAGTGCTTCAGCCGCTAC
CCCGACCACATGAAGCAGCACGACTTCTTCAAGTCCGCCATGCCCGAAGGCTACGTCCAGGAGCGCACCATCTTC
TTCAAGGACGACGGCAACTACAAGACCCGCGCCGAGGTGAAGTTCGAGGGCGACACCCTGGTGAACCGCATCGAG
CTGAAGGGCATCGACTTCAAGGAGGACGGCAACATCCTGGGGCACAAGCTGGAGTACAACTACAACAGCCACAAC
GTCTATATCATGGCCGACAAGCAGAAGAACGGCATCAAGGTGAACTTCAAGATCCGCCACAACATCGAGGACGGC
AGCGTGCAGCTCGCCGACCACTACCAGCAGAACACCCCCATCGGCGACGGCCCCGTGCTGCTGCCCGACAACCAC
TACCTGAGCACCCAGTCCGCCCTGAGCAAAGACCCCAACGAGAAGCGCGATCACATGGTCCTGCTGGAGTTCGTG
ACCGCCGCCGGGATCACTCTCGGCATGGACGAGCTGTACAAGTCCGGACTCAGATCTCGAGCTCAAGCTTCGAAT
TCTGCAGTCGACGGTACCACCATGAATAACCACGTGTCTTCAAAACCATCTACCATGAAGCTAAAACATACCATC
AACCCTATTCTTTTATATTTTATACATTTTCTAATATCACTTTATACTATTTTAACATACATTCCGTTTTATTTT
TTCTCCGAGTCAAGACAAGAAAAATCAAACCGAATTAAAGCAAAGCCTGTAAATTCAAAACCTGATTCTGCATAC
AGATCTGTTAATAGTTTGGATGGTTTGGCTTCAGTATTATACCCTGGATGTGATACTTTAGATAAAGTTTTTACA
TATGCAAAAAACAAATTTAAGAACAAAAGACTCTTGGGAACACGTGAAGTTTTAAATGAGGAAGATGAAGTACAA
CCAAATGGAAAAATTTTTAAAAAGGTTATTCTTGGACAGTATAATTGGCTTTCCTATGAAGATGTCTTTGTTCGA
GCCTTTAATTTTGGAAATGGATTACAGATGTTGGGTCAGAAACCAAAGACCAACATCGCCATCTTCTGTGAGACC
AGGGCCGAGTGGATGATAGCTGCACAGGCGTGTTTTATGTATAATTTTCAGCTTGTTACATTATATGCCACTCTA
GGAGGTCCAGCCATTGTTCATGCATTAAATGAAACAGAGGTGACCAACATCATTACTAGTAAAGAACTCTTACAA
ACAAAGTTGAAGGATATAGTTTCTTTGGTCCCACGCCTGCGGCACATCATCACTGTTGATGGAAAGCCACCGACC
TGGTCCGAGTTCCCCAAGGGCATCATTGTGCATACCATGGCTGCAGTGGAGGCCCTGGGAGCCAAGGCCAGCATG
GAAAACCAACCTCATAGCAAACCATTGCCCTCAGATATTGCAGTAATCATGTACACAGCTGGAGCCACAGGACTT
CCAAAGGGAGTCATGATCTCACATAGTAACATTATTGCTGGTATAACTGGGATGGCAGAAAGGATTCCAGAACTA
GGAGAGGAAGATGTCTACATTGGATATTTGCCTCTGGCCCATGTTCTAGAATTAAGTGCTGAGCTTGTCTGTCTT
TCTCACGGATGCCGCATTGGTTACTCTTCACCACAGACTTTAGCAGATCAGTCTTCAAAAATTAAAAAAGGAAGC
AAAGGGGATACATCCATGTTGAAACCAACACTGATGGCAGCAGTTCCGGAAATCATGGATCGGATCTACAAAAAT
GTCATGAATAAAGTCAGTGAAATGAGTAGTTTTCAACGTAATCTGTTTATTCTGGCCTATAATTACAAAATGGAA
CAGATTTCAAAAGGACGTAATACTCCACTGTGCGACAGCTTTGTTTTCCGGAAAGTTCGAAGCTTGCTAGGGGGA
AATATTCGTCTCCTGTTGTGTGGTGGCGCTCCACTTTCTGCAACCACGCAGCGATTCATGAACATCTGTTTCTGC
TGTCCTGTTGGTCAGGGATACGGGCTCACTGAATCTGCTGGGGCTGGAACAATTTCCGAAGTGTGGGACTACAAT
ACTGGCAGAGTGGGAGCACCATTAGTTTGCTGTGAAATCAAATTAAAAAACTGGGAGGAAGGTGGATACTTTAAT
ACTGATAAGCCACACCCCAGGGGTGAAATTCTTATTGGGGGCCAAAGTGTGACAATGGGGTACTATAAAAATGAA
GCAAAAACAAAAGCTGATTTCTTTGAAGATGAAAATGGACAAAGGTGGCTCTGTACTGGGGATATTGGAGAGTTT
GAACCCGATGGATGCTTAAAGATTATTGATCGTAAAAAGGACCTTGTAAAACTACAGGCAGGGGAATATGTTTCT

CTTGGGAAAGTAGAGGCAGCTTTGAAGAATCTTCCACTAGTAGATAACATTTGTGCATATGCAAACAGTTATCAT
TCTTATGTCATTGGATTTGTTGTGCCAAATCAAAAGGAACTAACTGAACTAGCTCGAAAGAAAGGACTTAAAGGG
ACTTGGGAGGAGCTGTGTAACAGTTGTGAAATGGAAAATGAGGTACTTAAAGTGCTTTCCGAAGCTGCTATTTCA
GCAAGTCTGGAAAAGTTTGAAATTCCAGTAAAAATTCGTTTGAGTCCTGAACCGTGGACCCCTGAAACTGGTCTG
GTGACAGATGCCTTCAAGCTGAAACGCAAAGAGCTTAAAACACATTACCAGGCGGACATTGAGCGAATGTATGGA
AGAAAATACCCATACGATGTTCCAGATTACGCTTGA

GFP-AA-ACSL3 amino acid sequence (986 amino acids, 110155.56 Da = 110 kDa)

MVSKGEELFTGVVPILVELDGDVNGHKFSVSGEGEGDATYGKLTLKFICTTGKLPVPWPTLVTTLTYGVQCFSRY
PDHMKQHDFFKSAMPEGYVQERTIFFKDDGNYKTRAEVKFEGDTLVNRIELKGIDFKEDGNILGHKLEYNYNSHN
VYIMADKQKNGIKVNFKIRHNIEDGSVQLADHYQQNTPIGDGPVLLPDNHYLSTQSALSKDPNEKRDHMVLLEFV
TAAGITLGMDELYKSGLRSRAQASNSAVDGTTMNNHVSSKPSTMKLKHTINPILLYFIHFLISLYTILTYIPFYF
FSESRQEKSNRIKAKPVNSKPDSAYRSVNSLDGLASVLYPGCDTLDKVFTYAKNKFKNKRLLGTREVLNEEDEVQ
PNGKIFKKVILGQYNWLSYEDVFVRAFNFGNGLQMLGQKPKTNIAIFCETRAEWMIAAQACFMYNFQLVTLYATL
GGPAIVHALNETEVTNIITSKELLQTKLKDIVSLVPRLRHIITVDGKPPTWSEFPKGIIVHTMAAVEALGAKASM
ENQPHSKPLPSDIAVIMYTAGATGLPKGVMISHSNIIAGITGMAERIPELGEEDVYIGYLPLAHVLELSAELVCL
SHGCRIGYSSPQTLADQSSKIKKGSKGDTSMLKPTLMAAVPEIMDRIYKNVMNKVSEMSSFQRNLFILAYNYKME
QISKGRNTPLCDSFVFRKVRSLLGGNIRLLLCGGAPLSATTQRFMNICFCCPVGQGYGLTESAGAGTISEVWDYN
TGRVGAPLVCCEIKLKNWEEGGYFNTDKPHPRGEILIGGQSVTMGYYKNEAKTKADFFEDENGQRWLCTGDIGEF
EPDGCLKIIDRKKDLVKLQAGEYVSLGKVEAALKNLPLVDNICAYANSYHSYVIGFVVPNQKELTELARKKGLKG
TWEELCNSCEMENEVLKVLSEAAISASLEKFEIPVKIRLSPEPWTPETGLVTDAFKLKRKELKTHYQADIERMYG
RKYPYDVPDYA*

Plasmid JF1262

The following sequence of A3Nt-mcherry is composed of the first 135 amino acids of the human ACSL3 (highlighted in purple; NCBI GenBank accession: BC041692.1) fused to mcherry (highlighted in red; NCBI GenBank accession: MG323876.1) by a linker.

A3Nt-mcherry nucleotide sequence

ATGAATAACCACGTGTCTTCAAAACCATCTACCATGAAGCTAAAACATACCATCAACCCTATTCTTTTATATTTT
ATACATTTTCTAATATCACTTTATACTATTTTAACATACATTCCGTTTTATTTTTCTCCGAGTCAAGACAAGAA
AAATCAAACCGAATTAAAGCAAAGCCTGTAAATTCAAAACCTGATTCTGCATACAGATCTGTTAATAGTTTGGAT
GGTTTGGCTTCAGTATTATACCCTGGATGTGATACTTTAGATAAAGTTTTTACATATGCAAAAAACAAATTTAAG
AACAAAAGACTCTTGGGAACACGTGAAGTTTTAAATGAGGAAGATGAAGTACAACCAAATGGAAAAATTTTTAAA
AAGGTTATTCTTGGACAGTATAATTGGCTTGCGGATCCACCGGTGGATCCTACCATGGTGAGCAAGGGCGAGGAG
GATAACATGGCCATCATCAAGGAGTTCATGCGCTTCAAGGTGCACATGGAGGGCTCCGTGAACGGCCACGAGTTC
GAGATCGAGGGCGAGGGCGAGGGCCGCCCCTACGAGGGCACCCAGACCGCCAAGCTGAAGGTGACCAAGGGTGGC
CCCCTGCCCTTCGCCTGGGACATCCTGTCCCCTCAGTTCATGTACGGCTCCAAGGCCTACGTGAAGCACCCCGCC
GACATCCCCGACTACTTGAAGCTGTCCTTCCCCGAGGGCTTCAAGTGGGAGCGCGTGATGAACTTCGAGGACGGC
GGCGTGGTGACCGTGACCCAGGACTCCTCCCTGCAGGACGGCGAGTTCATCTACAAGGTGAAGCTGCGCGGCACC
AACTTCCCCTCCGACGGCCCCGTAATGCAGAAGAAGACCATGGGCTGGGAGGCCTCCTCCGAGCGGATGTACCCC
GAGGACGGCGCCCTGAAGGGCGAGATCAAGCAGAGGCTGAAGCTGAAGGACGGCGGCCACTACGACGCTGAGGTC
AAGACCACCTACAAGGCCAAGAAGCCCGTGCAGCTGCCCGGCGCCTACAACGTCAACATCAAGTTGGACATCACC
TCCCACAACGAGGACTACACCATCGTGGAACAGTACGAACGCGCCGAGGGCCGCCACTCCACCGGCGGCATGGAC
GAGCTGTACAAGTAA

A3Nt-mcherry amino acid sequence (379 amino acids, 43165.18 Da = 43 kDa)

MNNHVSSKPSTMKLKHTINPILLYFIHFLISLYTILTYIPFYFFSESRQEKSNRIKAKPVNSKPDSAYRSVNSLD
GLASVLYPGCDTLDKVFTYAKNKFKNKRLLGTREVLNEEDEVQPNGKIFKKVILGQYNWLADPPVDPTMVSKGEE
DNMAIIKEFMRFKVHMEGSVNGHEFEIEGEGEGRPYEGTQTAKLKVTKGGPLPFAWDILSPQFMYGSKAYVKHPA
DIPDYLKLSFPEGFKWERVMNFEDGGVVTVTQDSSLQDGEFIYKVKLRGTNFPSDGPVMQKKTMGWEASSERMYP
EDGALKGEIKQRLKLKDGGHYDAEVKTTYKAKKPVQLPGAYNVNIKLDITSHNEDYTIVEQYERAEGRHSTGGMD
ELYK*

Acknowledgements

First of all, I would like to thank Prof. Dr. Joachim Füllekrug for supervising my PhD, provision of materials and equipment and for his helpful guidance in scientific issues. Your valuable critiques supported me in my learning processes, the development and performing of experiments and the efforts bringing together all pieces of work to write my PhD Thesis.

I would also like to thank Prof. Dr. Britta Brügger for being my first supervisor. Thanks also to my TAC members Prof. Dr. Britta Brügger, Prof. Dr. Joachim Füllekrug and Dr. Rainer Pepperkok for their useful input and suggestions in the TAC meetings and for participation in my oral examination. Thanks to Dr. Sebastian Schuck for participating in my PhD defense.

I would like to thank Prof. Dr. med. Dr. h. c. Stremmel for the chance to work on my PhD project in the department of Internal Medicine IV.

I wish to acknowledge the consistent cooperation and helpfulness offered by Dr. Margarete Poppelreuther. Thank you, Marga, for sharing your experimental skills and your scientific knowledge to promote me in my work.

A special thanks goes to Cassian for the helpful cooperation concerning the radiolabelling assays and to Tarik for the support in the lipid droplet quantification by ImageJ. Moreover, I would like to thank the other members of the Füllekrug Lab for their assistance and teamwork.

I would also like to thank Mike Heilemann and Marina Dietz from Goethe-University Frankfurt for the good cooperation in dSTORM microscopy.

Finally, I would like to express my great appreciation to my family and friends, who stood by me throughout my time as a PhD student. Mom and Dad, Julia and Jana Lea, thanks for always supporting me. I value every word and gesture of encouragement, big or small. Nico, thank you for cheering me on in all the moments of frustration and exhaustion, but also for getting excited about every little success on the way. I am grateful to have a family I can always count on! Without you this would not have been possible.